Reactor modelling of the pre-combustion chemical looping concept with coal-derived syngas and natural gas as feedstock

van Etten, M.P.C.

Award date:
2016

Technische Universiteit
Eindhoven
University of Technology

Process Engineering
Multiphase Reactor group (SMR)
Department of Chemical Engineering
and Chemistry

Den Dolech 2, 5612 AZ Eindhoven
P.O. Box 513, 5600 MB Eindhoven
The Netherlands
www.tue.nl

Graduation Committee:
Prof. Dr. Ir. M van Sint Annaland
Dr. F. Gallucci
Dr. Ir. J. van der Schaaf
Dr. V. Spallina

Author:
M.P.C. van Etten

Date:
June 2016

Reactor modelling of the pre-combustion chemical looping concept with coal-derived syngas and natural gas as feedstock

MSc. Thesis

Contents

Abstract

The pre-combustion chemical looping technology combines the advantages of chemical looping to convert a fuel into carbon dioxide and steam during the reduction stage with the advantages of producing a H_2/N_2 stream during the oxidation stage for a hydrogen fueled gas turbine or for ammonia synthesis.

In this work, the pre-combustion chemical looping is carried out in dynamically operated packed bed reactors operated at high pressure (>20 bar) and intermediate temperature (600-1000˚C). A numerical analysis shows the reactor behavior and performance of the complete process after multiple cycles in which reduction/oxidation phases are considered, combined with purge and heat removal phases.

Both syngas obtained from coal gasification and natural gas diluted with steam and carbon dioxide are considered as feed in the analysis, whereas a Fe-based oxygen carrier supported with Al_2O_3 has been selected for the process, mainly because it allows the production of hydrogen by water-splitting during the oxidation phase. Different active weight contents of the oxygen carrier are compared in order to investigate the effect of the axial solid temperature profile on the performance of the pre-combustion chemical looping concept.

For the case that coal-derived syngas is used as fuel for the reduction phase, the performance of the pre-combustion chemical looping concept is optimized by performing a sensitivity analysis of the heat removal flowrate on the power production by the gas turbine. Also the effect of the steam oxidation kinetics on the power production by the gas turbine is analyzed.

For the case that natural gas is used as fuel for the reduction phase, the performance of the pre-combustion chemical looping concept is optimized by performing a sensitivity analysis of the oxygen content of the inflowing oxidant gas stream on the ratio hydrogen to nitrogen of the produced outflowing oxidant gas stream needed for the synthesis of ammonia. Also the effect of the steam oxidation kinetics on this hydrogen to nitrogen ratio for the ammonia synthesis is analyzed.

1 Introduction

1.1 Energy consumption and climate change

The world energy demand has been increased continuously since the industrial revolution. The required power and heat has been generated mainly by combustion of fossil fuels, which resulted in large anthropogenic carbon dioxide emissions to the atmosphere. The combination of a rapidly growing world population and the increasing energy consumption per capita suggests that large investments are needed in order to secure sufficient energy supply at reasonable prices. On the other hand, the fossil fuel reserves are shrinking, while the transition towards a world economy based on sustainable energy is still in an early stage of development.

The relevance of this issue has been increased due to strong indications that human activities are affecting the climate on Earth. The International Panel on Climate Change (IPCC) has collected the results of substantial research efforts to obtain a comprehensive scientific framework describing the evolution of the climate over very long time-scales. According to the research of IPCC (2013), the effect of human activities on changes in the climate is very likely (probability of more than 90%) to have been dominating the natural variations in especially the past 50 years [1].

Among the various greenhouse gasses, the major anthropogenic contribution to the increased greenhouse effect is by carbon dioxide, which makes up for the largest additional radiative forcing (IPCC, 2013). The emissions of carbon dioxide are predominantly due to the burning of fossil fuels, especially in large scale combustion units used for power production, and in small distributed sources such as cars.

From 1900, the CO_2 concentrations in the atmosphere has risen from 300 to 390 ppm, which indeed has been associated to fossil fuel combustion, cement production and deforestation (IPCC, 2013). During these activities, only 43% of the released CO_2 remained in the atmosphere, the other 57% of the CO_2 has been reabsorbed in terrestrial ecosystems and the oceans (IPCC, 2013). Due to the reabsorption of CO_2 in the oceans, the acidity of the oceans has increased, which negatively influences the environment in the oceans.

The temperature on Earth is dependent on the radiative forces in the atmosphere, which influences the solar energy uptake by the Earth. Greenhouse gasses, like CO_2, CH_4, O_3 and halocarbons, when in the right concentration, have a positive influence on the radiative force and thus on the global temperature. Therefore, with the increase of greenhouse gas concentrations, especially CO_2, the balance on the radiative forces is altered, and the temperature is increased. During the last century, the temperature has increased by 0.8˚C (IPCC, 2013). The expectation for this century is that the

anthropogenic CO_2 emissions will continue, and rise to 421-936 ppm, which will result in a further global temperature rise of 1-3.7˚C (IPCC, 2013). This temperature rise will lead to a rising sea level, more extreme weather conditions, and the extinction of species.

For this reason, there is a growing body of opinion that urgent measures needs to be taken in order to mitigate climate change by reducing the anthropogenic emissions of greenhouse gases as soon as possible.

The long term solution to this problem requires that the fossil fuels will be replaced by sustainable (renewable) resources. Besides stabilizing the greenhouse gas concentrations, this replacement of fossil fuels by sustainable resources in order to avoid shortages in raw materials for the production of e.g. bulk chemicals. Nevertheless, in different energy scenarios the use of fossil fuels is projected to not only remain the dominant primary energy source for at least until halfway the current century, its absolute use is expected to increase significantly [2]. The transition towards a world economy based on energy supply via sustainable sources such as wind-, hydro-, and solar energy is expected to be a lengthy process that cannot be expected to be solely responsible for the stabilization of atmospheric greenhouse gas concentrations in this century.

Therefore, on the short term significant reductions of carbon dioxide emissions should be attained from energy savings, for example via efficiency improvements both in power production and consumer products, and as a consequence of public awareness. According to the assessment of IPCC (2014), this can be achieved by applying carbon capture and storage (CCS) to power production and energy intensive processes [3].

1.2 Carbon Capture and Storage

Carbon dioxide capture and storage technologies can be used to reduce carbon dioxide emissions from large stationary sources, particularly from fossil fuel-fired power plants, either existing or new generation. Essentially, CCS consists of three consecutive steps: (1) the CO_2 capture at the power plant, (2) the CO_2 transport to a suitable storage location, and (3) the long-term isolation of CO_2 from the atmosphere.

1.2.1 CO_2 capture

Three different general approaches have been proposed to obtain CO_2 at high purity from fossil-fuel fired power stations: (1) post-combustion capture for flue gases, in which nitrogen and carbon dioxide are separated, (2) pre-combustion capture for producing a carbon-free H_2 based fuel for a power cycle, and (3) oxyfuel combustion for generating a highly concentrated CO_2 stream after water condensation. With all of this three approaches, additional equipment is needed for CO_2-separation, purification and compression, which also requires a significant energy input. This will lead to a significant energy penalty with respect to a power plant without CO_2 capture. With the current available capture techniques, the power production efficiency of a coal-based power plant would drop from 42% to 31-33% [4]. Therefore, much research is dedicated in order to reduce this efficiency penalty by improving, or circumventing, the separations steps.

1.2.1.1 Post-combustion capture

With post-combustion capture, the carbon dioxide is removed after the combustion of the primary fuel in air, resulting in a flue gas stream that mainly consists of nitrogen. There are several approaches of interest in order to achieve this separation, including concepts based on chemical and physical absorption, adsorption processes using solid sorbents, cryogenic separation, and membrane processes. Due to the low pressure of the flue gas and the modest concentration of the CO_2 in the flue gas, chemical absorption (using an amine) is the preferably approach for this separation.

The principle of this technology is to firstly have a reaction of the carbon dioxide with an alkanolamine (e.g. monoethanolamine) in an absorption column. Consequently, the absorption liquid has to be regenerated in a stripping column, in which the carbon dioxide is stripped from the solvent using pressure and temperature differences, and recycled to the absorber. The most important challenges in this process are to decrease the large regeneration energy input, and to decrease the sensitivity of the absorption liquids for oxygen and water present in the flue gas stream.

For the short term, post-combustion capture appears to be the most interesting option for CCS. Technologies like amine scrubbing are already used in the industry, but are still expensive and very energy-intensive. Since this technology is an end-of-the-pipe solution, the implementation at new power plants which are based on the original designs will be possible. Also adjusting the existing power plants is an option, but the availability of land for the capture equipment can lead to restrictions, as well as the proportionally higher energy penalty as a consequence of the lower plant efficiency, and the remaining lifetime of the power plant.

Major concerns with post-combustion capture technologies are related to the strong decrease in the overall energy efficiency when CO_2 capture is applied. Therefore, a lot of research is in progress to obtain for example improved absorption liquids, stable sorbents or cheap membranes.

1.2.1.2 Pre-combustion capture

With pre-combustion capture, a mixture of hydrogen and carbon dioxide is produced from the primary fuel (typically natural gas or gasified coal) via a series of chemical reactions. Firstly, the hydrocarbon fuel is converted to a mixture of carbon monoxide and hydrogen (synthesis gas). The carbon monoxide is then converted to carbon dioxide in water gas shift reactors. Finally, the resulting mixture can be separated into a CO_2-rich stream, which can be compressed and stored, and a hydrogen stream that can be combusted in a power plant in order to generate power or heat.

Although the initial fuel conversion steps in this approach is more elaborated than with the traditional combustion process, the high concentrations of carbon dioxide produced in the water gas shift reactors (up to 60% after water condensation) simplifies the separation process [5]. This typically occurs via pressure swing adsorption or physical/chemical absorption.

1.2.1.3 Oxy-combustion capture

The principle of oxyfuel combustion is to avoid nitrogen-dilution of the carbon dioxide by burning the fuel with pure oxygen (instead of air) in a mixture with recycled flue gas only. In this case, a flue gas is obtained consisting of carbon dioxide, water and only small amount of nitrogen. After water condensation, a CO_2-rich stream is obtained, which can be compressed and stored.

One of the important challenges for using the oxyfuel combustion principle is minimizing the energy efficiency loss associated with the air separation. Air separation is typically carried out using cryogenic distillation, which makes it very energy-intensive. Therefore, the eventual rate of success if this technology may depend on the improvements to the current technology, or the development of novel air separation processes.

1.2.2 CO_2 transport

After the capture process, carbon dioxide should be transported to the storage site, except when it can be stored directly at the power plant. Transportation of CO_2 can be done via pipelines or ship transport. Both of these conceivable ways are mature technologies used in the oil and gas industries, and therefore no significant (technological) obstacles for the implementation of CCS with respect to CO_2 transport are foreseen. The main issues for the transport of carbon dioxide are the costs and safety, but so far neither of those issues have proved to be an obstacle in the current transport operations.

1.2.3 CO_2 storage

After CO_2 capture and storage, the carbon dioxide needs to be stored either permanently (sequestration) or at least for a long period (storage). Four options have been identified for the storage of carbon dioxide, namely geological storage, ocean storage, mineralization and industrial use. Both ocean storage and mineralization are still in research and demonstration phase, but it is believed that especially the public acceptance of ocean storage is doubtful in view of the possible damage done to the marine ecosystems, and that for mineralization the process will be too expensive due to the slow process kinetics. Industrial use of CO_2, in which carbon dioxide is converted into value-added products, is unlikely to become a factor of quantitative relevance, since there is a limited demand for carbon dioxide. This leaves geological storage to be considered as the most likely option for CO_2 storage on the short term.

Geological sequestration is the disposal of carbon dioxide in geological media. From an economic point of view, the use of carbon dioxide is of particular interest in order to promote the production of fossil fuels from almost depleted gas field (Enhanced Gas Recovery), oil fields (Enhanced Oil Recovery), or unmineable coal seams (Enhanced Coal Bed Methane Recovery). However, the fraction of carbon dioxide emitted that can be used for these purposes is relatively small [5], which makes the depleted gas and oil fields, and saline aquifers the most important options for carbon dioxide sequestration. The saline aquifers are rock formations saturated with water, where huge quantities of salts are dissolved, covered with an impermeable layer. The carbon dioxide will be injected into these spaces at around 1000 meters depth, and therefore will have a considerable geological stability. The capacity for the storage of carbon dioxide in geological formations is expected to be sufficiently large in order to cover the demand for CCS in the coming century. Also is expected that technological problems with carbon dioxide storage can be overcome, even though there are several issues that are not properly solved yet, since the knowledge from the oil and gas industries on the behavior of gas reservoirs can be used with this technology.

The possibility of CO_2 leakage from the storage sites should be of special concern, since when a significant fraction of the stored CO_2 would end up in the atmosphere, an additional contribution to the carbon dioxide emissions could be expected. However, from modeling and experimental studies, and already gained experience from the operation of natural gas reservoirs, it is expected that the amount of carbon dioxide retained in the reservoirs will exceed 99% even after 1000 years after injection [5]. On the short term, potential risks can be related to the abrupt leakage of CO_2 from a reservoir, and the immediate dangers anticipated for population and environment in the direct surroundings. This could be caused by a sudden failure of well closures, resulting in a rapid and potentially life-threatening release of carbon dioxide. Based on the experience with the existing gas reservoirs, it is expected that blow-outs can be contained, which means that there will be a limiting direct impact. A more gradual release of CO_2 may occur by for example rock fractures. For this case, especially the consequences of pollution of the groundwater have to be addressed. Therefore, accurate monitoring systems need to be developed, and careful site selection needs to be done.

1.2.4 Future market for CCS

When the decision to implement CCS is left to the market alone, the technology will never become successful. Carbon dioxide needs to be obtained at high purity and must be compressed in order to transport and store it, which means that there will be always a significant loss in energy efficiency. Since this is the parameter that the power sector has been optimizing over the past century, the energy companies would rather prefer to seek for further improvements of their current processes. This is the reason that governmental actions like fiscal incentives or environmental legislation are needed when CCS is considered as in important option to reduce anthropogenic emissions of CO_2.

In order to increase the chance of success for CCS, the development of improved processes for reducing the capture costs is needed, which is currently estimated to be in the order of 10-15 percentage points [6]. Obviously, this also means that a significant additional amount of fossil fuels must be burned, and therefore the depletion of coal and gas reserves is accelerated. In order to avoid this acceleration, novel technologies have to be developed in which the capture efficiencies is increased, while energy penalties are minimized. The Chemical Looping Combustion (CLC) process is a very interesting new technology for achieving a high reduction of the CO_2 emissions with a reduced energy penalty. This is due to fact that the separation CO_2 is integrated with the power production process, while direct contact between the fuel and air (and therefore N_2 dilution of the CO_2) is avoided.

1.3 This Thesis

In this thesis, a novel reactor concept for chemical looping is simulated, and the performance of this reactor concept concerning the power production and the production of a H_2/N_2-rich gas stream for ammonia production is analyzed for both the cases of coal-derived syngas and natural gas as the fuel.

First, the principle of chemical looping will be explained in Chapter 2. Also different chemical looping technologies that has been researched during the last few years will be reviewed, and eventual downsides of these technologies will be discussed. Finally, the pre-combustion chemical looping concept will be introduced, and the advantages in comparison with the other chemical looping technologies will be discussed.

In Chapter 3, a reactor model for the pre-combustion chemical looping concept will be provided. Therefore, first all reactions that are possible during the reduction will be explained. Since most of the reduction reactions by hydrogen and carbon monoxide are equilibrium reactions, also the equilibrium constant for this reactions will be discussed. When Al_2O_3 is used as inert material, full conversion of hydrogen and carbon monoxide during the reduction cycle is possible due to the formation of the spinel $FeAl_2O_3$, and therefore also this phenomenon will be explained. For the case that natural gas is used as fuel, the reductant stream consists mainly out of methane, steam and carbon dioxide, and therefore also the methane reforming reactions will be discussed. In the second part of this chapter, the oxidation reactions that are possible during the oxidation cycle will be explained. Since the oxidation reaction by oxygen are highly exothermic, there will be a temperature rise within the reactor, which will also be explained. Finally, the numerical model used for simulating the 1D adiabatic packed bed reactor system will be provided.

The results obtained from the reactor model for the case of coal-derived syngas as the fuel will be analyzed and discussed in Chapter 4. For this case, two heat management strategies are possible. For the first heat management strategy, the effect of the active weight fraction of the oxygen carrier on the performance of the PCCL concept will be determined concerning the power production downstream by a gas turbine. In order to optimize the performance of the PCCL concept, a sensitivity analysis of the heat removal flowrate on the power production by the gas turbine is performed. Since the hydrogen production during the oxidation cycle is highly dependent on the steam oxidation kinetics, the effect of the steam oxidation kinetics on the power production is determined by decreasing the reaction rate for the oxidation of $FeAl_2O_4$ to Fe_3O_4 by steam. For the second heat management strategy, also the effect of the active weight fraction of the oxygen carrier on the performance of the PCCL concept will be determined concerning the power production downstream by a gas turbine, and the performance will be compared to that of the first heat management strategy.

The results obtained from the reactor model for the case of natural gas as the fuel will be analyzed and discussed in Chapter 5. For this case, only one heat management strategy is possible. First, different active weight contents of the oxygen carrier are compared in order to investigate the effect of the axial solid temperature profile on the performance of the pre-combustion chemical looping concept. Since for the ammonia synthesis a hydrogen to nitrogen ratio of 3 is needed, the effect of the steam to air ratio of the inflowing oxidant stream on the hydrogen to nitrogen ratio of the produced gas stream during the oxidation cycle is analyzed. Also the effect of the steam oxidation kinetics on the production of a H_2/N_2-rich gas stream for the ammonia production will be analyzed.

In Chapter 6, the main conclusion obtained from the research are described for both the case that coal-derived syngas and natural gas is used as fuel for the reduction of the oxygen carrier.

Finally, the recommendations for future research concerning the further optimization of the performance for the pre-combustion chemical looping concept are described in Chapter 7.

2 Chemical Looping Combustion

2.1 Technology description

Chemical Looping Combustion has emerged as an alternative for conventional power production processes. CLC is based on the use of a metal oxide (oxygen carrier), which is sequentially oxidized in contact with air, and reduced in the presence of a reducing agent such as a fuel (see figure 2.1). Therefore, the separation of CO_2 is intrinsically integrated with the power production process by avoiding direct contact between the fuel and air.

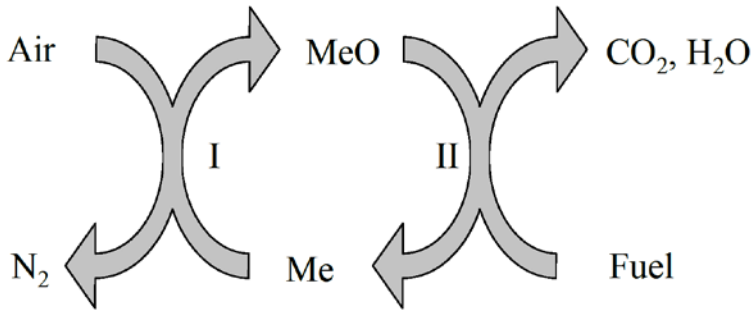

Figure 2.1 – Schematic overview of Chemical Looping Combustion.

During the reduction cycle, the metal oxide is reduced and a nitrogen-free mixture of CO_2 and H_2O is produced. Therefore, a very high purity of CO_2 can be reached after water condensation. Subsequently, the oxygen carrier is oxidized with air to its original state. The reactions involved with the CLC process are shown in equation 2.1 to 2.3, in case of coal-derived syngas as fuel, and the overall reaction is shown in equation 2.4.

$$n\,H_2 + n\,MeO \rightarrow n\,H_2O + n\,Me \quad [2.1]$$

$$m\,CO + m\,MeO \rightarrow m\,CO_2 + m\,Me \quad [2.2]$$

$$\frac{n+m}{2}O_2 + (n+m)\,Me \rightarrow (n+m)\,MeO \quad [2.3]$$

$$n\,H_2 + m\,CO + \frac{n+m}{2}O_2 \rightarrow n\,H_2O + m\,CO_2 \quad [2.4]$$

From an energy point of view, the oxidation reaction is always exothermic, so the O_2-depleted air is produced at high temperature. This hot outlet stream can be fed to a gas turbine for the production of electricity. The reduction reaction can be either exothermic or endothermic, depending both on the used oxygen carrier and the fuel type/composition. Since the CO_2 capture is integrated in the combustion step, a higher electrical efficiency of the complete plant can be achieved compared to the state-of-the-arte capture technologies.

2.2 Reactor concepts

2.2.1 Fluidized bed reactor concept

For the application of Chemical Looping Combustion several studies have been published in recent years, mainly based on a pressurized circulating fluidized bed reactor (CFBR) operated with natural gas [7-9] or sulfur-free syngas from a coal gasification unit as fuel for the CLC loop at high pressure [10,11]. In this reactor concept, the syngas is fed to the fuel reactor, where it reacts with the oxygen carrier to CO_2 and H_2O. Subsequently, the particles are transported to the air reactor (typically a riser), where hot air is produced via the oxidation of the oxygen carrier. In the end, the solids are recirculated to the fuel reactor, in which reduction of the oxygen carrier can take place again (see figure 2.2). At the reactor exits, the gas and the solids are separated by cyclones.

The favorable features for the application of fluidized beds in CLC processes are: (1) good gas-particle contact, (2) high gas throughput, allowing for compact reactors, (3) good temperature control with uniform temperature within the reactor due to vigorous particle mixing, and (4) continuous operations with time-independent temperature and composition of the product gases, which is favorable for the gas turbine downstream.

The main drawbacks of this reactor concept are related to the transport of the oxygen carrier. Not only cyclones are required in order to separate the particles from the hot air stream, but also an additional energy input is required to transport the particles. The gas solid separation is particularly difficult considering the desired operating conditions (high temperatures and pressures), and the fact that even fines from inevitable particle attrition need to be removed in order to protect the downstream gas turbine from rapid destruction.

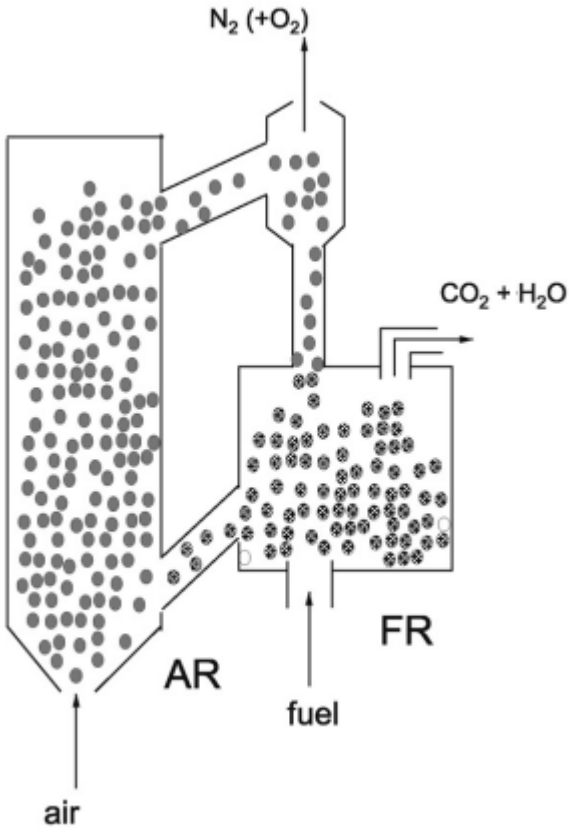

Figure 2.2 – Schematic overview of the circulating fluidized bed system.

2.2.2 Packed bed reactor concept

Since high pressure operation with interconnected fluidized bed reactors is a challenging and unproven technology, dynamically operated packed bed reactor technology for CLC has been recently proposed and studied [12-15]. With this concept, the difficulties with gas solid separations are intrinsically avoided, since the oxygen carrier particles remains stationary in the packed bed reactor, while the reactant gas feed is periodically switched.

A packed bed configuration for CLC consists of several dynamically operated reactors working in cycles. A process cycle consists of the following operating steps: oxidation, heat removal, purge and reduction. In order to have a pseudo-continuous hot gas stream entering the gas turbine(s), at least one reactor has to operate in each of the operating steps, which means that multiple dynamically operated packed bed reactors need to work in parallel.

In the first step, starting with a reduced oxygen carrier and a reactor temperature around 450-600°C, the oxygen carrier is oxidized with air (see figure 2.3). Heat is produced inside the reactor due to the highly exothermic oxidation reaction (step 1). When the complete bed is oxidized, and the heat front has reached the exit of the reactor, a hot air stream at around 1200°C is produced by feeding air at 450°C to the reactor (step 2). This hot stream of O_2-depleted air is send to a turbine for power production. The temperature of the inlet air stream to the heat removal reactor is obtained from adiabatic compression from ambient conditions to 20 bar.

After the heat is blown out of the reactor, the reactor needs to be purged with nitrogen in order to avoid direct contact between oxygen and the fuel (step 3). Then, the fuel is fed to the reactor for reducing the oxygen carrier, in which a CO_2/H_2O-rich stream is produced (step 4). This product stream is cooled down in order to obtain a high purity CO_2 stream after water condensation. Subsequently, the CO_2 stream can be compressed and sequestrated. After the reduction, the bed needs to be purged again (step 5).

Besides that the gas solid separation is intrinsically avoided, other advantages of reactor concepts based on packed bed operations are that the reactor design can be more compact, and that it allows for better utilization of the oxygen carrier. This is due to the fact that in a packed bed reactor the full oxygen capacity of the oxygen carrier is used, while in a fluidized bed reactor only part of the oxygen capacity of the oxygen carrier is used. This also means that the stability of the oxygen carrier needs to be assured over the entire oxidation range of the oxygen carrier. Nevertheless, the number of reduction/oxidation cycles that the oxygen carrier must undergo per unit of time is much smaller in the packed bed configuration, which is advantageous for the oxygen carrier lifetime.

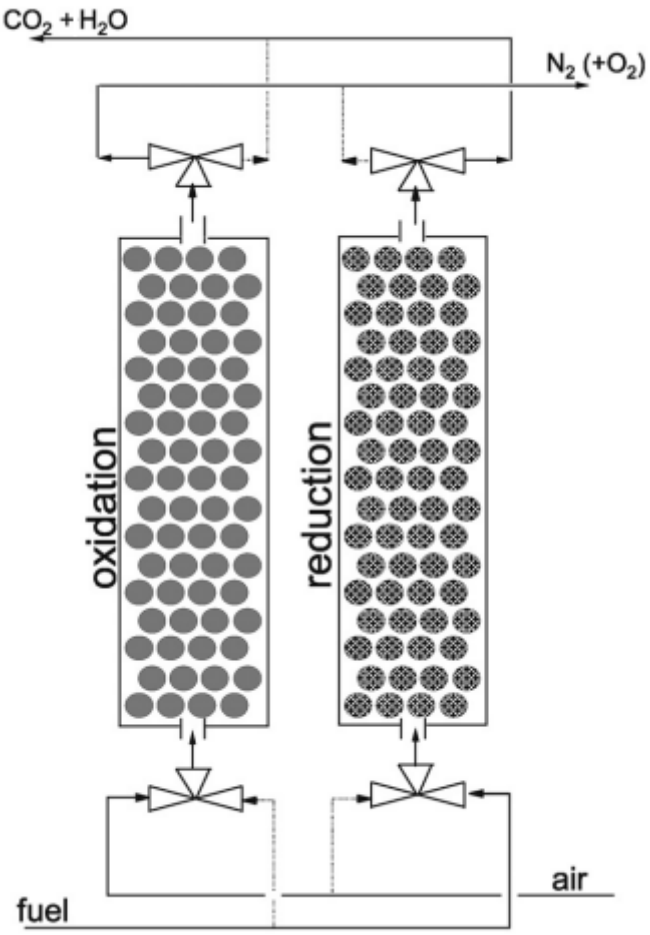

Figure 2.3 – Schematic overview of the dynamically operated packed bed reactors.

The main attention during the reduction of the oxygen carrier would be to avoid fuel slip in order to reach a high CO_2 capture efficiency, and efficient use of the fuel.

Although a high performance is expected for CLC in a packed bed reactor, this configuration requires a large number of high temperature switching valves and CLC reactors placed in parallel for a large-scale power plant. This is particularly because of the large number of reactors that is required for the heat removal phase. There is also a possibility of large temperature gradients within the reactors, meaning that heat management strategies needs to be defined in order to avoid overheating or excessive cooling of some parts of the reactor bed. Another drawback of this reactor concept is that there is a need of rather large particles in order to avoid high pressure drops, which can be disadvantageous for the mass transfer of the gaseous reactants to the particle pores.

2.2.3 Chemical looping hydrogen production

A different approach is the combination of chemical looping with the steam-iron process. With this approach, first the oxygen carrier, Fe_2O_3, is reduced to Fe/FeO in a fuel reactor. Subsequently, the oxygen carrier is oxidized to Fe_3O_4 by reaction with steam in the steam reactor. During this steam oxidation a pure stream of H_2 can be produced after steam condensation. The last step is the full oxidation of Fe_3O_4 to Fe_2O_3 with air. The integration of the steam-iron process with chemical looping for power and hydrogen co-production has been discussed by several authors for coal-derived syngas [16-19], natural gas [20-21], and solid fuels [22-24] as reducing agents.

The reactor loop is based on two counter-current moving bed reactors for respectively the fuel and steam reactors (see figure 2.4), allowing for higher oxygen carrier conversions compared to fluidized bed reactors, while achieving complete fuel conversion. The oxidation of Fe_3O_4 to Fe_2O_3 by air takes place in the air reactor (typically a riser), where a hot O_2-depleted air stream is produced. A similar reactor concept for the production of hydrogen is the combination of the chemical looping concept with the steam-iron process by using dynamically operated packed bed reactors instead of the moving bed reactors [25-26].

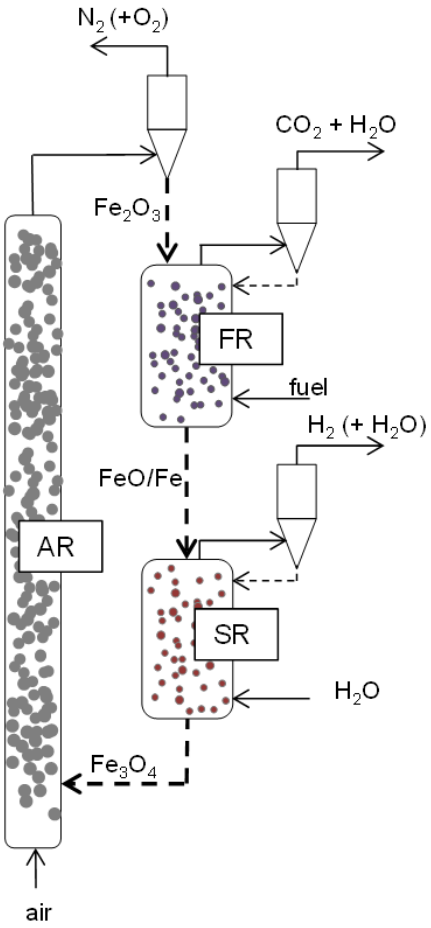

Figure 2.4 – Schematic overview of the reactor design for chemical looping hydrogen production using moving beds.

2.2.4 Pre-combustion chemical looping (PCCL)

A novel reactor concept for the production of a hydrogen rich gas stream for power or ammonia production is based on the pre-combustion chemical looping technology using dynamically operated packed bed reactors. Compared to the previous discussed concepts, the oxidation of the oxygen carrier with steam and air occurs simultaneously, producing a product stream containing N_2, H_2 and unreacted H_2O (see figure 2.5). After water condensation, a product stream of nitrogen and hydrogen can be obtained, which can be used as feedstock for e.g. the ammonia production process. During the reduction cycle, a gaseous fuel is directly converted into a nitrogen-free mixture of CO_2 and H_2O, and a pure CO_2 stream can be obtained after water condensation.

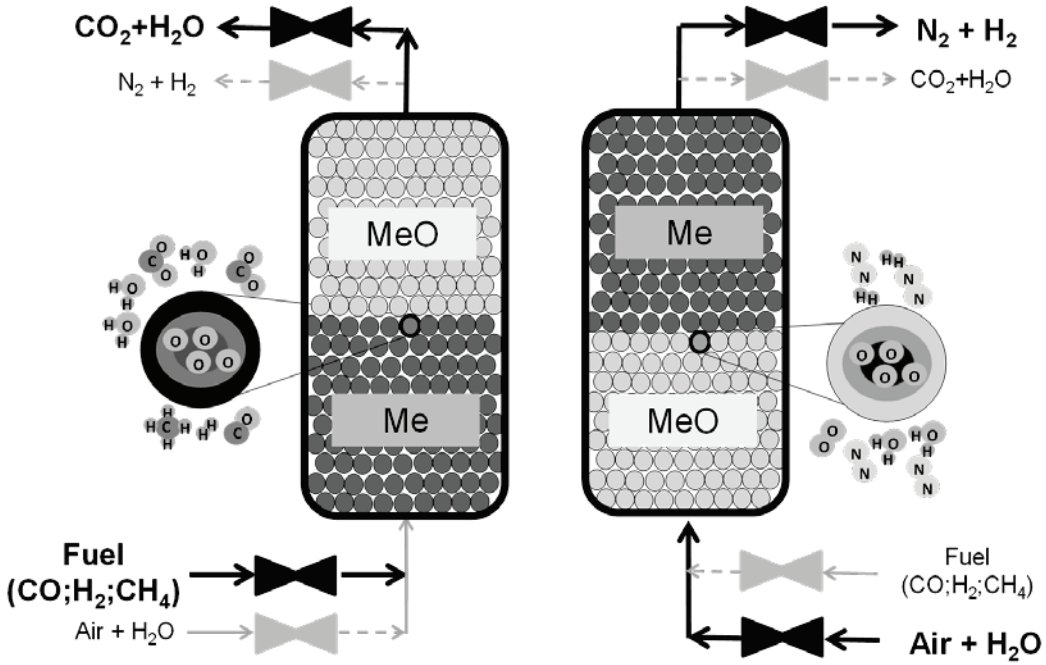

Figure 2.5 – Schematic overview of the reactor design for pre-combustion chemical looping (PCCL) technology.

Due to the partial oxidation of the oxygen carrier by steam, there will be a smaller temperature rise within the bed in comparison with the packed bed reactor configuration where the oxygen carrier is oxidized by only oxygen (air). Therefore, this process can be carried out at elevated pressures, but at intermediate temperature (in the range of 600-900°C), which means that challenging components such as HT-switching valves and piping are not required in the PCCL concept. Since the overall heat of reaction is lower, the number of reactors needed for heat removal phase can be decreased.

This concept has a strong process intensification, since this process includes the primary fuel combustion, the inherent CO_2 separation, and the production of a H_2/N_2-rich stream, which can be used for power of ammonia production, in a single reactor loop.

3 Reactor model for PCCL

3.1. Reduction cycle

It is generally established that the reduction of hematite (Fe_2O_3) to metallic iron (Fe) follows either a two or three step reaction sequence. The reduction of hematite to metallic iron is always through magnetite (Fe_3O_4), and depending on the reaction conditions also through wüstite (FeO). Whether the two or three step reaction sequence occurs depends on the reaction temperature. If there is a rich hydrogen or carbon monoxide atmosphere, the reduction of Fe_3O_4 directly to metallic iron takes place at temperatures lower than 570˚C, while at temperatures higher than 570˚C, FeO will be the intermediate stable compound during the reduction of Fe_3O_4 to metallic iron.

The reduction of Fe_2O_3 to Fe_3O_4 will always give a full conversion of the reducing agents, which means that hydrogen and carbon monoxide will be fully converted to steam and carbon dioxide. Unfortunately, the reduction reactions of magnetite and wüstite with hydrogen and carbon monoxide will not obtain a full conversion of the reducing agents, due to thermodynamic constraints. This also means that the reverse reactions, oxidation with steam and carbon dioxide, are possible for this equilibrium reactions when there is a rich steam or carbon dioxide atmosphere. All possible reduction reactions by hydrogen and carbon monoxide can be found in equation 3.1-3.8, and a graphical overview, including the boundary conditions, can be found in Figure 3.1.

$$3\,Fe_2O_3 + H_2 \rightarrow 2\,Fe_3O_4 + H_2O \qquad [3.1]$$

$$\frac{1}{4}\,Fe_3O_4 + H_2 \leftrightarrow \frac{3}{4}\,Fe + H_2O \qquad T < 570°C \qquad [3.2]$$

$$Fe_3O_4 + H_2 \leftrightarrow 3\,FeO + H_2O \qquad T > 570°C \qquad [3.3]$$

$$FeO + H_2 \leftrightarrow Fe + H_2O \qquad T > 570°C \qquad [3.4]$$

$$3\,Fe_2O_3 + CO \rightarrow 2\,Fe_3O_4 + CO_2 \qquad [3.5]$$

$$\frac{1}{4}\,Fe_3O_4 + CO \leftrightarrow \frac{3}{4}\,Fe + CO_2 \qquad T < 570°C \qquad [3.6]$$

$$Fe_3O_4 + CO \leftrightarrow 3\,FeO + CO_2 \qquad T > 570°C \qquad [3.7]$$

$$FeO + CO \leftrightarrow Fe + CO_2 \qquad T > 570°C \qquad [3.8]$$

For example, Figure 3.1B shows that at temperatures higher than 570˚C, the reduction of Fe_3O_4 to FeO takes place when the steam to hydrogen ratio is smaller than the equilibrium constant for Fe_3O_4/FeO, and the subsequent reduction of FeO to Fe takes place when the steam to hydrogen ratio is also smaller than the equilibrium constant for FeO/Fe.

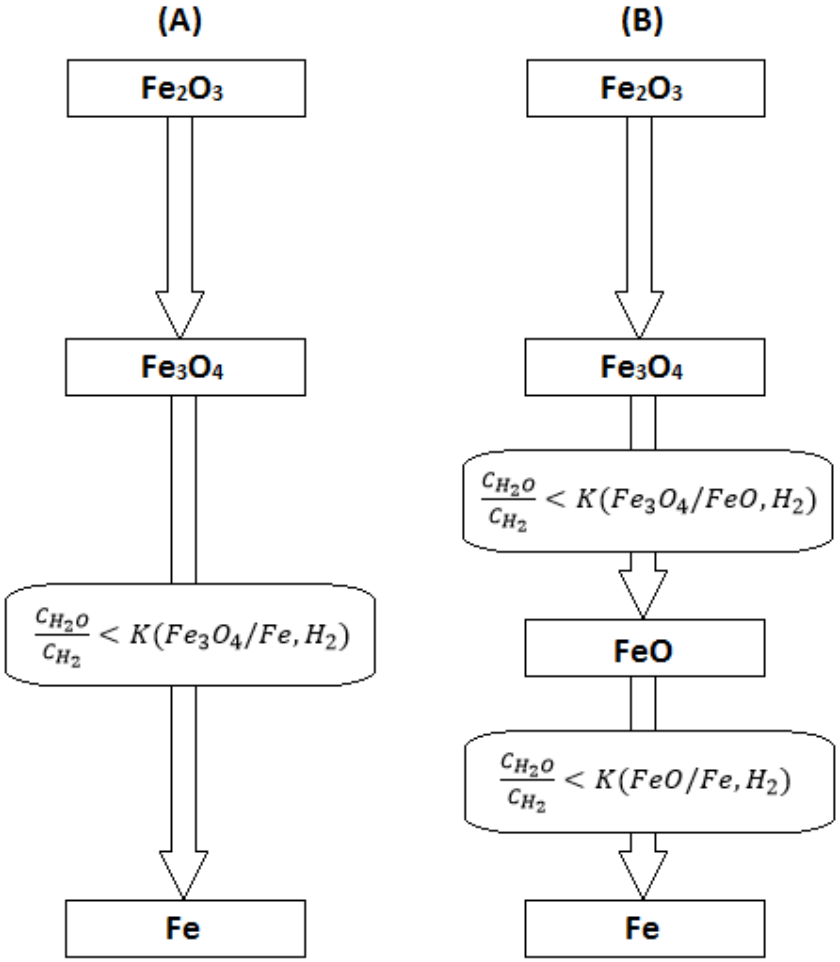

Figure 3.1 – Schematic overview of the reduction reactions by hydrogen for: (A) T < 570˚C, and (B) T > 570˚C.

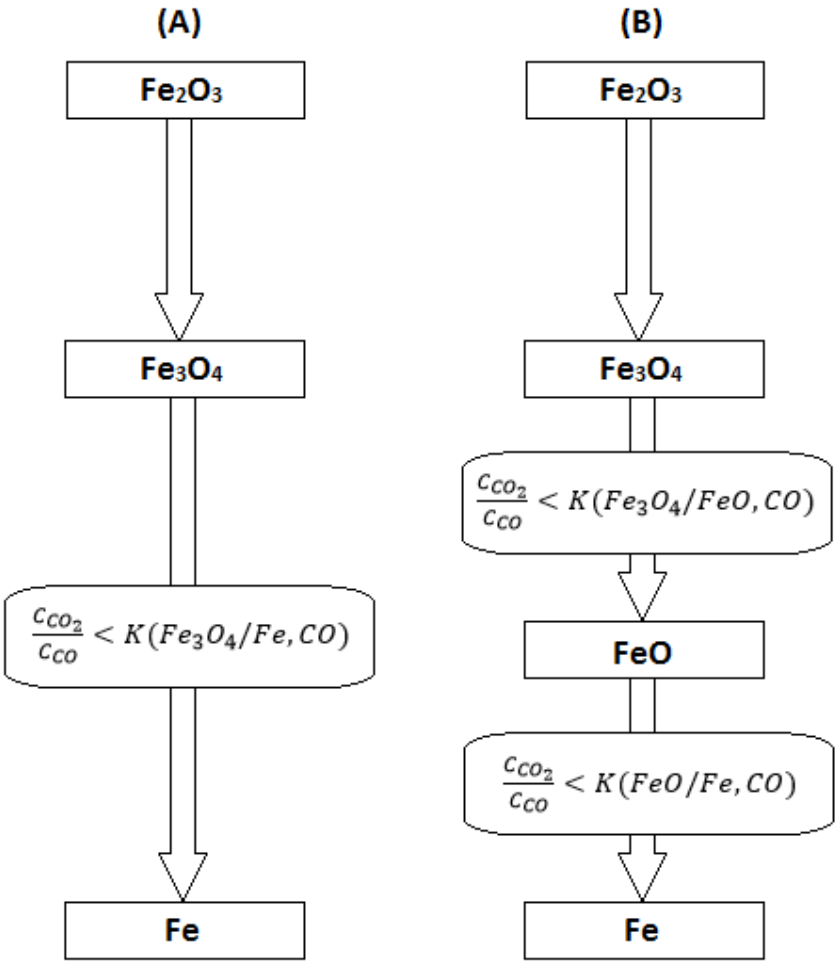

Figure 3.2 – Schematic overview of the reduction reactions by carbon monoxide for: (A) T < 570˚C, and (B) T > 570˚C.

3.1.1 Equilibrium constant

The equilibrium constant describes the solid phase equilibrium lines as a function of the gas composition. The equilibrium constant is also a function of the temperature. Expressions for the equilibrium constants were already described by several authors [27-28]. An overview of the expressions suggested by Coetsee et al. and Valipour et al. is shown in Table 3.1, and a graphical representation of the equilibrium constants in a hydrogen/steam and a carbon monoxide/carbon dioxide environment as a function of the temperature are shown in respectively Figure 3.3 and 3.4.

From the graphical representations of the equilibrium constants in Figure 3.3 and 3.4 can be seen that at high temperatures the equilibrium constant for Fe_3O_4/FeO from Valipour et al. is much higher than that of Coetsee et al., and even has a value twice as high at 1250 K. Figure 3.4 clearly shows that for the equilibrium lines suggested by Coetsee et al. there is a disconnection of the equilibrium lines at the transition temperature (843 K) for FeO formation.

Due to this inconsistencies, new equilibrium constant expressions are derived in this work by using HSC Chemistry software. This software calculates the equilibrium concentrations of steam and hydrogen (or carbon dioxide and carbon monoxide) at each temperature. The equilibrium constant can be obtained from dividing either the equilibrium concentration of H_2O by H_2, or CO_2 by CO. The obtained expressions for the equilibrium constants are shown in Table 3.2, and a graphical representation of the equilibrium lines (including the equilibrium lines from Coetsee et al. and Valipour et al.) are shown in Figure 3.5 and 3.6.

Table 3.1 – Overview of equilibrium constant expressions from literature

Reaction	**Expression for equilibrium constant**	
	Coetsee et al. [27]	*Valipour et al. [28]*
$Fe_3O_4 + H_2 \leftrightarrow 3\ FeO + H_2O$	$10^{(2.2523 - 2034.4/T)}$	$e^{(8.46 - 7916.6/T)}$
$FeO + H_2 \leftrightarrow Fe + H_2O$	$10^{(0.4404 - 806.56/T)}$	$e^{(0.9317 - 1586.9/T)}$
$0.25\ Fe_3O_4 + H_2 \leftrightarrow 0.75\ Fe + H_2O$	$10^{(1.7157 - 1706.95/T)}$	-
$Fe_3O_4 + CO \leftrightarrow 3\ FeO + CO_2$	$10^{(0.6601 - 270.33/T)}$	$e^{(4.58 - 3585.64/T)}$
$FeO + CO \leftrightarrow Fe + CO_2$	$10^{(-1.2239 + 1031.9/T)}$	$e^{(-2.946 + 2744.63/T)}$
$0.25\ Fe_3O_4 + CO \leftrightarrow 0.75\ Fe + CO_2$	$10^{(-0.3653 + 412.2/T)}$	-

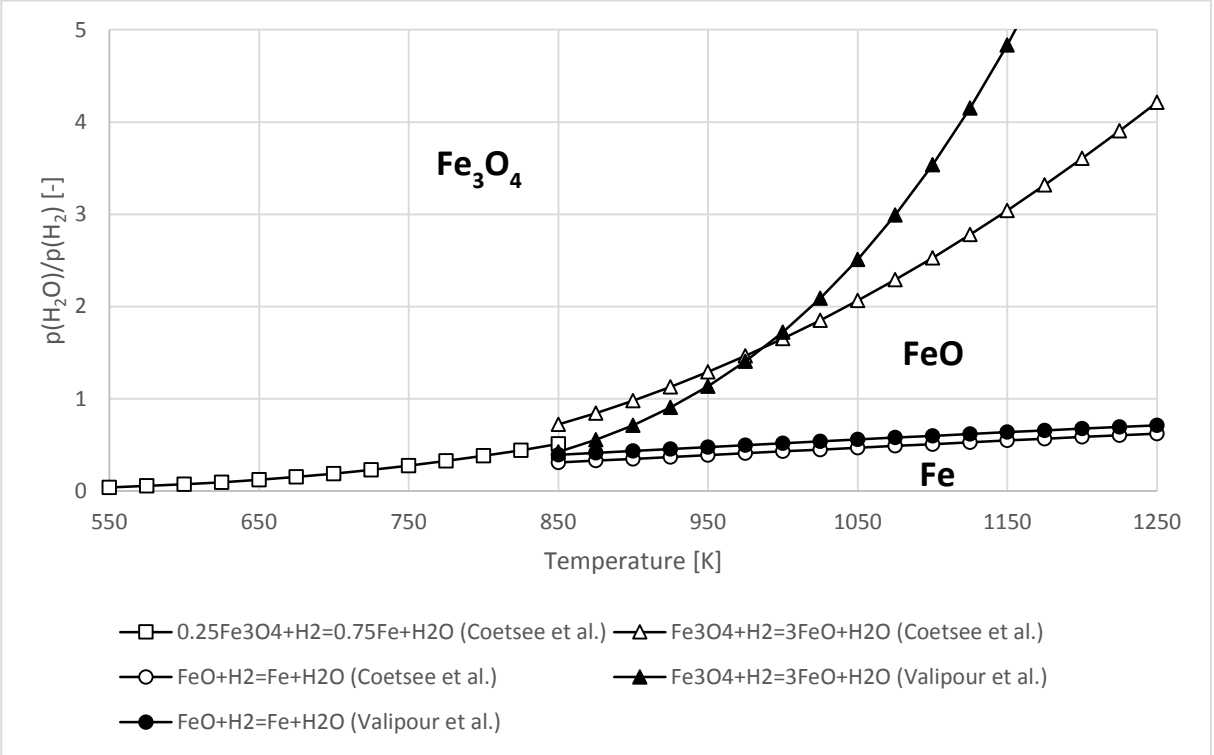

Figure 3.3 – Equilibrium constants from literature in a hydrogen/steam environment as a function of the temperature

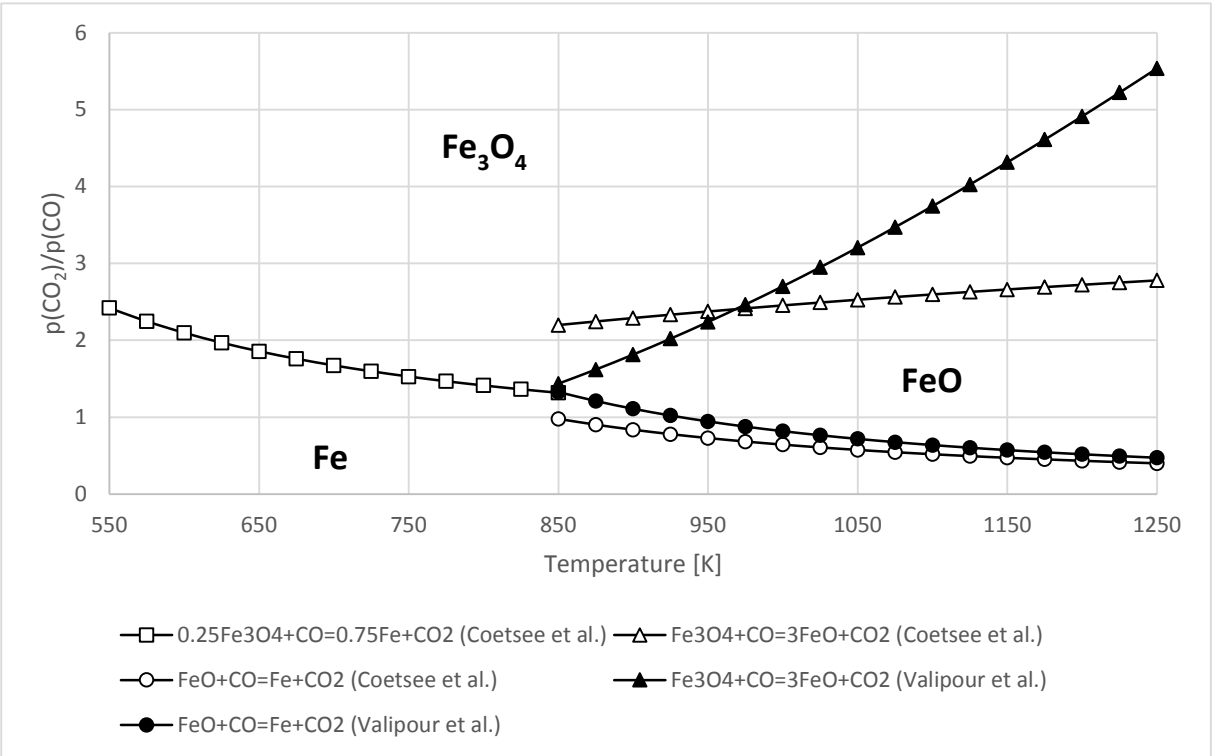

Figure 3.4 – Equilibrium constants from literature in a carbon monoxide/carbon dioxide environment as a function of the temperature

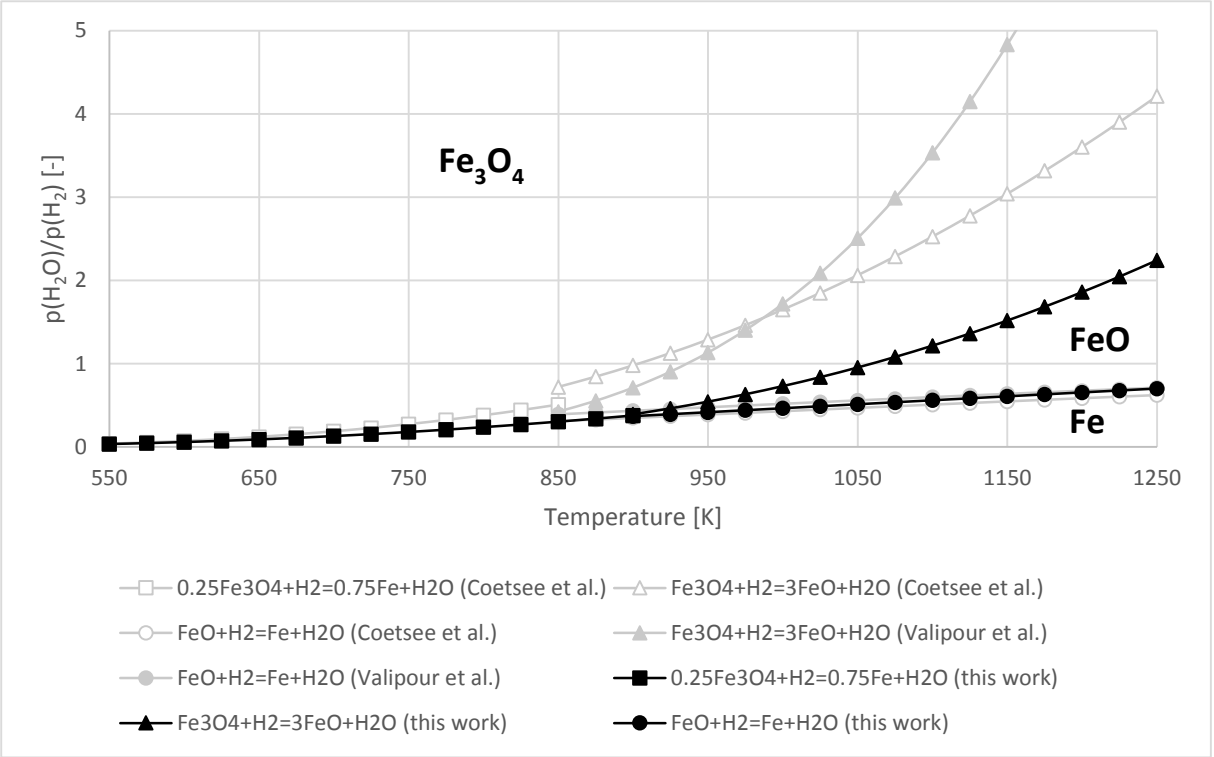

Figure 3.5 - Equilibrium constants derived from HSC in a hydrogen/steam environment as a function of the temperature

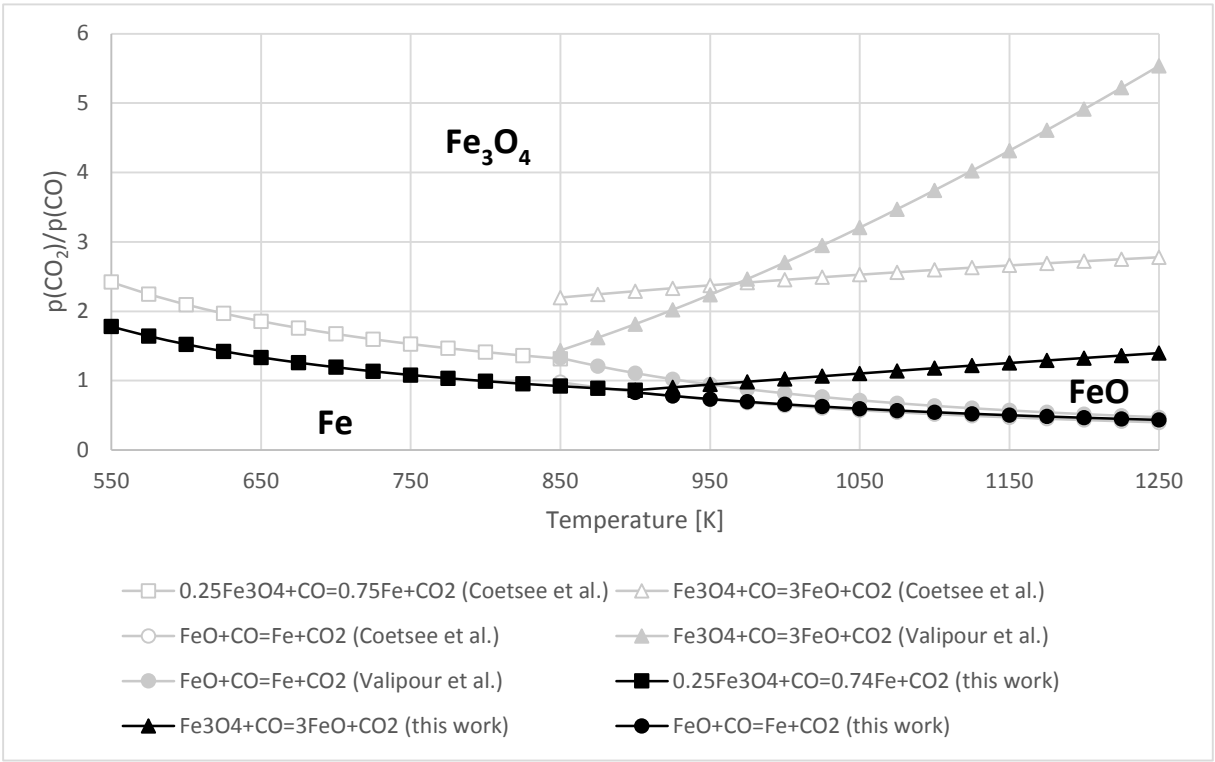

Figure 3.6 - Equilibrium constants derived from HSC in a carbon monoxide/carbon dioxide environment as a function of the temperature

Table 3.2 – Overview of equilibrium constant expressions derived in this work

Reaction	Expression for equilibrium constant
$Fe_3O_4 + H_2 \leftrightarrow 3\ FeO + H_2O$	$10^{(2.2523 - 2034.4/T)}$
$FeO + H_2 \leftrightarrow Fe + H_2O$	$10^{(0.4404 - 806.56/T)}$
$0.25\ Fe_3O_4 + H_2 \leftrightarrow 0.75\ Fe + H_2O$	$10^{(1.7157 - 1706.95/T)}$
$Fe_3O_4 + CO \leftrightarrow 3\ FeO + CO_2$	$10^{(0.6601 - 270.33/T)}$
$FeO + CO \leftrightarrow Fe + CO_2$	$10^{(-1.2239 + 1031.9/T)}$
$0.25\ Fe_3O_4 + CO \leftrightarrow 0.75\ Fe + CO_2$	$10^{(-0.3653 + 412.2/T)}$

Figure 3.5 shows that the equilibrium lines for Fe_3O_4/Fe and FeO/Fe in a steam/hydrogen atmosphere as suggested by Coetsee et al. and Valipour et al. have a good fit with the obtained results from equilibrium analysis with the HSC Chemistry Software. Unfortunately, the equilibrium lines for Fe_3O_4/FeO as suggested by Coetsee et al. and Valipour et al. have significantly higher values for the equilibrium constant than the equilibrium line that are obtained from equilibrium analysis with the HSC Chemistry Software.

Figure 3.6 shows that the equilibrium lines for FeO/Fe in a carbon dioxide/carbon monoxide atmosphere as suggested by Coetsee et al. and Valipour et al. also have a good fit with the obtained results from equilibrium analysis with the HSC Chemistry Software. The equilibrium lines for Fe_3O_4/Fe and Fe_3O_4/FeO as suggested by Coetsee et al. and Valipour et al. are significantly higher than the equilibrium lines that are obtained from equilibrium analysis with the HSC Chemistry Software.

The meaning of this lower values for the equilibrium constant is that at equilibrium the concentration of the reducing agent is higher. For example for the reduction of Fe_3O_4 to FeO by hydrogen: when the equilibrium constant is lower, the steam to hydrogen ratio at equilibrium is also lower, which means that the hydrogen concentration is relatively high. This higher concentration of H_2 at equilibrium leads to a lower hydrogen conversion when the hydrogen excess is not used for other reactions, like the reduction of Fe_2O_3 to Fe_3O_4, which gives a full conversion of hydrogen.

The results from equilibrium analysis with HSC also clearly shows a triple point at 900 K (627˚C) for both steam/hydrogen and carbon dioxide/carbon monoxide atmosphere. Above this temperature, FeO is formed as a stable intermediate during the reduction of Fe_3O_4 to metallic iron. This triple point is significantly higher than 570˚C as described by Coetsee et al.

Assumed for this research is that equilibrium constant expressions obtained with HSC can be used for describing the ratio of steam to hydrogen and carbon dioxide to carbon monoxide at equilibrium.

3.1.2 Reduction pathways

According to Patrick et al. [29], the sequence for particles composed by Fe_2O_3 and Al_2O_3 is Fe_2O_3-Fe_3O_4-$FeAl_2O_4$-Fe. $FeAl_2O_4$ is a spinel named hercynite, which can be seen as a combination of FeO and Al_2O_3. Thermodynamic calculations show that $FeAl_2O_4$ is formed as a stable compound at H_2O/H_2 ratios ranging from 0.01 to 365 000 at 950˚C, which is the only stable compound. Therefore, the reduction of Fe_2O_3 to $FeAl_2O_4$ results in a full conversion of hydrogen and carbon monoxide conversion to steam and carbon dioxide. This means that the bed is completely reduced to $FeAl_2O_4$ at the moment of hydrogen and carbon monoxide breakthrough.

The complete reduction of Fe_2O_3 to $FeAl_2O_4$ is an improvement on the used oxygen capacity of the bed in comparison with reduction of Fe_2O_3 in the absence of Al_2O_3. In the latter case, the bed is only partially reduced to FeO, at the moment of hydrogen and carbon monoxide breakthrough, while the rest of the bed is only reduced to Fe_3O_4. The part of the bed that is not reduced to FeO is dependent on the equilibrium constant, since this determines the excess of hydrogen and carbon monoxide during the equilibrium reaction of Fe_3O_4 to FeO. The excess of hydrogen and carbon monoxide is used for the reduction of Fe_2O_3 to Fe_3O_4 further on in the reactor. Therefore the excess of hydrogen and carbon monoxide determines how fast the bed is reduced to Fe_3O_4, and the hydrogen/carbon monoxide breakthrough takes place.

The spinel $FeAl_2O_4$ is formed out of FeO and Al_2O_3 with a molar ratio of one. When the molar ratio of FeO to Al_2O_3 is lower than one, there is an excess of Al_2O_3, which means that all Fe_2O_3 can be reduced to $FeAl_2O_4$ (Figure 3.7A). But when the molar ratio of FeO to Al_2O_3 is higher than one, there is not enough Al_2O_3 for reducing all Fe_2O_3 to $FeAl_2O_4$, which is the case when the weight fraction Fe_2O_3 is higher than 0.439. When the weight fraction Fe_2O_3 is higher than 0.439, the Fe in excess remains as Fe_3O_4. At steam to hydrogen or carbon dioxide to carbon monoxide ratios higher than the equilibrium constant for reduction of Fe_3O_4 to Fe, the final products for the reduction of Fe_2O_3 are $FeAl_2O_4$ and Fe_3O_4 (Figure 3.7B). When the steam to hydrogen or carbon dioxide to carbon monoxide ratio is smaller than the equilibrium constant for reduction of Fe_3O_4 to Fe, the final products for the reduction of Fe_2O_3 are $FeAl_2O_4$ and Fe (Figure 3.7C).

In this research, only particles composed of Fe_2O_3 and Al_2O_3 with weight fraction Fe_2O_3 lower than 0.439 are considered. Therefore, the reduction of Fe_3O_4 to Fe that occurs at weight fractions Fe_2O_3 of 0.439 and higher, and the corresponding equilibrium constant, were beyond the scope of this research. This means that the reduction of Fe_2O_3 to $FeAl_2O_4$ by hydrogen and carbon monoxide will always follow pathway A from Figure 3.7. The reaction equations for these reduction reactions can be found in equation 3.9 and 3.10.

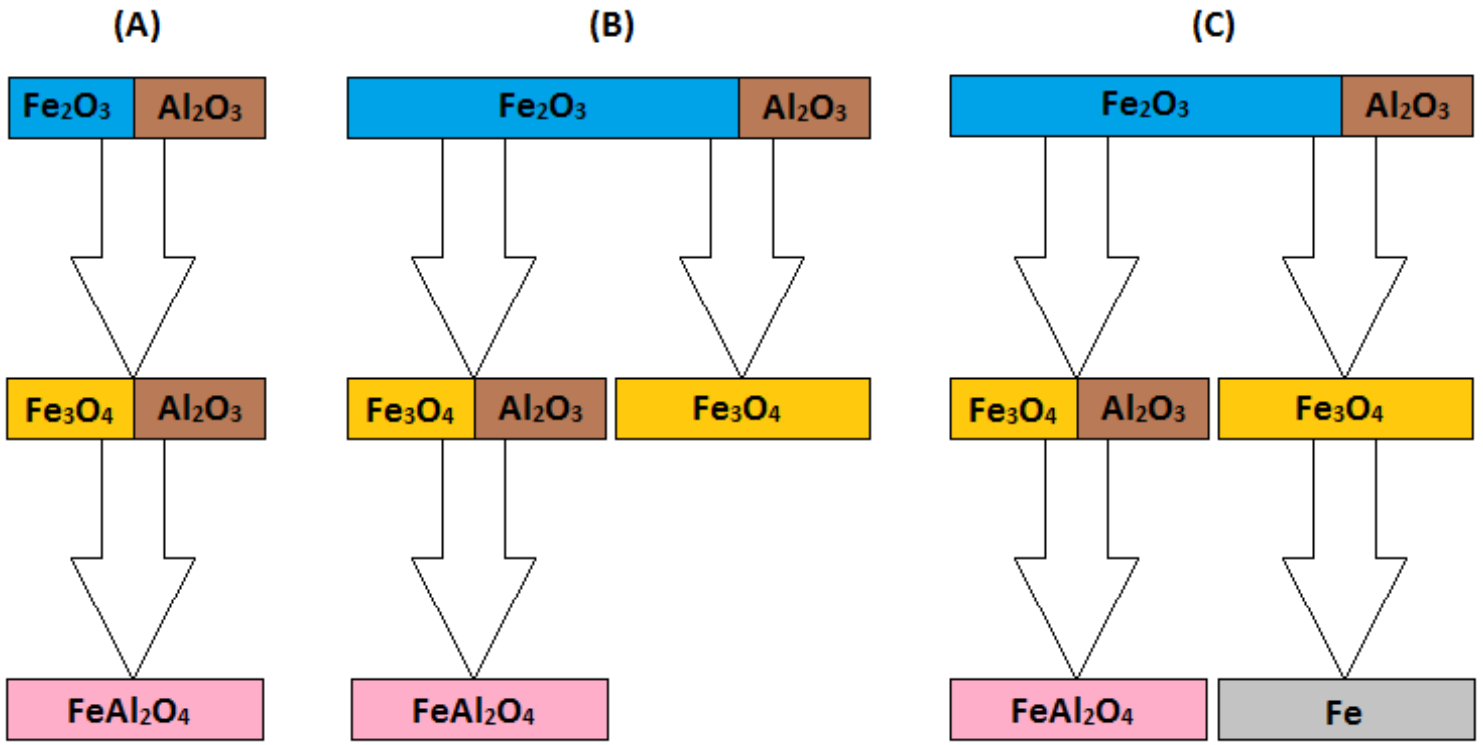

Figure 3.7 – pathways for reduction of particles composed of Fe_2O_3 and Al_2O_3: (A) w(Fe_2O_3) < 0.439, (B) w(Fe_2O_3) > 0.439 and ratio H_2O (or CO_2) to H_2 (or CO) > equilibrium constant for reduction of Fe_3O_4 to Fe, and (C) w(Fe_2O_3) > 0.439 and ratio H_2O (or CO_2) to H_2 (or CO) < equilibrium constant for reduction of Fe_3O_4 to Fe.

$$Fe_2O_3 + 2\,Al_2O_3 + H_2 \rightarrow 2\,FeAl_2O_4 + H_2O \quad [3.9]$$

$$Fe_2O_3 + 2\,Al_2O_3 + CO \rightarrow 2\,FeAl_2O_4 + CO_2 \quad [3.10]$$

In all experiments performed by Abad et al. [30], subsequent oxidation with oxygen showed complete regeneration of the oxygen carrier to Fe_2O_3, which means that $FeAl_2O_4$ is an active phase during both reduction and oxidation cycles.

According to Abad et al. [30], the expression for the reaction rate (r) of the reduction of Fe_2O_3 to $FeAl_2O_4$ by hydrogen and carbon monoxide, assuming chemical reaction control in the grain, can be described by the following equation:

$$r = \frac{3(1-\varepsilon)}{r_g} k_R C_{g,i}^n \quad \left[\frac{mol_i}{m_R^3 s}\right] \quad [3.11]$$

In which ε is the porosity, defined by the product of the bed porosity and solid porosity ($\varepsilon = \varepsilon_{bed}\varepsilon_s$), r_g is the grain radius, defined by the BET-surface area and the solid density, $C_{g,i}$ is the concentration of either carbon monoxide or hydrogen, and n is the reaction order. The grain radius and the bed porosity were assumed to be respectively 0.26 µm and 0.6. The solid porosity is not constant throughout the reactor, and changes due to oxygen transfer during reduction and oxidation. For the equations for calculating the solid porosity during reduction and oxidation, the reader is referred to Appendix A.

The reaction rate constants (k_R) were assumed to follow Arrhenius-type temperature dependences:

$$k_R = k_0 exp(-E_a/RT) \quad \left[\frac{mol_i^{1-n} m^{3n-2}}{s}\right] \quad [3.12]$$

In which k_0 is the pre-exponential factor, and E_a is the activation energy. An overview of the kinetic parameters for these reduction reactions is given in Table 3.3.

Table 3.3 – Kinetic parameters for the reduction of Fe_2O_3 to $FeAl_2O_4$ by hydrogen and carbon monoxide

	H_2	***CO***
$\boldsymbol{k_0\ [mol_i^{1-n} m^{3n-2} s^{-1}]}$	9.0 x 10^{-4}	2.5 x 10^{-4}
$\boldsymbol{E_a\ [kJ\ mol^{-1}]}$	24	20
$\boldsymbol{n\ [-]}$	0.8	1.0

3.1.3 Methane reforming

Methane is one of the main components of natural gas. There are two possible pathways for the reduction of Fe_2O_3 by methane, namely by methane steam reforming or by methane dry reforming. Both reforming reactions are equilibrium reactions. Expressions for the equilibrium constant of both reforming reactions are determined from equilibrium analysis with HSC Chemistry Software, and can be described by the following equation for respectively methane steam reforming and methane dry reforming:

$$K_{SR} = 10266.76 \times 10^6 \exp(-26830/T + 30.11) \qquad [Pa^2] \qquad [3.13]$$

$$K_{DR} = 5.17 \times 10^{-8} \exp(8700/T) \qquad \left[\frac{1}{Pa}\right] \qquad [3.14]$$

During methane steam reforming, carbon monoxide and hydrogen are produced, while steam is used for the reforming of methane:

$$CH_4 + H_2O \leftrightarrow CO + 3\,H_2 \qquad [3.15]$$

Combining this equation with equation 3.9 and 3.10 for the reduction of Fe_2O_3 to $FeAl_2O_4$ by respectively hydrogen and carbon monoxide, the following equation for the overall reduction of Fe_2O_3 to $FeAl_2O_4$ by methane via methane steam reforming can be obtained:

$$4\,Fe_2O_3 + 8\,Al_2O_3 + CH_4 \rightarrow 8\,FeAl_2O_4 + 2\,H_2O + CO_2 \qquad [3.16]$$

The reduction of Fe_2O_3 to $AlFe_2O_4$ is not an equilibrium reactions, which means that there will be a full conversion of hydrogen and carbon monoxide. Since both hydrogen and carbon monoxide are products during the methane steam reforming, the equilibrium for the methane steam reforming will be shifted towards the product side.

Carbon monoxide and hydrogen are also the products during methane dry reforming when carbon dioxide is used for the reforming of methane, only the molar ratio of the reaction products is different, as can be seen from the following equation:

$$CH_4 + CO_2 \leftrightarrow 2\,CO + 2\,H_2 \qquad [3.17]$$

Combining this equation with equation 3.9 and 3.10 for the reduction of Fe_2O_3 to $FeAl_2O_4$ by respectively hydrogen and carbon monoxide, the following equation for the overall reduction of Fe_2O_3 to $FeAl_2O_4$ by methane via methane dry reforming can be obtained:

$$4\,Fe_2O_3 + 8\,Al_2O_3 + CH_4 \rightarrow 8\,FeAl_2O_4 + H_2O + 2\,CO_2 \qquad [3.18]$$

The overall reduction of Fe_2O_3 to $FeAl_2O_4$ by methane via methane dry reforming will also give a full conversion of hydrogen and carbon monoxide. The only difference between the methane steam reforming and methane dry reforming is the molar ratio of produced steam to carbon dioxide. The higher molar ratio of carbon dioxide to steam produced during methane dry reforming is more favorable from a carbon capture efficiency point of view, which is the amount of carbon dioxide over the total amount of gasses after water condensation, since the amount of other gasses like N_2 and Ar that leave the reactor will not change.

Since the reduction of Fe_2O_3 to $FeAl_2O_4$ by methane consist out of two sequential steps, namely the steam or dry methane reforming, and the reduction of Fe_2O_3 to $FeAl_2O_4$ by hydrogen and carbon monoxide, the reaction rate of the overall reduction depends on the reaction with the slowest kinetics. Therefore, also the reaction kinetics for the both steam and dry methane reforming are needed for determining the overall reaction rate of the reduction of Fe_2O_3 to $FeAl_2O_4$ by methane.

The expression of the reaction rate (r) for methane steam reforming and methane dry reforming are given in equation 3.19 and 3.20. These rate expressions were developed by Abashar et al. [31] for methane reforming over a Nickel catalyst. Assumed is that Fe_2O_3/Al_2O_3 and $Ni/MgAl_2O_4$ will have similar catalytic behavior for the reforming of methane, which needs to be verified experimentally. It is also possible to add some Nickel to the solid in order to enhance the methane reforming reactions.

$$r_{SR} = \rho_s w_{cat} \frac{\frac{k_{R,SR}}{P_{H_2}^{2.5}}\left(P_{CH_4}P_{H_2O} - \frac{P_{H_2}^3 P_{CO}}{K_{SR}}\right)}{\left(1 + K_{CH_4}P_{CH_4} + K_{H_2}P_{H_2} + K_{CO}P_{CO} + \frac{K_{H_2O}P_{H_2O}}{P_{H_2}}\right)^2} \qquad \left[\frac{mol_{CH_4}}{m_R^3\, s}\right] \qquad [3.19]$$

$$r_{DR} = \rho_s w_{cat} \frac{k_{R,SR1}k_{R,SR2}K_{DR}P_{CH_4}P_{CO_2}}{k_{R,SR1}K_{DR}P_{CH_4}P_{CO_2} + k_{R,SR1}P_{CH_4} + k_{R,SR2}K_{DR}P_{CO_2}} \qquad \left[\frac{mol_{CH_4}}{m_R^3\, s}\right] \qquad [3.20]$$

The adsorption constants for the gaseous components can be described by the following equations:

$$K_{ad,CH_4} = 6.65 \times 10^{-9} \exp(4604.28/T) \qquad \left[\frac{1}{Pa}\right] \qquad [3.21]$$

$$K_{ad,H_2} = 6.12 \times 10^{-14} \exp(9971.13/T) \qquad \left[\frac{1}{Pa}\right] \qquad [3.22]$$

$$K_{ad,CO} = 8.23 \times 10^{-10} \exp(8497.71/T) \qquad \left[\frac{1}{Pa}\right] \qquad [3.23]$$

$$K_{ad,H_2O} = 1.77 \times 10^{5} \exp(-10666.35/T) \qquad [-] \qquad [3.24]$$

The reaction rate constants ($k_{R,SR}$, $k_{R,DR1}$ and $k_{R,DR2}$) follow the Arrhenius-type temperature dependences, and can be described by the following equations:

$$k_{R,SR} = 8.336 \times 10^{17} \exp(-240100/RT) \qquad \left[\frac{mol\ Pa^{0.5}}{kg\ s}\right] \qquad [3.25]$$

$$k_{R,DR1} = 2.61 \times 10^{-3} \exp(-35750/RT) \qquad \left[\frac{mol}{kg\ s\ Pa}\right] \qquad [3.26]$$

$$k_{R,DR2} = 5.35 \times 10^{2} \exp(-62355/RT) \qquad \left[\frac{mol}{kg\ s}\right] \qquad [3.27]$$

The solid bulk density is the total mass of the solids per cubic meter of reactor, and can be calculated with the following equation:

$$\rho_s = \varepsilon_{bed}\varepsilon_s / \left(\sum \frac{w_i}{\rho_i}\right) \qquad \left[\frac{kg_s}{m_R^3}\right] \qquad [3.28]$$

At temperatures higher than 600˚C, the reaction rate for methane steam reforming is much higher than that of methane dry reforming. This means that the equilibrium for methane steam reforming is reached faster than that of methane dry reforming, and the ratio of produced hydrogen to produced carbon monoxide will be around 3 (see equation 3.3). The reaction rate for the reduction of Fe_2O_3 to $FeAl_2O_4$ by hydrogen is one order of magnitude higher than the reaction rate for the methane steam reforming at temperatures between 600-1000˚C. The reaction rate for the reduction of Fe_2O_3 to $FeAl_2O_4$ by carbon monoxide is of the same order of magnitude as the methane steam reforming. Since hydrogen is converted to steam faster than carbon monoxide is converted to carbon dioxide, additional hydrogen is produced via the water gas shift (section 3.1.5). Overall, this means that, the reaction front for the reduction of Fe_2O_3 to $FeAl_2O_4$ will be always faster than that of methane steam reforming, and the equilibrium for methane steam reforming will be shifted to the product side. Finally, this also means that there will not be a breakthrough of methane before total reduction of the bed.

3.1.4 Water gas shift

The water gas shift is an equilibrium reaction between carbon monoxide and steam on the one side, and carbon dioxide and hydrogen on the other side:

$$CO + H_2O \leftrightarrow H_2 + CO_2 \quad [3.29]$$

The reaction rate for the water gas shift can be described by the following equation:

$$r_{SR} = \rho_s w_{cat} \frac{\frac{k_{R,WGS}}{P_{H_2}}\left(P_{CO}P_{H_2O} - \frac{P_{H_2}P_{CO_2}}{K_{WGS}}\right)}{\left(1 + K_{CH_4}P_{CH_4} + K_{H_2}P_{H_2} + K_{CO}P_{CO} + \frac{K_{H_2O}P_{H_2O}}{P_{H_2}}\right)^2} \quad \left[\frac{mol_{CO}}{m_R^3\, s}\right] \quad [3.30]$$

The reaction rate constants ($k_{R,WGS}$) follows the Arrhenius-type temperature dependences, and can be described by equation 3.31. The kinetic parameters for the reaction rate constant are taken from Abashar et al. [31].

$$k_{R,DR1} = 12.19 \exp(-67130/RT) \quad \left[\frac{mol}{kg\, s\, Pa}\right] \quad [3.31]$$

Since the water gas shift reaction is an equilibrium reaction, also an expression for the equilibrium constant is needed, which can be described by the following equation.

$$K_{WGS} = \exp\,(4400/T - 4.063) \quad [-] \quad [3.32]$$

3.1.5 Carbon deposition

Carbon deposition always needs to be avoided, since this will lead to poisoning of the oxygen carrier. Also the presence of carbon during the oxidation cycle will result in the production of carbon dioxide, which decreases the CO_2 capture efficiency. Carbon deposition can take place due to the methane decomposition reaction, the Boudouard reaction and the heterogeneous water-gas reaction, as described by respectively equation 3.33 to 3.35.

$$CH_4 \leftrightarrow C + 2\,H_2 \quad [3.33]$$

$$2\,CO \leftrightarrow C + CO_2 \quad [3.34]$$

$$CO + H_2 \leftrightarrow C + H_2O \quad [3.35]$$

Metallic iron is a catalyst for the carbon deposition reactions, and therefore the formation of metallic iron needs to be avoided. Therefore, the weight fraction Fe_2O_3 was always below 0.429 during this research. This means that all Fe_2O_3 can be reduced to $FeAl_2O_4$, and the formation of metallic iron is avoided.

3.2 Oxidation cycle

3.2.1 Temperature rise

Oxidation reactions with oxygen are highly exothermic, as can be seen from the enthalpy of reaction in Figure B3 and B4 from Appendix B. Therefore, a high temperature rise within the bed will take place. The maximum temperature rise within the reactor can be derived from the overall energy balance over the packed bed. In order to derive the energy balance, first information about the front velocities within the bed is needed. Figure 3.8 shows a schematic representation of the anticipated concentration profiles of the gaseous reactant (oxygen) and the temperature evolution is depicted. Here, an ideal system is considered in which the rate at which the non-catalytic gas-solid reaction proceeds is infinitely high, and where axial conduction and dispersion effects can be neglected. Also, assumed is that there are no heat and mass transfer limitations between the gas and solid phase and that the system can be considered as pseudo-homogeneous.

Initially, assumed is that the solid material is fully reduced, the gas present in the bed is non-reactive and the entire system is at uniform initial temperature (T_0). The system is fed with a reactive gas flow, also at temperature T_0. As a consequence of the gas-solid reaction, a reaction front propagates through the bed with velocity w_1. Due to the reaction heat, the temperature of the bed changes, and the same reaction front can be observed in the temperature profile. Along with the reaction front, a heat front propagates through the bed as a consequence of the temperature difference between the bed and the incoming gas flow. The velocity at which this heat front moves is referred to as w_2.

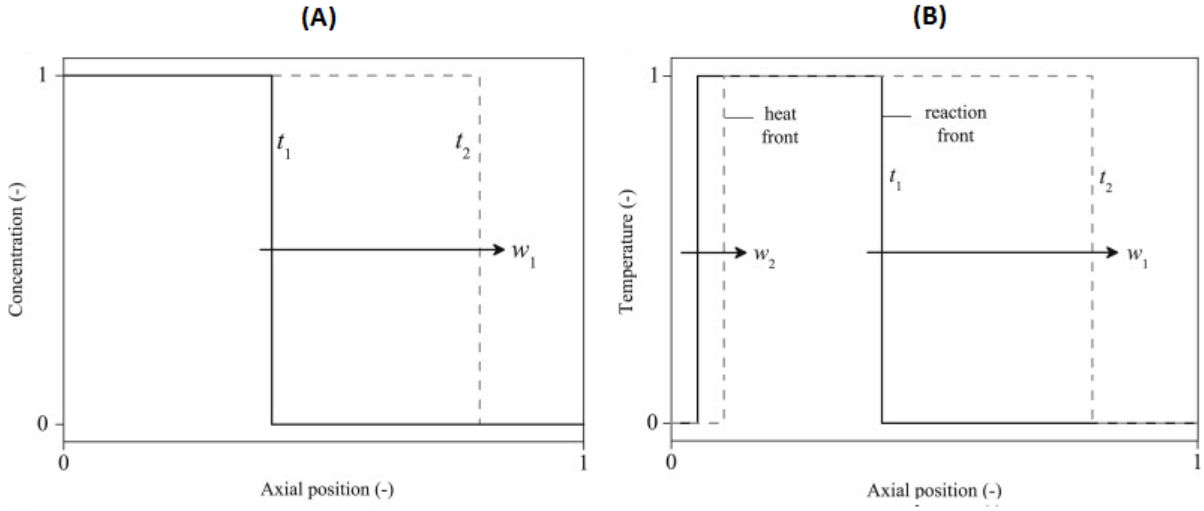

Figure 3.8 – schematic representation of the evolution of: (A) the dimensionless axial concentration profile of the gaseous reactant, and (B) the axial dimensionless temperature profiles in a packed bed CLC reactor.

Considering the temperature profiles depicted in Figure 3.8, neglecting the volumetric heat capacity of the gas phase relative to the solid phase, and assuming that the reaction front propagates more rapidly through the bed than the heat front, an overall simplified energy balance can be formulated for the system:

$$\frac{\rho_g v_g w_{g,i}^{in}}{M_{g,i}}\left(-\Delta H_{R,i}\right) = \varepsilon_s \rho_s C_{p,s}(w_1 - w_2)(T_1 - T_0) \quad [3.36]$$

Therefore, the expected maximum temperature change in the packed bed reactor is given by:

$$\Delta T = (T_1 - T_0) = \frac{\rho_g v_g w_{g,i}^{in}(-\Delta H_{R,i})}{\varepsilon_s \rho_s C_{p,s} M_{g,i}(w_1 - w_2)} \quad [3.37]$$

Assuming that at the heat front the heat present in the solid material is transferred to the gas phase, and at the reaction front all the gaseous reactant fed reacts with a known, stoichiometric amount of the solid material, expressions for respectively the reaction front velocity and heat front velocity are obtained:

$$w_1 = \frac{\rho_g v_g w_{g,i}^{in} M_{act}}{\varepsilon_s \rho_s w_{act}^0 M_{g,i} \zeta} \quad [3.38]$$

$$w_2 = \frac{\rho_g v_g C_{p,g}}{\varepsilon_s \rho_s C_{p,s}} \quad [3.39]$$

ζ denotes the stoichiometric ratio of number of moles of gas and solid material needed in the reaction, ω_{act}^0 denotes the weight content of the active solid material in the oxygen carrier at the initial state, and M_{act} is the molecular weight of the initially present active material. By combining equation 3.37 to 3.39, the temperature change in a packed bed reactor can be expressed by the following equation:

$$\Delta T = \frac{\left(-\Delta H_{R,i}\right)}{\frac{C_{p,s} M_{act}}{w_{act}^0 \zeta} - \frac{C_{p,g} M_{g,i}}{w_{g,i}^{in}}} \quad [3.40]$$

From this equation for the temperature change in a packed bed reactor can be seen that maximum temperature increase due to an oxidation reaction is independent of the gas flow rate. This is very important in relation to the reactor's flexibility to changes in production capacity. The maximum temperature is only influenced by the properties of the gas phase and the solid material, as long as the reaction front propagates faster through the reactor than the heat. If the difference in front velocities is small, no temperature plateau is produced, but rather a moving temperature peak. When the oxidation reaction is very fast, there is almost no influence of the reaction kinetics on the maximum temperature change. Therefore, a possible decrease in the activity of the oxygen carrier will not directly affect the temperature increase obtained in the bed. For the reduction cycle, the same derivation and conclusions are also valid.

3.2.2 Oxidation pathways

The reaction kinetics for the oxidation with oxygen are fast. Therefore, the formation of the intermediate oxidation states (FeO and Fe_3O_4) can be neglected, and the final oxidation state (Fe_2O_3) is formed directly. The reaction equations for the oxidation reactions by oxygen can be described by equation 3.41 to 3.43, and a schematic overview of all possible oxidation reactions by oxygen can be found in Figure 3.9.

$$\frac{4}{3}\,Fe + O_2 \rightarrow \frac{2}{3}\,Fe_2O_3 \qquad [3.41]$$

$$4\,FeO + O_2 \rightarrow 2\,Fe_2O_3 \qquad [3.42]$$

$$4\,Fe_3O_4 + O_2 \rightarrow 6\,Fe_2O_3 \qquad [3.43]$$

Another purpose of the oxidation cycle is the production of hydrogen, which can be produced via the steam-iron process. The oxidation by steam is the reverse reaction of the reduction by hydrogen. Since the reduction of Fe_2O_3 to Fe_3O_4 by hydrogen is not an equilibrium reaction, the oxidation of Fe_3O_4 to Fe_2O_3 is not possible. Therefore, Fe_3O_4 is the highest possible oxidation state during oxidation by steam for an iron-based oxygen carrier. Whether the reduction by hydrogen or the oxidation by steam takes place is dependent on the equilibrium constant of the reaction. When the ratio steam to hydrogen is higher than the equilibrium constant, the oxidation reaction by steam will take place. Normally during the oxidation cycle, a mixture of steam and air is fed to the reactor, which means that the ratio steam to hydrogen is infinitely high at the reactor inlet. Therefore, the oxidation by steam will always take place.

The oxidation of metallic iron by steam follows either a one-step or two-step reaction pathway, depending on the temperature. Since FeO is only stable at temperatures higher than 570˚C, the one-step pathway will take place at temperatures lower than 570˚C, and the two-step pathway will take place at temperatures higher than 570˚C. Therefore, the reaction equations for the oxidation reactions by steam can be described by equation 3.44-3.46. A schematic overview of all possible oxidation reactions by steam can be found in Figure 3.10.

$$\frac{3}{4}Fe + H_2O \leftrightarrow \frac{1}{4}\,Fe_3O_4 + H_2 \qquad T < 570°C \qquad [3.44]$$

$$Fe + H_2O \leftrightarrow FeO + H_2 \qquad T > 570°C \qquad [3.45]$$

$$3\,FeO + H_2O \leftrightarrow Fe_3O_4 + H_2 \qquad T > 570°C \qquad [3.46]$$

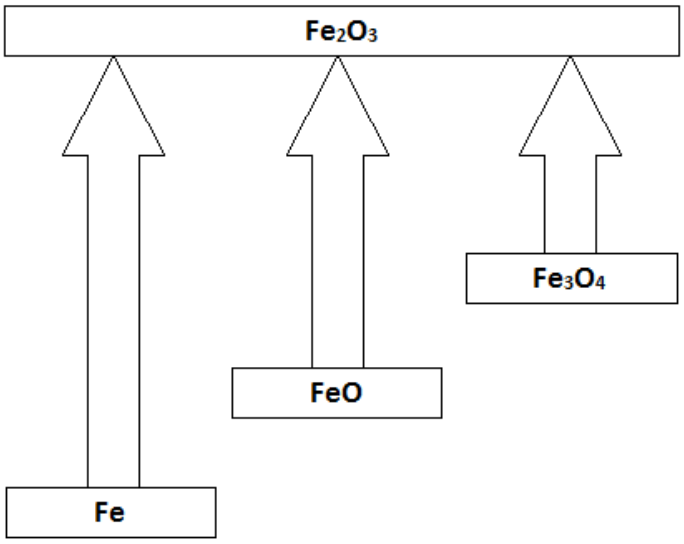

Figure 3.9 – overview of oxidation reaction by oxygen

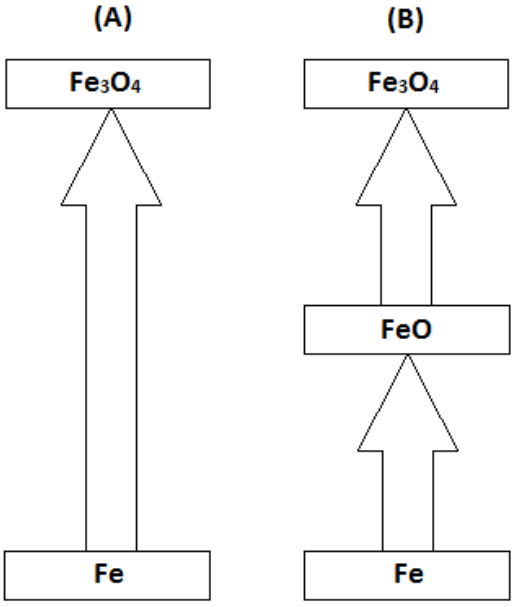

Figure 3.10 – overview of oxidation (equilibrium) reactions by steam at temperatures:
(A) lower than 570˚C, and (B) higher than 570˚C.

During reduction, the bed is fully reduced to $FeAl_2O_4$, when the weight fraction Fe_2O_3 is below 0.429. Assumed is that the spinel $FeAl_2O_4$ behaves like a combination of FeO and Al_2O_3. Since there is no reduction to metallic iron, the oxidation reactions of metallic iron by both oxygen and steam will not take place. Therefore, only two possible reaction pathways for the oxidation of $FeAl_2O_4$ to Fe_2O_3 are possible: (1) the oxidation of $FeAl_2O_4$ to Fe_2O_3 by oxygen, and (2) the oxidation of $FeAl_2O_4$ to Fe_3O_4 by steam with the sequential oxidation of Fe_3O_4 to Fe_2O_3 by oxygen. An overview of these two oxidation pathways can be found in Figure 3.11.

Therefore, the reaction equations for these oxidation pathways can be found in equation 3.47 to 3.49.

$$3\ FeAl_2O_4 + H_2O \leftrightarrow Fe_3O_4 + 3\ Al_2O_3 + H_2 \quad [3.47]$$

$$4\ FeAl_2O_4 + O_2 \rightarrow 2\ Fe_2O_3 + 4\ Al_2O_3 \quad [3.48]$$

$$4\ Fe_3O_4 + O_2 \rightarrow 6\ Fe_2O_3 \quad [3.49]$$

The oxidation of $FeAl_2O_4$ to Fe_3O_4 by steam is an equilibrium reaction, which means that the equilibrium constant needs to be included in the reaction rate expressions. For the equilibrium constant for this oxidation reaction is assumed that $FeAl_2O_4$ behaves like a mixture of FeO and Al_2O_3. Therefore, the expression for the equilibrium constant from Table 3.2 for the equilibrium between FeO and Fe_3O_4 in a H_2O/H_2 atmosphere can be used.

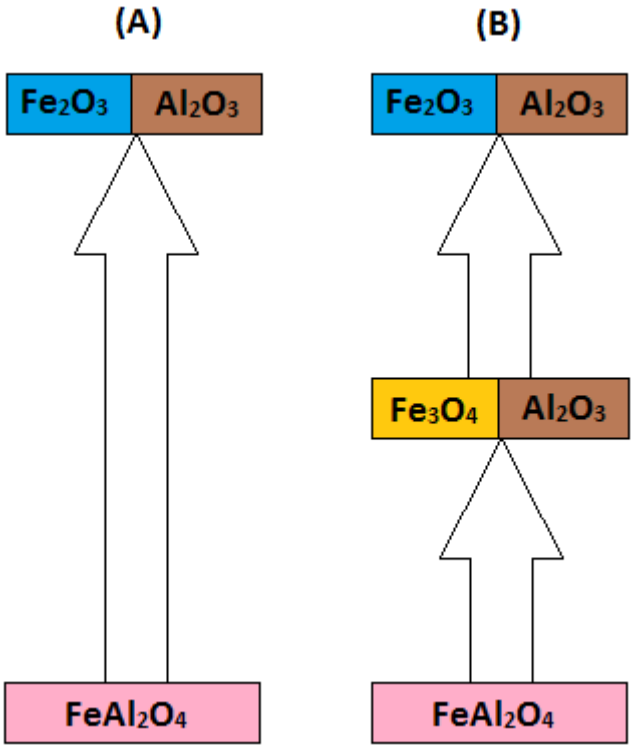

Figure 3.11 – overview of the possible oxidation pathways: (A) The oxidation of $FeAl_2O_4$ to Fe_2O_3 by oxygen, and (B) the oxidation of $FeAl_2O_3$ to Fe_3O_4 by steam with the sequential oxidation of Fe_3O_4 to Fe_2O_3 by oxygen.

For the oxidation of $FeAl_2O_4$ to Fe_3O_4 by steam, the reaction rate equation as suggested by Coetsee et al. [27] can be described by the following equation:

$$r = (1-\varepsilon)k_R M_{v,FeO}\left(C_{H_2O} - C_{H_2O}^{eq}\right) \qquad \left[\frac{mol_{H_2O}}{m_R^3\, s}\right] \qquad [3.50]$$

In which ε is the porosity, k_R is the reaction rate constant, $M_{v,FeO}$ is the mass of FeO per pellet volume, and $C_{H_2O}^{eq}$ is the equilibrium concentration of steam. The reaction rate constant follows the Arrhenius-type temperature dependence. The kinetic parameters for the steam oxidation of $FeAl_2O_4$ to Fe_3O_4 are taken from Coetsee et al. [27], and are shown Table 3.4.

It is assumed that $FeAl_2O_4$ behaves like ilmenite ($FeTiO_3$) during the oxidation with oxygen. Therefore, for the oxidation of $FeAl_2O_4$ to Fe_2O_3 by oxygen, the reaction rate, as suggested by Spallina et al. [32], can be described by the following equation:

$$r = (1-\varepsilon)k_R \frac{M_{v,FeO}}{M_{FeO}} \frac{3b}{\rho_m r_g} C_{O_2} \qquad \left[\frac{mol_{O_2}}{m_R^3\, s}\right] \qquad [3.51]$$

In which $M_{v,FeO}$ is the molecular weight of FeO, b is the stoichiometric factor of the reaction, ρ_m is the molar solid density, and r_g is the grain radius (0.26 μm). The kinetic parameters for the oxidation of $FeAl_2O_4$ to Fe_2O_3 by oxygen are taken from Abad et al. [30], and are shown in Table 3.4.

For the oxidation of Fe_3O_4 to Fe_2O_3 by oxygen, the reaction rate, as suggested by Monsen et al. [33], can be described by the following expression:

$$r = (1-\varepsilon)k_R C_{O_2} \qquad \left[\frac{mol_{O_2}}{m_R^3\, s}\right] \qquad [3.52]$$

The kinetic parameters for the oxidation of Fe_3O_4 to Fe_2O_3 by oxygen are taken from Monsen et al. [33], and are also shown in Table 3.4

Table 3.4 – Kinetic parameters for the oxidation of $FeAl_2O_4$ to Fe_3O_4 by steam.

	k_o	E_a
$\mathbf{3\ FeAl_2O_4 + H_2O \leftrightarrow Fe_3O_4 + 3\ Al_2O_3 + H_2}$	133 m^3/kg s	54 kJ/mol
$\mathbf{4\ FeAl_2O_4 + O_2 \rightarrow 2\ Fe_2O_3 + 4\ Al_2O_3}$	1.9 x 10^{-3} m/s	25.5 kJ/mol
$\mathbf{4\ Fe_3O_4 + O_2 \rightarrow 6\ Fe_2O_3}$	1.0 x 10^{-4} 1/s	51 kJ/mol

3.3 Packed bed reactor model

In order to study the complete process consisting of multiple oxidation/reduction cycles, a numerical model was developed by Noorman et al. [34], based on a 1D adiabatic packed bed reactor model. This model is developed with Borland® Delphi™ software, within Twente University.

The component mass balances for the gas phase can be described by:

$$\varepsilon_g \rho_g \frac{\partial \omega_{i,g}}{\partial t} = -\rho_g v_g \frac{\partial \omega_{i,g}}{\partial x} + \frac{\partial}{\partial x}\left(\rho_g D_{ax,eff} \frac{\partial \omega_{i,g}}{\partial x}\right) + \varepsilon_s r_i M_i \quad [3.53]$$

In which the axial mass dispersion (Edwards and Richardson, 1968) is:

$$D_{ax} = \left(\frac{0.73}{ReSc} + \frac{0.5}{\varepsilon_g + \frac{9.7\varepsilon_g^2}{ReSc}}\right) v_g d_p \quad [3.54]$$

The component mass balances for the solid phase can be described by:

$$\varepsilon_s \rho_s \frac{\partial \omega_{s,j}}{\partial t} = \varepsilon_g r_j M_j \quad [3.55]$$

The energy balance (gas and solid phase) can be described by:

$$\left(\varepsilon_g \rho_g C_{p,g} + \varepsilon_s \rho_s C_{p,s}\right)\frac{\partial T}{\partial t} = -\rho_s v_g C_{p,g} \frac{\partial T}{\partial x} + \frac{\partial}{\partial x}\left(\lambda_{ax} \frac{\partial T}{\partial x}\right) + \varepsilon_g r_i \Delta H_{R,i} \quad [3.56]$$

In which the effective axial heat dispersion (Vortmeyer and Berninger, 1982) is:

$$\lambda_{ax} = \lambda_{bed,0} + \frac{RePr\lambda_g}{Pe_{ax}} + \frac{Re^2 Pr^2 \lambda_g}{6(1-\varepsilon_g)Nu} \quad [3.57]$$

With the equation for the Nusselt number (Gunn, 1978) of:

$$Nu = \left(7 - 10\varepsilon_g + 5\varepsilon_g^2\right)\left(1 + 0.7Re^{0.2}Pr^{1/3}\right) + \left(1.33 - 2.4\varepsilon_g + 1.2\varepsilon_g^2\right)Re^{0.7}Pr^{1/3} \quad [3.58]$$

And the equation for the heat Péclet axial number (Gunn and Misbah, 1993) of:

$$Pe_{ax} = \frac{2\left(0.17 + 0.33 exp\left[-\frac{24}{Re}\right]\right)}{1 - \left(0.17 + 0.33 exp\left[-\frac{24}{Re}\right]\right)} \quad [3.59]$$

Expressions for the heat of reactions and the solid heat capacities can be found in respectively Table B1 and B2 of Appendix B.

Finally, the momentum balance can be described by the Ergun equation:

$$-\frac{dp}{dx} = 150 \frac{\eta_g v_g}{d_p^2} \frac{(1-\varepsilon_g)^2}{\varepsilon_g^3} + 1.75 \frac{\eta_g v_g^2}{d_p} \frac{(1-\varepsilon_g)}{\varepsilon_g^3} \quad [3.60]$$

4 Results and discussion: coal-derived syngas

The performance of the PCCL concept concerning the power production and the co-production of a H_2/N_2-rich stream for the production of ammonia will be discussed and optimized in this chapter for the case that coal-derived syngas is used as fuel.

Heat is stored within the reactor due to the highly exothermic oxidation reactions by oxygen. This heat can be removed from the reactor either after the oxidation or the reduction cycle. Therefore, two heat management strategies are possible.

First the results will be shown and discussed for the first heat management strategy, in which the heat is removed from the reactor after the oxidation cycle. For this case, the effect of the active weight fraction of the oxygen carrier on the power production by the gas turbine and the corresponding turbine efficiency will be analyzed. For the active weight fraction of oxygen carrier with the highest power production by the gas turbine, the effect of the heat removal flowrate on the power production will be determined in order to optimize the power production. Finally, the performance of the PCCL concept from this heat management strategy is further optimized by decreasing the cycle time in order to increase the mole fraction of hydrogen in the outflowing oxidant stream. Since the kinetics for the steam oxidation are not validated yet, the effect of the steam oxidation kinetics on the power production will be determined by decreasing the reaction rate constant for steam oxidation. Finally, the possibility of producing a H_2/N_2-rich gas stream for the production of ammonia is discussed for this heat management strategy.

For the second heat management strategy, in which the heat is removed from the reaction after the reduction cycle, also the effect of the active weight fraction of the oxygen carrier on the power production will be determined and the performance will be compared to that of the first heat management strategy. Also the possibility for producing a H_2/N_2-rich stream for the production of ammonia will be discussed for this heat management strategy, and will be compared to that of the first heat management strategy.

4.1 Heat management strategy 1

During the reduction cycle, the oxygen carrier is reduced with coal-derived syngas. The syngas obtained from the gasification of coal, is a mixture of H_2, H_2O, CO and CO_2. The inlet conditions of the fuel entering the reactor during the reduction cycle are given in Table 4.1.

The oxygen carrier is oxidized with a mixture of steam and air during the oxidation cycle. As described in section 3.2, hydrogen is produced only via pathway B by the oxidation of $FeAl_2O_4$ to Fe_3O_4 by steam. In order to maximize the hydrogen production, the oxygen to steam ratio of the oxidant inlet stream should not be too high. When the oxygen to steam ratio fed to the reactor is higher than the oxygen to steam ratio needed for the oxidation of Fe_3O_4 to Fe_2O_3 by oxygen and the oxidation of $FeAl_2O_4$ to Fe_3O_4 by steam, there will be an excess of oxygen. Therefore, part of the $FeAl_2O_4$ is directly oxidized to Fe_2O_3 by oxygen via pathway A, and the amount of hydrogen that can be produced decreases. Since the oxidation of $FeAl_2O_4$ to Fe_3O_4 by steam is an equilibrium reaction, there will always be an equilibrium between steam and hydrogen throughout the reactor, which means that part of the steam fed to the reactor will not be converted to hydrogen. This steam excess is dependent on the temperature, and therefore the exact oxygen to steam ratio needed for the oxidation cycle in order to only have oxidation of the oxygen carrier via pathway B is hard to predict. When the oxygen to steam ratio is smaller than this value, the reaction front for the oxidation of $FeAl_2O_4$ to Fe_3O_4 by steam will be faster than the reaction front for the oxidation of Fe_3O_4 to Fe_2O_3 by oxygen. Therefore, the two reaction fronts for oxidation by steam and oxygen are separated, and the direct oxidation of $FeAl_2O_4$ by oxygen is avoided, and the hydrogen production is maximized. The inlet conditions for the oxidant stream, as suggested in the thesis of Fabio Arienti [35], will be used for modelling the oxidation cycle, and are given in Table 4.1.

Heat is removed from the reactor during the heat removal cycle, with a gas stream of 700°C. This temperature of the heat removal gas stream is needed in order to have sufficient fast kinetics of the reduction and oxidation reactions in the subsequent reduction and oxidation cycle. In order to obtain a gas stream of 700°C, part of the produced hydrogen during the oxidation cycle is combusted with oxygen from an adiabatic compressed air stream at 440°C and 20.5 bar. During the combustion of hydrogen with oxygen, steam is formed, and therefore the gas stream entering the heat removal cycle will consist out of N_2, O_2 and H_2O. The inlet composition of the gas stream needed for the heat removal cycle is calculated with Aspen Plus, and is given in Table 4.1.

Table 4.1 – Inlet condition for the reduction, oxidation, heat removal and purge cycle

		Reduction	Oxidation	Heat Removal	Purge
Mole fraction [mol_i/mol_g]	**Ar**	0.010	0.0044	0.0088	-
	CO	0.336	-	-	-
	CO_2	0.341	0.0001	0.0003	-
	H_2	0.137	-	-	-
	H_2O	0.164	0.5217	0.0588	-
	N_2	0.012	0.3738	0.7561	1.0
	O_2	-	0.1000	0.1760	-
Temperature [˚C]		517.0	447.2	700.0	397.5
Pressure [bar]		20.5	20.5	20.5	20.5
Flowrate [$kg/m^2/s$]		1.0	0.73	-	0.10

4.1.1 Coal-derived syngas power plant integrated with the PCCL process

In order to have a pseudo-continuous hot gas stream entering the gas turbine, at least one reactor has to operate in each of the operating steps, which means that multiple dynamically operated packed bed reactors need to work in parallel. The cycle time of each operating step needs to be the same, unless several reactors are operated in parallel for one operating step.

A flowsheet of the pre-combustion chemical looping concept for power production for pseudo-continuous operation is made with Aspen Plus. For the Aspen Plus model, the solids are not taken into account, since during one oxidation/reduction cycle the oxygen carrier is first reduced from Fe_2O_3 to $FeAl_2O_4$ during the reduction cycle, and sequentially oxidized back to Fe_2O_3 during the oxidation cycle. For the oxidation by steam, steam is split into hydrogen and oxygen by water-splitting. Therefore, the overall reaction can be seen as:

$$n\,H_2 + m\,CO + \left(\frac{n+m}{2}\right)(1-x)\,O_2 \;+\; (n+m)x\,H_2O \rightarrow n\,H_2O + m\,CO_2 + \;(n+m)x\,H_2 \qquad [4.1]$$

The flowsheet of the pre-combustion chemical looping concept for power production is shown in Figure 4.1, and can be described by the following steps:

1) Air compression

The air needed for both the oxidation and heat removal cycle is adiabatically compressed from ambient conditions to pressure of 20.5 bar and a temperature of 440˚C. An isentropic compressor is used for the Aspen model with an isentropic efficiency of 0.92, and a mechanical efficiency of 0.995.

2) Oxidation reactor

Part of the compressed air steam is mixed with a steam stream, in order to obtain a steam/air mixture with the desired mole fraction of oxygen, and is fed to the oxidation reactor. The oxidation reactor is modeled by four sequential steps: (1) separator for the separation of oxygen from the inflowing gas stream, (2) stoichiometric reactor for the water-splitting reaction, (3) separator for the separation of the produced oxygen from the gas stream exiting the water-splitting reactor, and (4) heater for heating the outflowing gas stream. Since the oxidation by steam is an equilibrium reactor, not all steam will be converted to hydrogen and oxygen. This steam excess determines the conversion of the water-splitting reaction. The outflowing gas stream consists out of nitrogen, hydrogen and steam. The heater for heating the outflowing gas stream is needed since there will be a temperature difference between the gas streams entering and exiting the reactor.

3) Reduction reactor

Coal-derived syngas from the coal-gasification unit is fed to a Gibbs reactor. In the Gibbs reactor, the hydrogen and carbon monoxide is fully converted to steam and carbon monoxide. This outflowing gas stream is also heated by a heater, since there will be a temperature difference between the gas streams entering and exiting the reactor.

4) Heating heat removal inlet stream

Part of the produced hydrogen from the outflowing gas stream of the oxidation reactor is combusted in order to obtain a gas stream of 700˚C needed for the heat removal cycle. The combustion reactor is simulated in Aspen Plus with a Gibbs reactor. The net duty is set to zero, and the amount of the hydrogen-rich outflowing gas stream from the oxidation reactor is calculated with a design spec in order to obtain a temperature of 700°C for the outflowing gas stream from the combustor.

5) Heat removal reactor

During the heat removal cycle, the produced heat during the reduction and the oxidation cycle is removed from the reactor by feeding a gas stream of 700°C. The heat removal reactor is simulated as a heater in Aspen Plus, in which the temperature of the outflowing gas stream can be set to the desired value.

6) Heating heat removal outlet stream

The high temperature outflowing gas stream from the heat removal reactor is heated further by combustion of the residual part of the produced hydrogen from the outflowing gas stream of the oxidation reactor. This further heating of the outflowing gas stream from the heat removal reactor is advantageous for the power production in the subsequent gas turbine, since a higher temperature of the inflowing gas stream to the gas turbine will result in a higher power production by the gas turbine. The combustion of the residual produced hydrogen during the oxidation cycle is simulated in Aspen Plus with a Gibbs reactor. The net duty is set zero, so the temperature of the outflowing gas stream from the combustor is calculated by the Aspen model.

7) Gas turbine

The outflowing gas stream from the combustor is fed to the gas turbine. In the gas turbine, power is produced by adiabatically expanding the high temperature and high pressure gas stream to atmospheric pressure. The temperature of the outflowing gas stream from the gas turbine is dependent on the temperature of the inflowing gas stream, and is calculated by the Aspen model. The gas turbine is simulated as an isentropic turbine with an isentropic efficiency of 0.92, and a mechanical efficiency of 0.995.

8) Heat recovery gas turbine outlet stream

Additional power can be produced from the heat of the outflowing streams from the gas turbine. Therefore, the outflowing gas stream from the gas turbine is cooled down to 120°C. This is simulated in the Aspen Plus model as a cooler.

9) Heat recovery reduction outlet stream

Additional power can also be produced from the heat of the outflowing stream from the reduction reactor by integrating a steam cycle. Therefore, the outflowing gas stream from the reduction reactor is cooled down to ambient temperature. However, water condensation takes place at 100°C. Since during water condensation the temperature of the gas stream will remain constant, the heat recovery from the outflowing gas stream from the reduction reactor is only before the water condensation.

The additional power production by cooling down the outflowing gas streams from both the gas turbine and the reduction reactor are beyond the scope of this research. Therefore, these power productions are not included in the calculations for the produced power, which means that when there is referred to the power production this is always the produced power by the gas turbine.

For a full description of the coal-derived syngas power plant integrated with the PCCL process, the reader is referred to the article Spallina et al. [35].

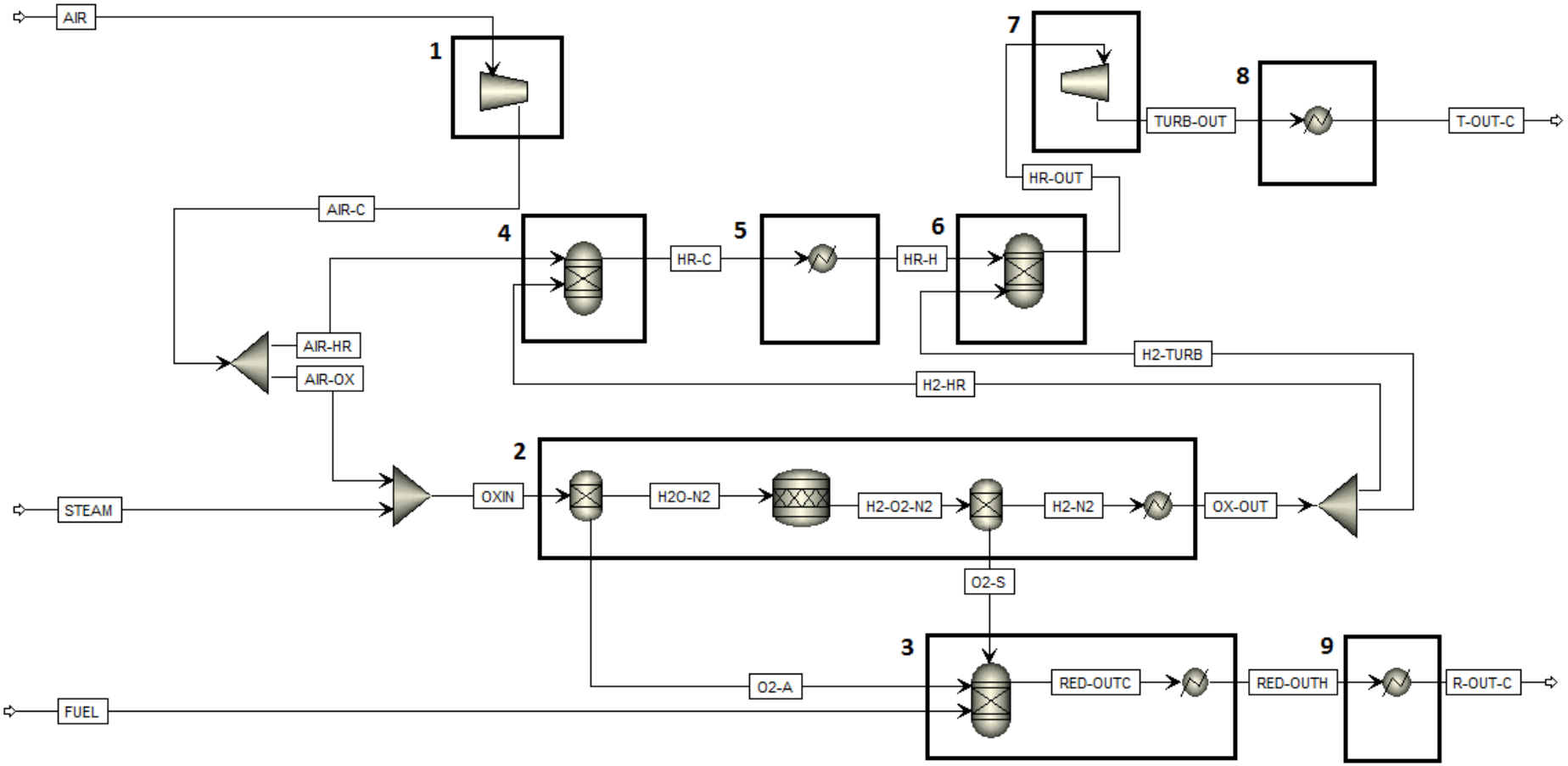

Figure 4.1 – Aspen flowsheet of the reduction, oxidation and heat removal reactors, including the gas turbine, for pseudo-continuous operation of heat removal strategy 1

4.1.2 Determining flowrate for oxidation and heat removal cycle

The ratio of oxidant to reductant flowrate is determined by the mole fractions of the reacting components according to equation 4.1, and the equilibrium constant for the steam oxidation. The equilibrium constant, which is temperature dependent, determines the ratio of produced hydrogen to unreacted steam, and therefore determines the flowrate needed for complete oxidation of the oxygen carrier during the oxidation cycle. Assumed is that during the reduction cycle there will be a full conversion of hydrogen and carbon monoxide to steam and carbon dioxide.

Since the amount of steam that will be converted to hydrogen is temperature dependent, the amount of converted steam during the oxidation cycle needs to be determined in order to determine the flowrate for the oxidation cycle. From the Delphi model, the fraction of converted steam was calculated to be 0.636.

The needed flowrate for the oxidation cycle is determined by combining the results from the Delphi model with the Aspen Plus model. Therefore, the conversion of the water-splitting reaction was set to the fraction of converted steam as obtained from the Delphi model, and a design spec was introduced in which the oxidant flowrate was the changing variable in order to obtain the same outlet composition as obtained from the Delphi model. A ratio of oxidant to reduction flowrate of 0.73 was determined from the Aspen Plus model, which means that for a reductant flowrate of 1 kg/m^2/s a oxidant flowrate of 0.73 kg/m^2/s is needed for the case that coal-derived syngas is used as fuel.

During the oxidation cycle, a temperature rise within the reactor takes place due to the highly exothermic oxidation reaction by oxygen. This temperature rise increases with increasing active weight fraction of the oxygen carrier, and therefore also the power production by the gas turbine will increase. Therefore, different active weight fractions of oxygen carrier were simulated in order to determine the effect of the active weight fraction of the oxygen carrier on the performance of the pre-combustion chemical looping concept for power production. The active weight fraction Fe_2O_3 should be below 0.439, in order to avoid the formation of metallic iron. Therefore, three solid materials were simulated with different active weight fraction of Fe_2O_3, namely 0.2, 0.3 and 0.4.

The needed heat removal flowrate is dependent on difference between the temperature of the inflowing heat removal stream (700°C) and the temperature of the bed before the heat removal cycle. Since the temperature of the outflowing heat removal stream changes with changing active weight fraction of the oxygen carrier, the heat removal flowrate needs to be determined for each case individually.

In order to determine the heat removal flowrate, first the average temperature of bed before the heat removal cycle needs to be determined. These average bed temperatures before the heat removal cycle

were determined for the three different active weight fractions of Fe_2O_3 with the Delphi model, and are 804.2°C, 874.8°C and 930.3°C for the case that the active weight fraction of Fe_2O_3 is respectively 0.2, 0.3 and 0.4.

The needed heat removal flowrate is determined by combining the results from the Delphi model with Aspen Plus model. Therefore, a design spec was introduced in which the heat removal flowrate was the changing variable in order to obtain the temperature of the outflowing heat removal stream as determined from the Delphi model. From this Aspen Plus simulations, heat removal flowrates of 10.5 kg/m^2/s, 7.6 kg/m^2/s and 4.9 kg/m^2/s were obtained for the case that the active weight fraction of Fe2O3 is respectively 0.2, 0.3 and 0.4.

When the needed heat removal flowrate increases, also the amount of hydrogen needed for heating the inflowing heat removal stream to 700°C by combustion of the produced hydrogen increases. The results from the Aspen Plus model showed that for the case that the active weight fraction of Fe_2O_3 is 0.2 the needed heat removal flowrate is so high that there is not enough hydrogen produced during the oxidation cycle for heating the inflowing heat removal stream to 700°C by combustion of the produced hydrogen. A maximum temperature of 677°C of the inflowing heat removal stream is obtained from the Aspen Plus model for the case that the active weight fraction of Fe_2O_3 is 0.2, a heat removal flowrate of 10.5 kg/m^2/s and all produced hydrogen during the oxidation cycle is combusted.

For the case that the active weight fraction of Fe_2O_3 is 0.2, the temperature of the inflowing heat removal stream was adjusted to 677°C in the Delphi model. Due to this lower temperature of the inflowing heat removal stream, an average temperature of the outflowing heat removal stream of 773.6°C was obtained from the Delphi model. Since the temperature difference between the inflowing and outflowing heat removal stream remains almost the same, the heat removal flowrate obtained from the Aspen Plus model still can be used for further analysis with the Delphi model.

In order to have a pseudo-continuous operation, the cycle time for each operating step needs to be the same, unless several reactors are operated in parallel for one operating step. During the calculation of the ratio of oxidant to reductant flowrate, this was already taken into account, even as for determining the heat removal flowrate with the Aspen Plus model. The cycle time is dependent on the active weight fraction of the oxygen carrier, and the dimensions of the reactor. For the Delphi simulations, the reactor length was 2 meter and the reactor diameter was 0.5 meter, and therefore the needed cycle time for each operating step for the case that the active weight fraction of Fe_2O_3 is 0.2, 0,3 and 0.4 is respectively 165, 255 and 355 seconds.

Gas velocities of the inflowing gas stream of around 0.5 m/s are preferable for operation in packed-bed reactors. This is not the case for the heat removal cycle, and therefore the heat removal flowrate for the case that the active weight fraction of Fe_2O_3 is 0.2 was divided by 3, and the heat removal flowrates for the cases that the active weight fractions of Fe_2O_3 are 0.3 and 0.4 were divided by 2. Therefore, the heat removal flowrate for the case that the active weight fraction of Fe_2O_3 is 0.2, 0.3 and 0.4 is respectively 3.5 kg/m^2/s, 3.8 kg/m^2/s and 2.45 kg/m^2/s.

Since the amount of heat removal gas that is fed to the heat removal reactor is decreased by either a factor 3 or 2, the time needed for the heat removal cycle needs to be increased by a either a factor 3 or 2. This means that three heat removal reactors need to operate in parallel for the case that the active weight fraction of Fe_2O_3 is 0.2, and two heat removal reactors need to operate in parallel for the case that the active weight fraction of Fe_2O_3 is 0.3 or 0.4. Therefore, the cycle time (τ) for the case that the active weight fraction of Fe_2O_3 is 0.2, 0.3 and 0.4 is respectively 495, 510 and 710 seconds.

For the case that three heat removal reactors in parallel are needed, the operating steps of each reactor are shown in Figure 4.2.

	R1	R2	R3	R4	R5	R6	R7
τ	**RED**	**P**	**OX**	**HR**	**HR**	**HR**	**P**
τ	**P**	**OX**	**HR**	**HR**	**HR**	**P**	**RED**
τ	**OX**	**HR**	**HR**	**HR**	**P**	**RED**	**P**
τ	**HR**	**HR**	**HR**	**P**	**RED**	**P**	**OX**
τ	**HR**	**HR**	**P**	**RED**	**P**	**OX**	**HR**
τ	**HR**	**P**	**RED**	**P**	**OX**	**HR**	**HR**
τ	**P**	**RED**	**P**	**OX**	**HR**	**HR**	**HR**

Figure 4.2 – Operating steps of each reactor for the case that three heat removal reactors in parallel are needed.

4.1.3 Effect of active weight fraction of Fe_2O_3 on performance of the PCCL concept

Now all the inlet conditions are known for the three cases with different active weight fractions of Fe_2O_3, the performance of the pre-combustion chemical looping concept can be determined with the results from the Delphi model. Several cycles were simulated with the Delphi model in order to obtain results at steady state. The steady state is reached, when the temperature profile of the bed at the start of the cycle is the same as at the end of the cycle. All the results shown in this report are obtained from cycles at which steady state was reached.

From the Delphi simulations, the bed temperatures as a function of the reactor length at a certain time, and the outlet temperatures as a function of the time can be obtained. The bed temperature profiles at the end of each cycle, and the outlet temperature during each cycle for the case that the active weigh fraction of Fe_2O_3 is 0.2 are shown in respectively Figure 4.3 and 4.4.

From the bed temperature profile of Figure 4.3 can be seen that there is a small temperature decrease during the reduction cycle, which means that the reduction reactions are overall endo-thermic. The lower temperature at the inlet of the reduction reactor is due to the low temperature of the fuel (517˚C). The small increase in temperature at around 0.2 m is caused by the water gas shift reaction, which is exothermic. From Figure 4.3 also can be seen that the temperature rise during the oxidation cycle is around 125˚C, and that the heat is removed during heat removal cycle.

From the outlet temperature profile of Figure 4.4, the average outlet temperature during the heat removal cycle can be calculated. The average outlet temperature during the heat removal is 770.9˚C, with a minimum of 680˚C and a maximum of 800˚C (blue line). Since three heat removal reactors are working in parallel, and each heat removal reactor is working in a different mode (HR1, HR2 or HR3), the average temperature of the three heat removal outlet streams can be calculated (orange line). Due to the parallel heat removal cycles, the temperature fluctuations are decreased.

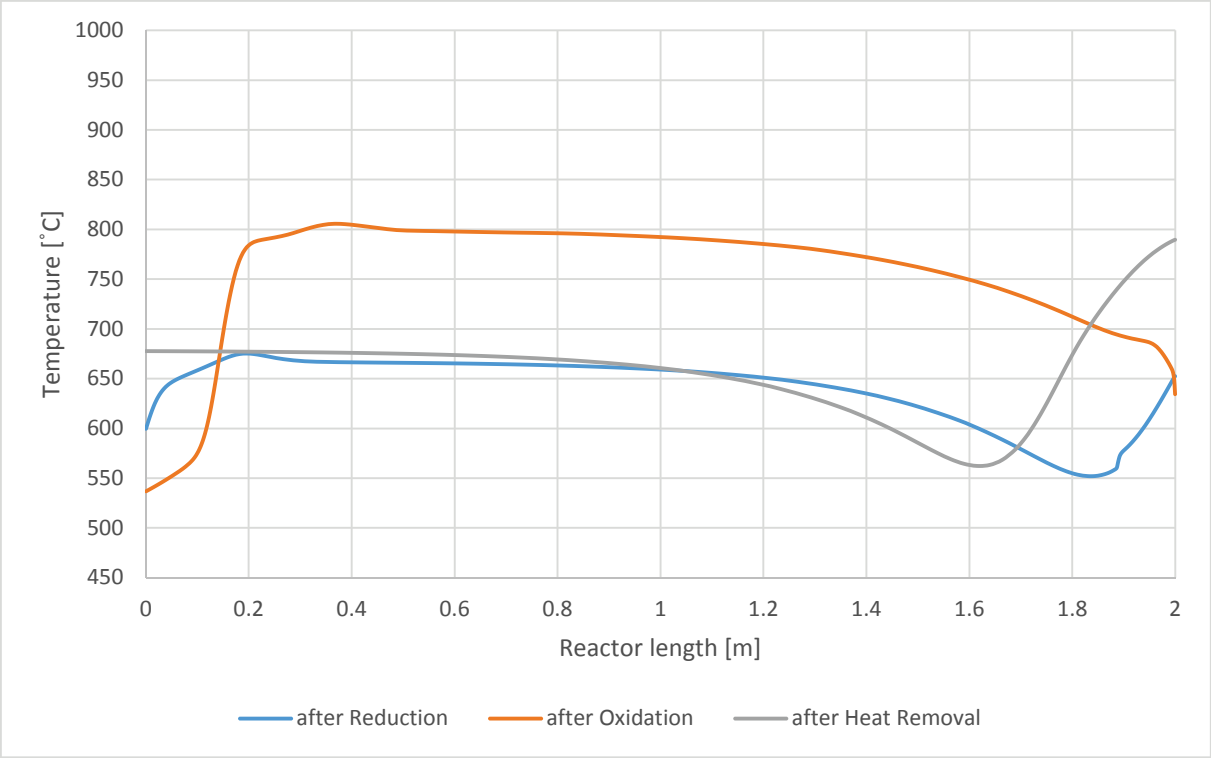

Figure 4.3 – Bed temperature profiles as a function of the reactor length after reduction, oxidation and heat removal for the case that the active weight fraction of Fe_2O_3 is 0.2

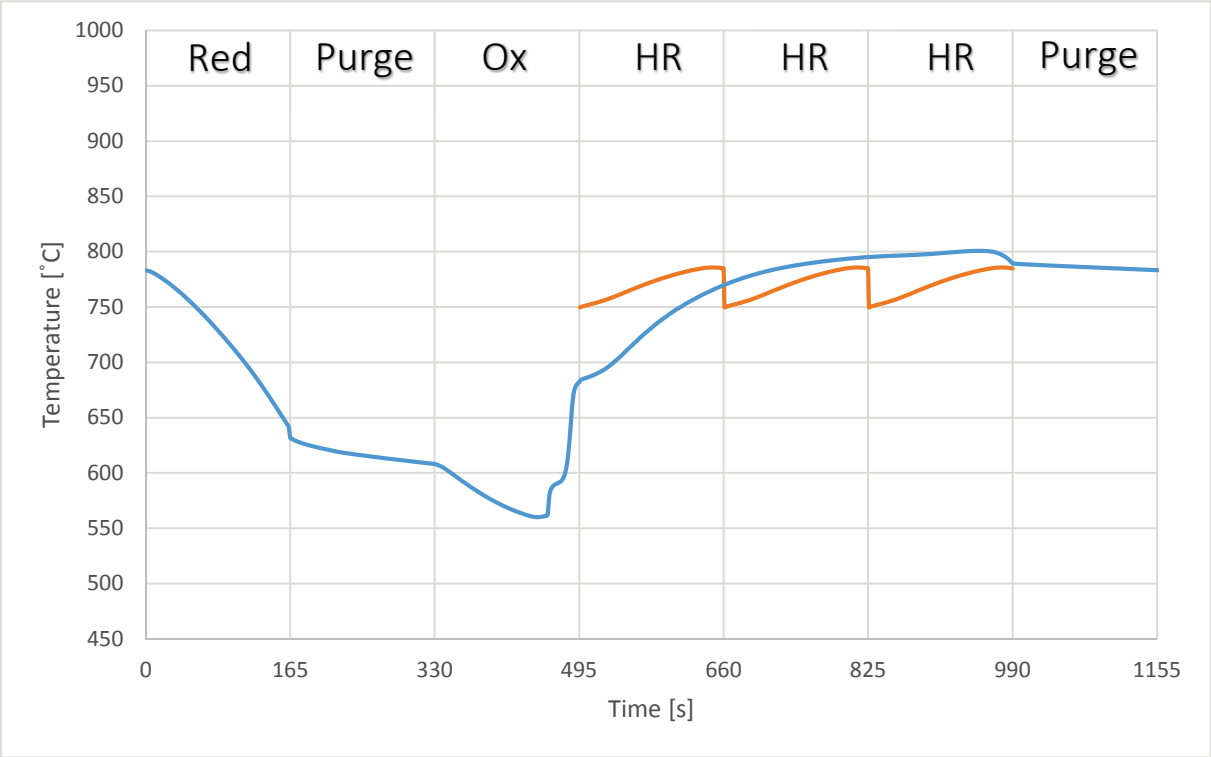

Figure 4.4 – Outlet gas temperature as a function of time during sequentially reduction, purge, oxidation, heat removal and purge for the case that the active weight fraction of Fe_2O_3 is 0.2

The bed temperature profiles after each cycle are obtained from the Delphi simulations, and are shown in Figure 4.5 and 4.6 for the active weight fraction Fe_2O_3 of respectively 0.3 and 0.4. From Figure 4.5 and 4.6 can be seen that the temperature rise within the bed due to the exothermic oxidation of Fe_3O_4 to Fe_2O_3 by oxygen increases with increasing active weight fraction of Fe_2O_3, which is ± 200˚C for the case that the active weight fraction of Fe_2O_3 is 0.3, and ± 275˚C for the case that the active weight fraction of Fe_2O_3 is 0.4. Comparison of the bed temperature profiles after the heat removal cycle shows that the heat removal flowrate for the case that the active weight fraction Fe_2O_3 is 0.3 is relatively high in comparison with the heat removal flowrate for the case that the active weigh fraction Fe_2O_3 is 0.4, since the bed temperature at the exit of the reactor is around 150˚C lower.

Since the bed is colder at the end of the reactor for the case that the active weight fraction Fe_2O_3 is 0.3, also the temperature of the outflowing gas stream from the subsequent reduction cycle will be lower at the beginning of the cycle. This can be seen from the outlet gas temperature profiles during each cycle of Figure 4.7 and 4.8 for active weight fraction Fe_2O_3 of respectively 0.3 and 0.4.

From comparison of the outlet gas temperature profiles of Figure 4.7 and 4.8 can also be seen that the temperature fluctuations during the heat removal cycle are higher for the case that the active weight fraction Fe_2O_3 is 0.3. This is also due to the relative higher heat removal flowrate, since the bed is cooled down until a lower temperature for this case.

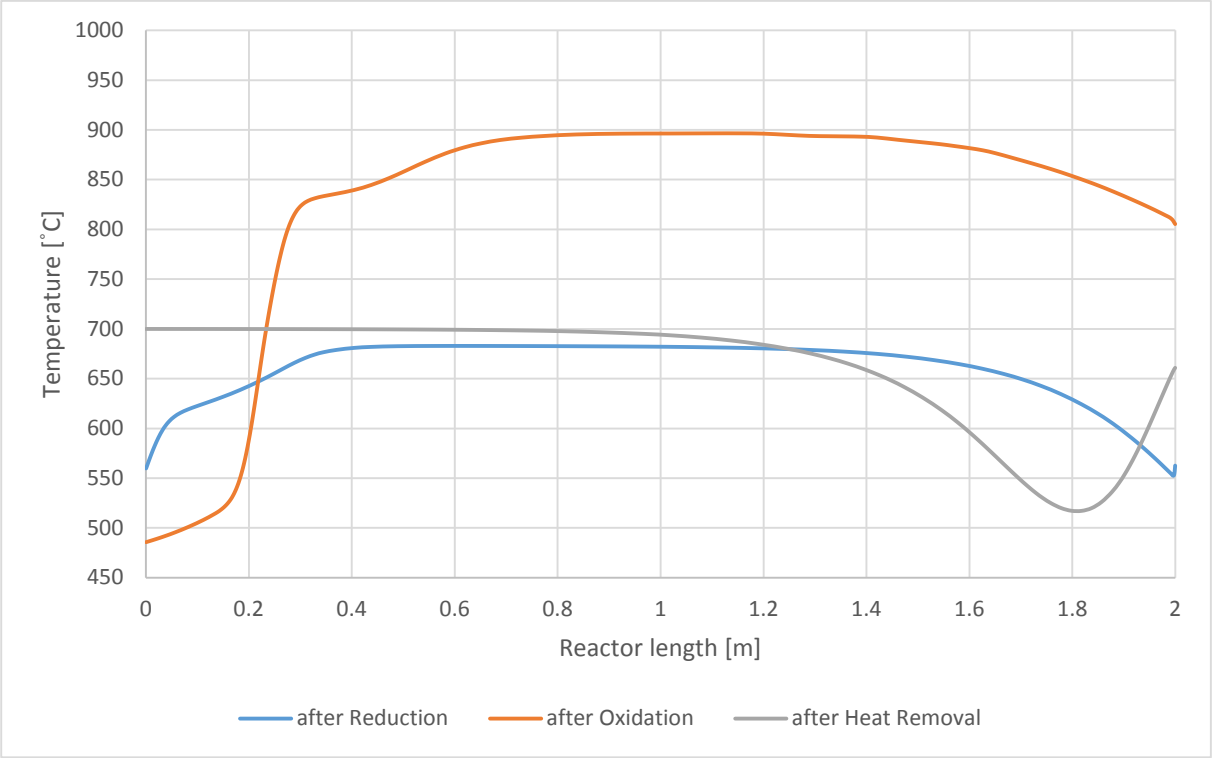

Figure 4.5 - Bed temperature profiles as a function of the reactor length after reduction, oxidation and heat removal for the case that the active weight fraction of Fe_2O_3 is 0.3

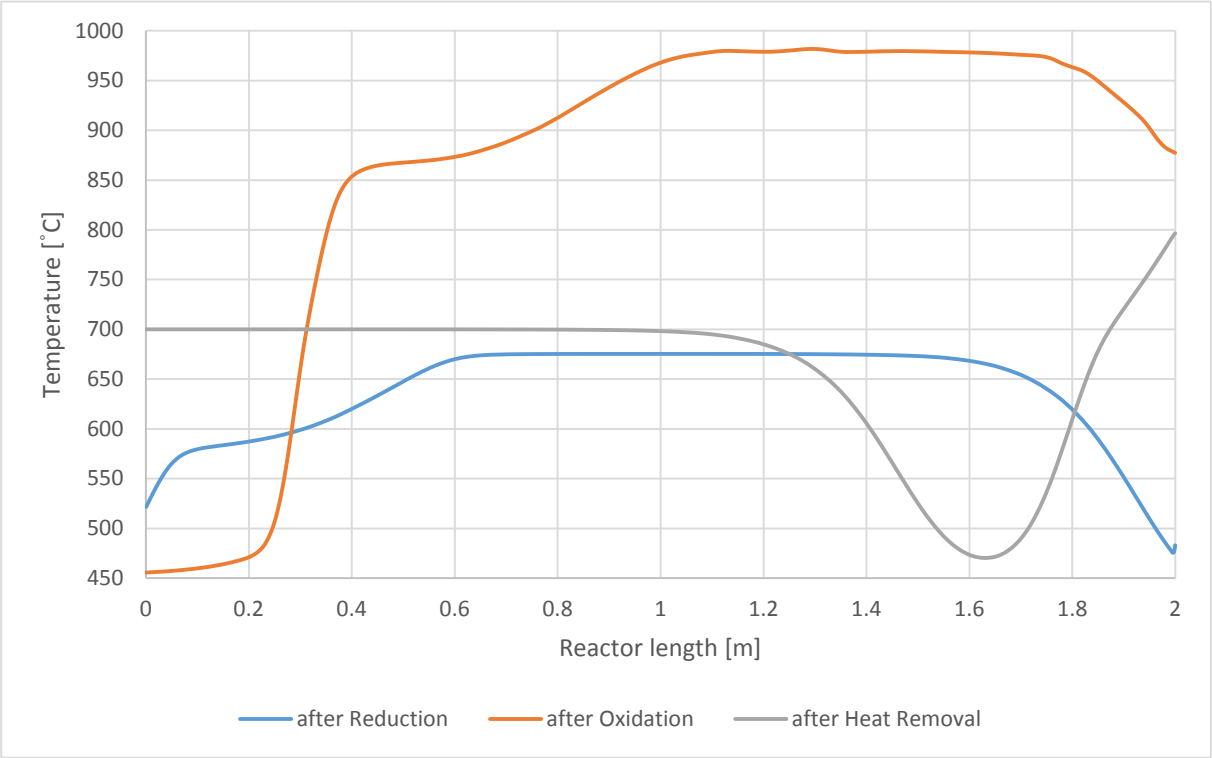

Figure 4.6 - Bed temperature profiles as a function of the reactor length after reduction, oxidation and heat removal for the case that the active weight fraction of Fe_2O_3 is 0.4

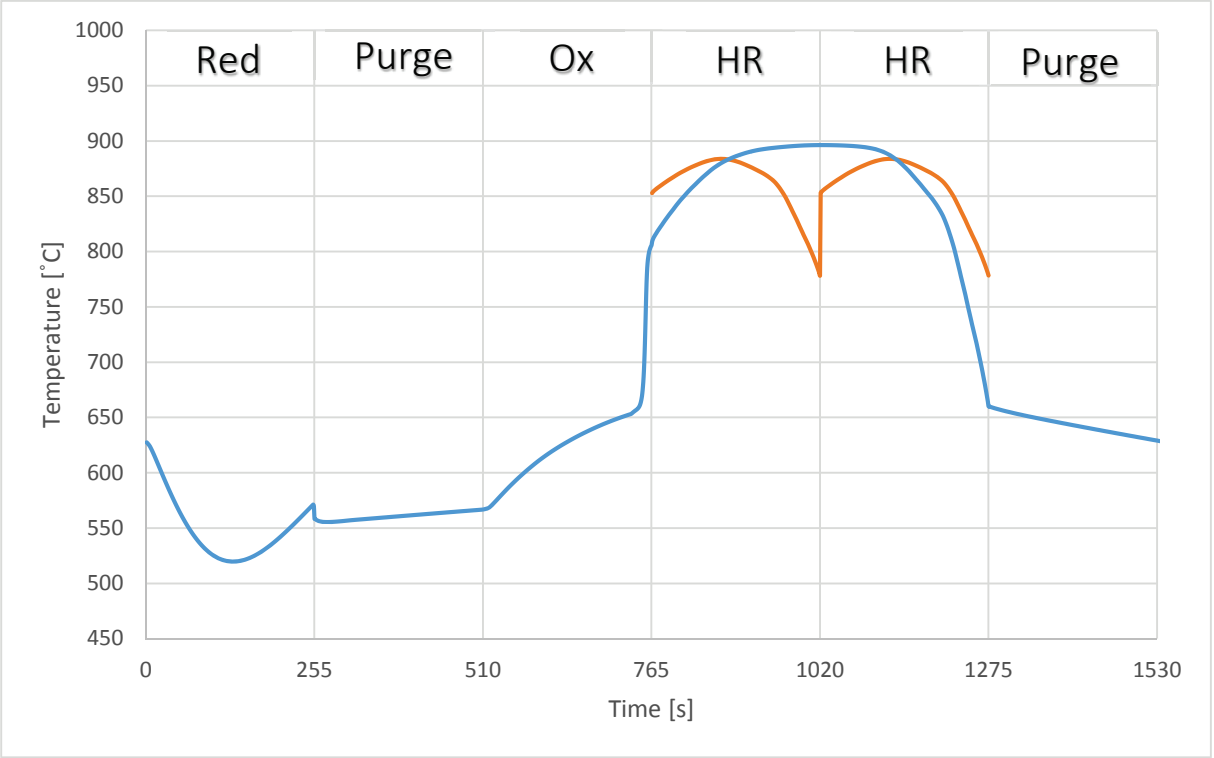

Figure 4.7 – Outlet gas temperature as a function of time during sequentially reduction, purge, oxidation, heat removal and purge for the case that the active weight fraction of Fe_2O_3 is 0.3

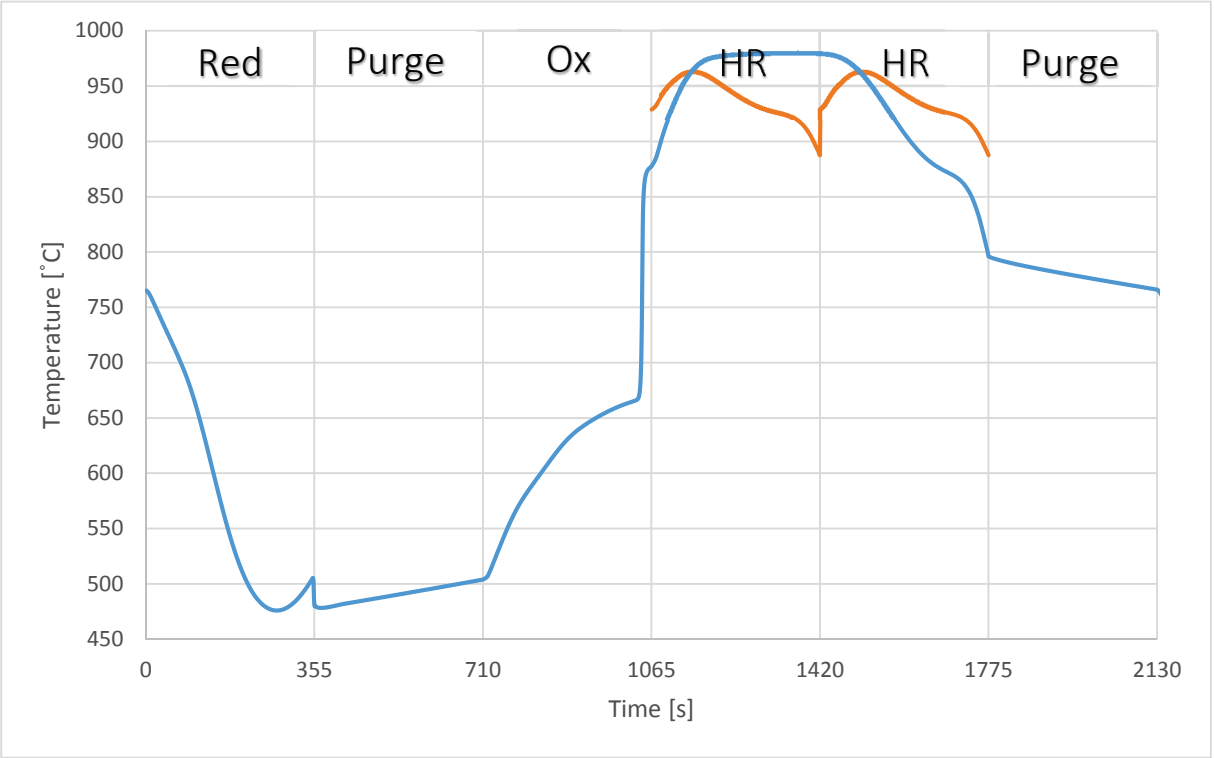

Figure 4.8 – Outlet gas temperature as a function of time during sequentially reduction, purge, oxidation, heat removal and purge for the case that the active weight fraction of Fe_2O_3 is 0.4

The average temperatures of the gas stream exiting the heat removal reactor are calculated from the outlet temperature profiles of Figure 4.7 and 4.8, and are 864.5˚C and 938.0˚C for the case that the active weight fraction of Fe_2O_3 is respectively 0.3 and 0.4. These high temperature gas streams exiting the heat removal reactors are heated up further by combustion with the part of the produced hydrogen that is left after heating up the air stream needed for the heat removal cycle from 440˚C to 700˚C. The ratio of the amount of hydrogen needed for heating the air stream for the heat removal cycle to the total amount of hydrogen, the temperatures of the gas stream entering and exiting the heat removal reactor, and the temperature of the gas stream entering the gas turbine after further heating of the heat removal outlet stream by combustion with the other part of the produced hydrogen can be found in Table 4.2 for the three different active weight fractions of Fe_2O_3.

The produced power by the gas turbine can be calculated by subtracting the power needed for compression of the ambient air stream to 20.5 bar from the power produced by expanding the high temperature and high pressure gas stream in the gas turbine.

The gas turbine efficiency is the ratio of the overall produced power by the gas turbine to the lower heating value of the fuel:

$$\eta_{turbine} = \frac{P_{turbine}}{LHV_{fuel}} \qquad [4.2]$$

The lower heating value of the fuel can be calculated with equation 4.3, and has a value of 886.83 kW for a fuel inlet stream (F_{fuel}) of 1 kg/m^2/s and a reactor diameter of 0.5 m.

$$LHV_{fuel} = F_{fuel}(\sum_i^n w_i LHV_i)A \qquad [4.3]$$

For calculating this gas turbine efficiency, the power needed for the coal gasification unit, and the additional power production that can be obtained from the heat of the outflowing gas streams from the reduction reactor and the gas turbine are not taken into account.

The produced power by the gas turbine and the gas turbine efficiency are calculated for the three cases with different active weight fractions of Fe_2O_3 with the Aspen Plus model, and are shown in Table 4.2. The results clearly show that the produced power, and therefore the gas turbine efficiency is the highest for the case that the active weight fraction of Fe_2O_3 is 0.4.

Table 4.2 – Overview of performance related results of the pre-combustion chemical looping concept for three different active weight fractions of Fe_2O_3

	$w_{Fe_2O_3} = 0.2$	$w_{Fe_2O_3} = 0.3$	$w_{Fe_2O_3} = 0.4$
H_2(HR)/H_2(Total) [-]	1.000	0.848	0.533
Inlet temperature HR reactor [˚C]	678.3	700	700
Outlet temperature HR reactor [˚C]	770.9	864.5	938.0
Inlet temperature gas turbine [˚C]	770.9	903.3	1109.8
Produced power by gas turbine [kW]	310.29	351.17	370.55
Gas turbine efficiency [-]	0.350	0.396	0.417

The outlet compositions of the gaseous components as a function of time is shown in Figure 4.9. Figure 4.9 shows that there is only a small fuel slip at the end of the reduction cycle. Figure 4.9 also shows that the oxygen breakthrough starts at 20 seconds before the end of the oxidation cycle, which means that the oxygen carrier is already fully oxidized. The hydrogen production, due to oxidation of $FeAl_2O_4$ to Fe_3O_4 by steam, is already finished after around 90 percent of the cycle time, and the mole fraction of hydrogen is zero for 10 percent of the time. The mole fraction of hydrogen can be increased by decreasing the oxidant flowrate. This is advantageous for the power production, since on average more hydrogen will be available for heating up the outlet heat removal stream. Therefore, the temperature of the gas stream entering the gas turbine is higher, and the production of power increases. In order to have the oxygen breakthrough at exactly the end of the oxidation cycle, the oxidant flowrate was decreased from 0.73 to 0.70 kg/m^2/s.

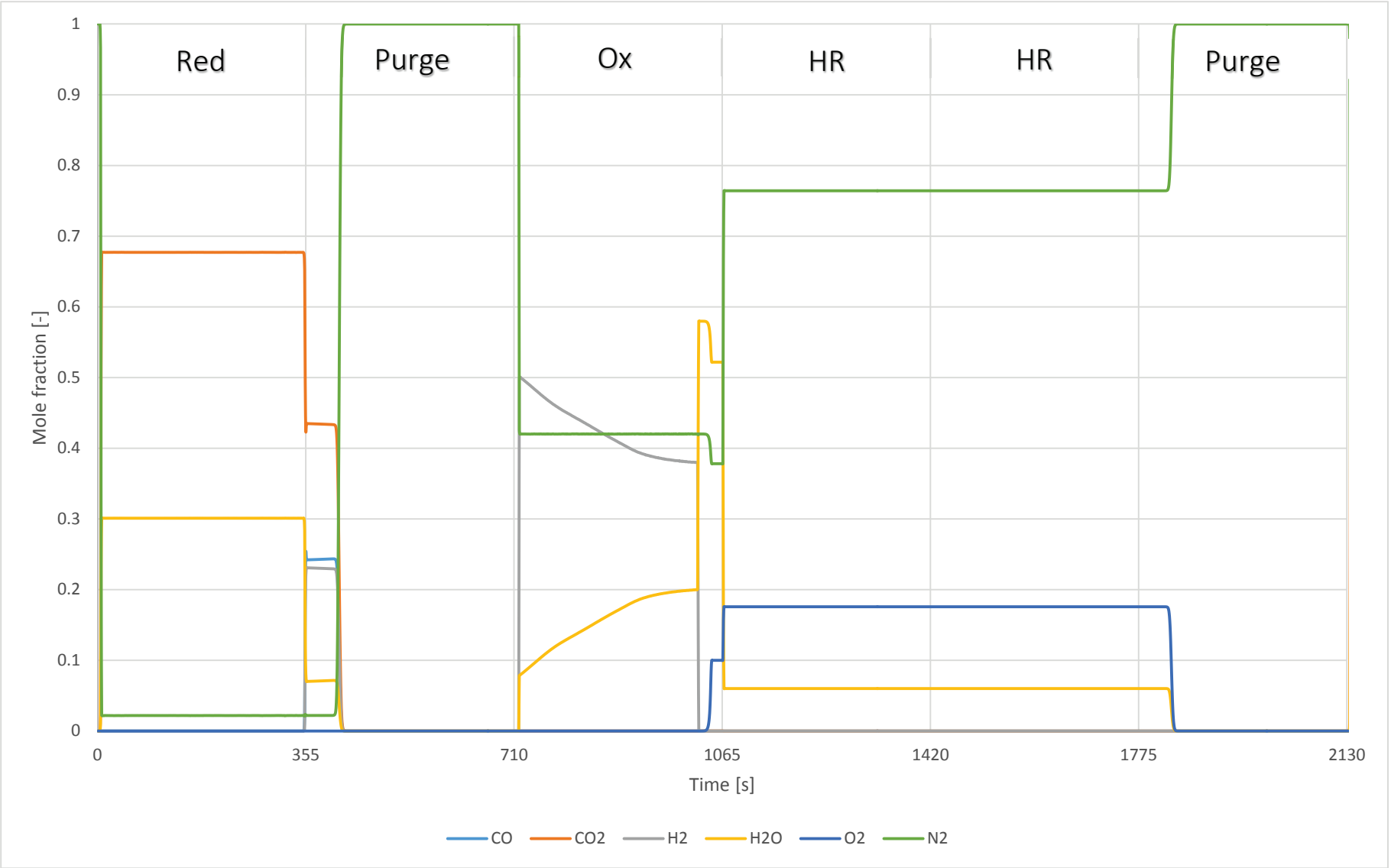

Figure 4.9 – Outlet composition of gaseous components as a function of time

4.1.4 Effect of Heat Removal flowrate on the performance of the PCCL concept

A sensitivity analysis was carried out for the case that the active weight fraction of Fe_2O_3 is 0.4, in order to optimize the power production. During this sensitivity analysis, the effect of the heat removal flowrate on the power production was analyzed. Therefore, the heat removal flowrate was varied between 4.6 and 6.2 kg/m^2/s, with intervals of 0.2 kg/m^2/s, while all the other inlet conditions remained the same.

Both the temperature and the flowrate of the stream entering the gas turbine affect the power production. By varying the heat removal flowrate, the average temperature of the outflowing stream from the heat removal reactor changes. The average temperatures of outflowing gas streams from the reduction, oxidation and heat removal cycle are obtained from simulations with Delphi, and are shown in Figure 4.10 for the different heat removal flowrates. The temperatures of the gas streams entering the gas turbine are obtained for each heat removal flowrate from simulations with the Aspen Plus model, and are also shown in Figure 4.10.

From Figure 4.10 can be seen that the average temperature of the heat removal outlet stream decreases with increasing heat removal flowrate. This is due to the fact that when almost all stored heat is removed from the reactor, the temperature of the bed at the outlet of the reactor decreases, and a heat removal stream at lower temperature is obtained at the end of the heat removal cycle. When the heat removal flowrate is increased, a higher part of the produced hydrogen is needed for pre-heating the air stream for the heat removal cycle to 700˚C. This means that less hydrogen is available for further heating of the gas stream after the heat removal cycle, and the temperature of the inflowing gas stream to the gas turbine also decreases.

The produced power increases with increasing heat removal flowrate, but also the needed power for air compression increases. The inlet temperature of the gas stream entering the turbine decreases with increasing heat removal flowrate, which hampers the increasing power production by the gas turbine. Therefore, a maximum in the power production is expected at a certain heat removal flowrate. With the Aspen Plus model, the power production by the turbine and the corresponding turbine efficiency were calculated for each of the heat removal flowrates. The turbine efficiency as a function of the heat removal flowrate is shown in Figure 4.1 (blue squares), and indeed shows that an optimal turbine efficiency can be reached with a heat removal flowrate of 5.6 kg/m^2/s.

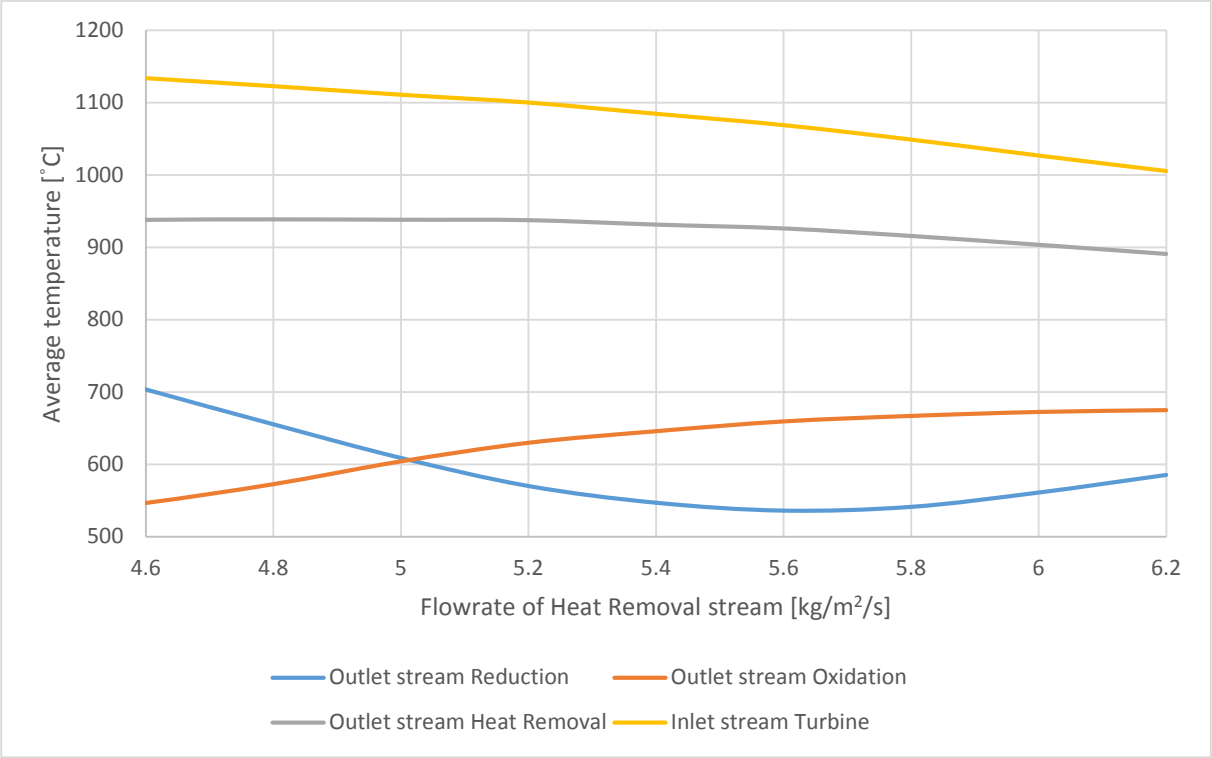

Figure 4.10 – Average temperatures of the Reduction, Oxidation and Heat Removal outlet stream, and the Turbine inlet stream as a function of the heat removal flowrate

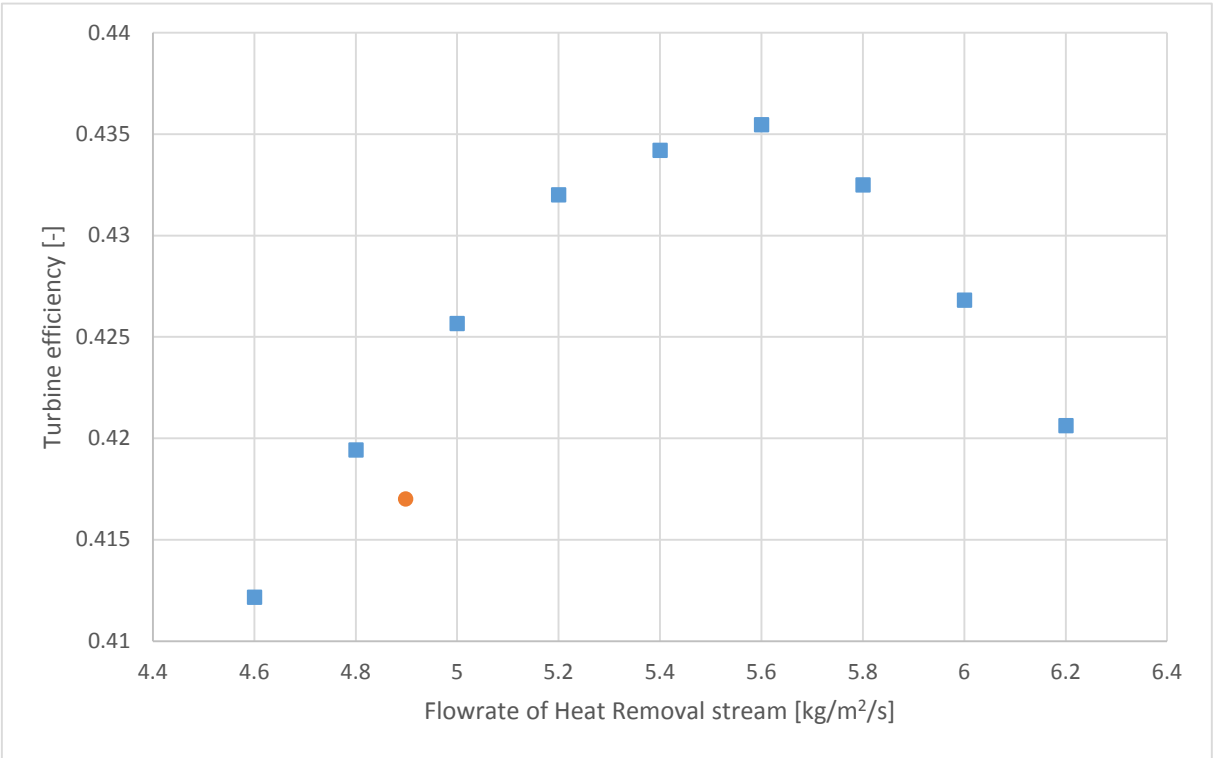

Figure 4.11 – Turbine efficiency as a function of the heat removal flowrate (blue squares: oxidant flowrate of 0.70 kg/m²/s, orange dot: oxidant flowrate of 0.73 kg/m²/s)

The maximum power production by the turbine at a heat removal flowrate of 5.8 kg/m^2/s can also be explained by the fact the temperature of the outflowing gas from the reduction cycle is at a minimum. Therefore, a maximum amount of heat is flowing out of the reactor during the oxidation and heat removal cycle, which is sequentially used for the power production.

The orange dot in Figure 4.12 represents the turbine efficiency for the previous case before the oxidant flowrate was decreased from 0.73 to 0.70 kg/m^2/s. From Figure 4.11 can be seen that the turbine efficiency is indeed increased by decreasing the oxidant flowrate.

It is possible that the obtained optimal heat removal flowrate changes when the downstream power production from the heat of the outflowing gas streams is taken into account. Since this additional power production is out of the scope of this project, future research is needed in order to determine the effect of this additional power production from the outflowing gas streams on the optimal heat removal flowrate obtained in this research.

The outlet compositions of the gaseous reactants as a function of time is shown in Figure 4.12 for the case that the heat removal flowrate is 5.8 kg/m^2/s. From Figure 4.12 can be seen that the fuel breakthrough takes place at the moment that the cycle is switched from reduction to purge. Figure 4.12 also shows that there is still an oxygen breakthrough before the end of the oxidation cycle, and that in the last 10 seconds of the oxidation cycle no hydrogen is produced. The average mole fraction of hydrogen in the outflowing oxidant stream can be increased by decreasing the cycle time from 355 to 345 seconds. Due to this higher mole fraction of hydrogen in the outflowing oxidant stream, the outlet stream from the heat removal reactor can be heated up to a higher temperature, which is advantageous for power production by the gas turbine and the corresponding turbine efficiency.

The outlet compositions of the gaseous components as a function of time is shown in Figure 4.13 for the case that the cycle time of each operating step was decreased by 10 seconds. Figure 4.13 shows that the hydrogen production is completed at the moment that the oxidation cycle is stopped. At the beginning of the oxidation cycle, there is narrow peak at which the mole fraction of steam is high. This peak can be explained by the fact that the cycle time is too short for complete reduction during the reduction cycle, and therefore a small part of the produced hydrogen is used for reduction of the last part of the oxygen carrier in the bed that was not reduced during the reduction cycle.

In order to avoid that part of the produced hydrogen reacts away during the oxidation cycle, a somewhat higher reduction flowrate is needed, so the bed will be completely reduced by the fuel during the reduction cycle. Eventually, this will also lead to a little higher turbine efficiency, since the average mole fraction of hydrogen increases.

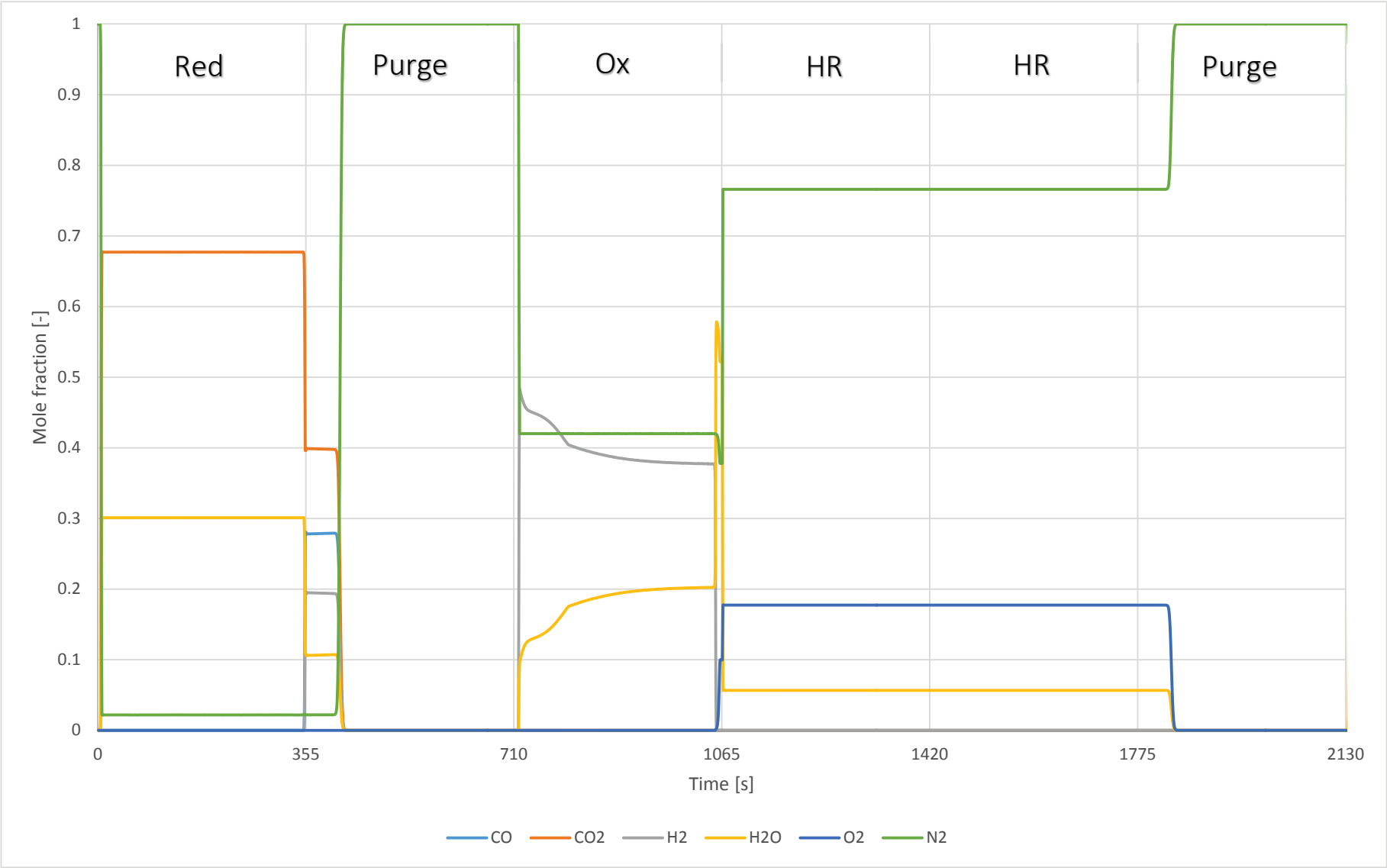

Figure 4.12 - Outlet composition of gaseous components as a function of time for the case that the heat removal flowrate is 5.6 kg/m²/s

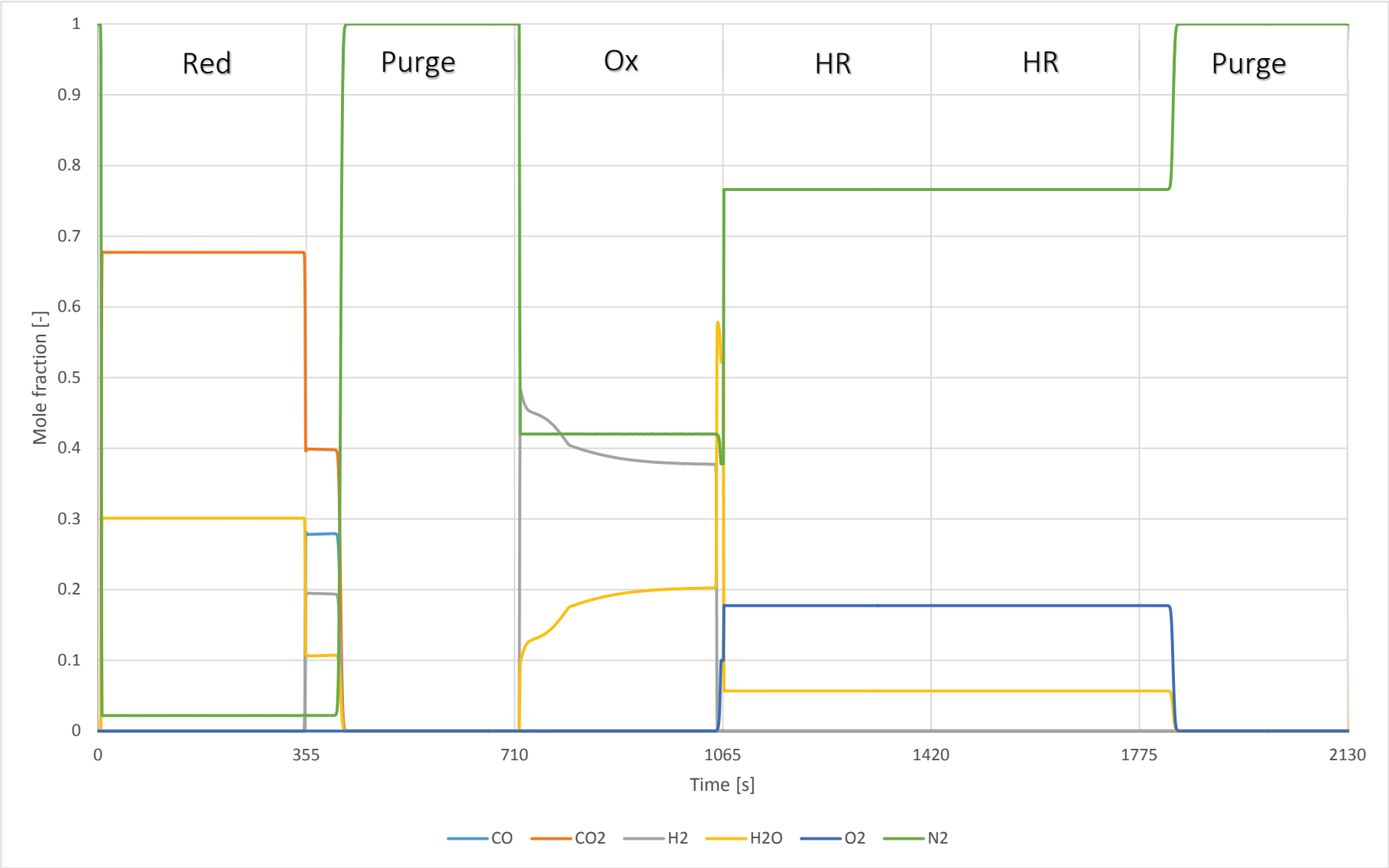

Figure 4.13 - Outlet composition of gaseous components as a function of time for the case of maximum power production and a reduction of the cycle time by 10 seconds

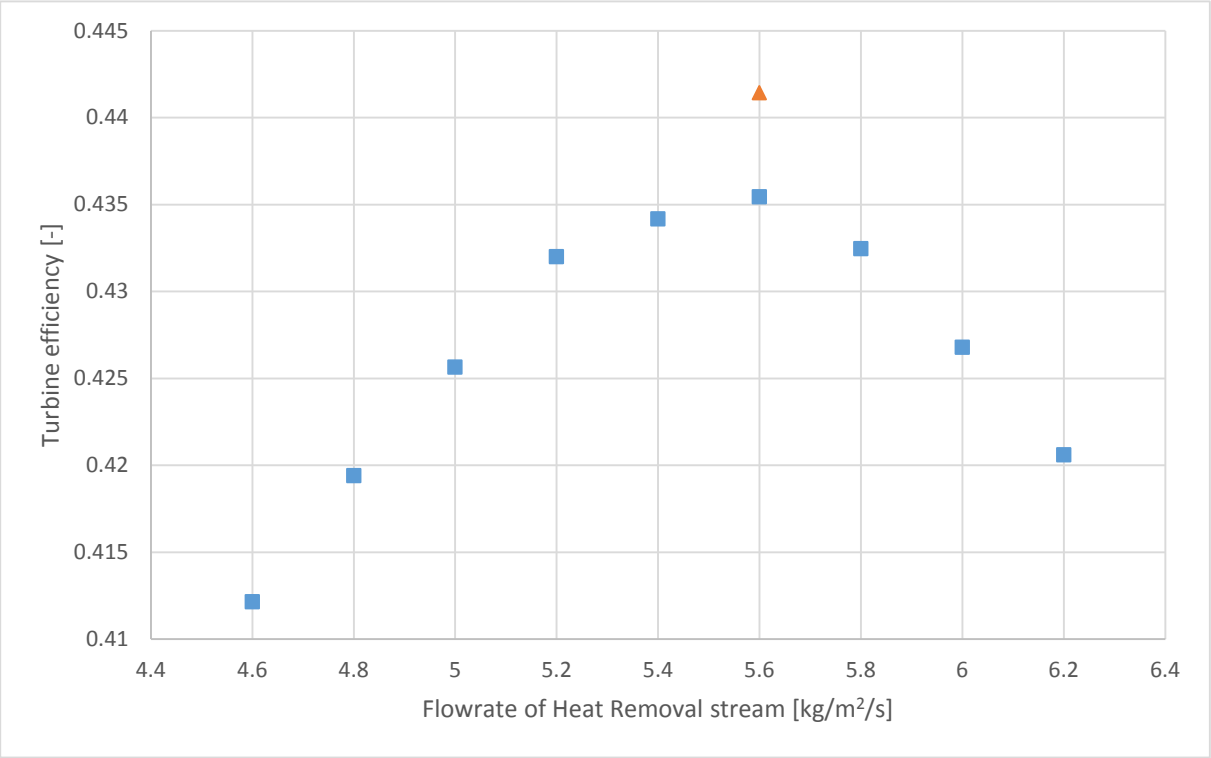

Figure 4.14 - Turbine efficiency as a function of the heat removal flowrate (red triangle: oxidant flowrate of 0.70 kg/m2/s with cycle time of 345 s, blue squares: oxidant flowrate of 0.70 kg/m^2/s with cycle time of 355 s, orange dot: oxidant flowrate of 0.73 kg/m^2/s with cycle time of 355 s)

The performance of the gas turbine for the case of reduced cycle time was determined with the Aspen Plus model. A power production by the gas turbine of 486.58 kW, and a turbine efficiency of 0.4414 were obtained. As can be seen from Figure 4.14, this cycle time reduction resulted in a turbine efficiency improvement of around 0.6 percent points.

The average outlet compositions during the reduction and oxidation cycle are shown in Table 4.3. From Table 4.3 can be seen that average mole fraction of hydrogen and carbon monoxide are zero, which means that there is no fuel slip during the reduction cycle. Also can be seen that there are only three components exiting the reactor during the reduction cycle, which are carbon dioxide, nitrogen and steam. A high purity carbon dioxide stream can be obtained after water condensation since the mole fraction of nitrogen in the outflowing stream from the reduction cycle is relatively small. The carbon dioxide purity can be calculated by dividing the mole fraction of carbon dioxide by the mole fraction of the gaseous components after water condensation, which is one minus the mole fraction of steam. The carbon dioxide purity for this case is 96.8 %.

Table 4.3 – Average outlet compositions during the reduction and oxidation cycle

		Reduction	Oxidation
Mole fraction [mol_i/mol_g]	**CO**	0.000	0.000
	CO_2	0.677	0.000
	H_2	0.000	0.395
	H_2O	0.301	0.184
	N_2	0.023	0.420
	O_2	0.000	0.000

4.1.5 Effect of steam oxidation kinetics on performance of the PCCL concept

As described in section 3.2, there are two possible pathways for the oxidation of the oxygen carrier, namely the oxidation of $FeAl_2O_4$ to Fe_2O_3 by oxygen and the oxidation of $FeAl_2O_4$ to Fe_3O_4 by steam and the subsequent oxidation of Fe_3O_4 to Fe_2O_3 by oxygen. Since the oxidation of $FeAl_2O_4$ to Fe_3O_4 by steam is crucial for the hydrogen production during the oxidation cycle, the effect of the steam oxidation kinetics on the reactor performance of the pre-combustion chemical looping concept needs to be analyzed.

At Eindhoven University of Technology, research is still ongoing for determining the reaction kinetics for the steam oxidation of $FeAl_2O_4$. Since the results are not available yet, the reaction rate constant for the oxidation of $FeAl_2O_4$ by steam as suggested by Coetsee et al. [27] were decreased by a factor 2, 10 and 100, in order to analyze the effect of slower steam oxidation kinetics on the performance of the pre-combustion chemical looping concept.

The average outlet composition of the gas stream exiting the oxidation reactor, the average outlet temperature of the outflowing heat removal stream, the average temperature of the gas stream entering the gas turbine, and the produced power by the gas turbine with the corresponding turbine efficiency are shown in Table 4.4 for the three cases that the reaction rate constant for the steam oxidation were decreased, even as the original case without reaction rate constant adjustment. Table 4.4 shows that the average mole fraction of hydrogen in the outflowing oxidant stream decreases with decreasing reaction rate constant for the steam oxidation. In comparison with the original case, the decrease in average mole fraction of hydrogen is small for the case that the reaction rate constant is decreased by a factor 2 and 10, while it is rather large for the case that the reaction rate constant is decreased by a factor 100. This can be explained with the profiles of the weight fractions Fe_3O_4 as a function of the reactor length in Figure 4.15. The profiles for the weight fractions of Fe_3O_4 as a function of the reactor length are obtained from the Delphi model after 200 seconds of oxidation.

Table 4.4 – Overview of performance related results of the pre-combustion chemical looping concept for original case and the case that the reaction rate constant is was divided by a factor 2, 10 and 100

		k	k/2	k/10	k/100
Mole fraction [mol_i/mol_g]	**CO**	0.000	0.000	0.000	0.000
	CO_2	0.000	0.000	0.000	0.000
	H_2	0.386	0.384	0.376	0.359
	H_2O	0.193	0.194	0.201	0.221
	N_2	0.420	0.420	0.420	0.420
	O_2	0.002	0.002	0.002	0.002
Outlet temperature HR reactor [˚C]		926.3	922.6	923.4	936.9
Inlet temperature gas turbine [˚C]		1069.1	1063.8	1057.7	1055.3
Produced power gas turbine [kW]		386.34	382.68	378.45	376.45
Turbine efficiency [-]		0.4356	0.4315	0.4267	0.4245

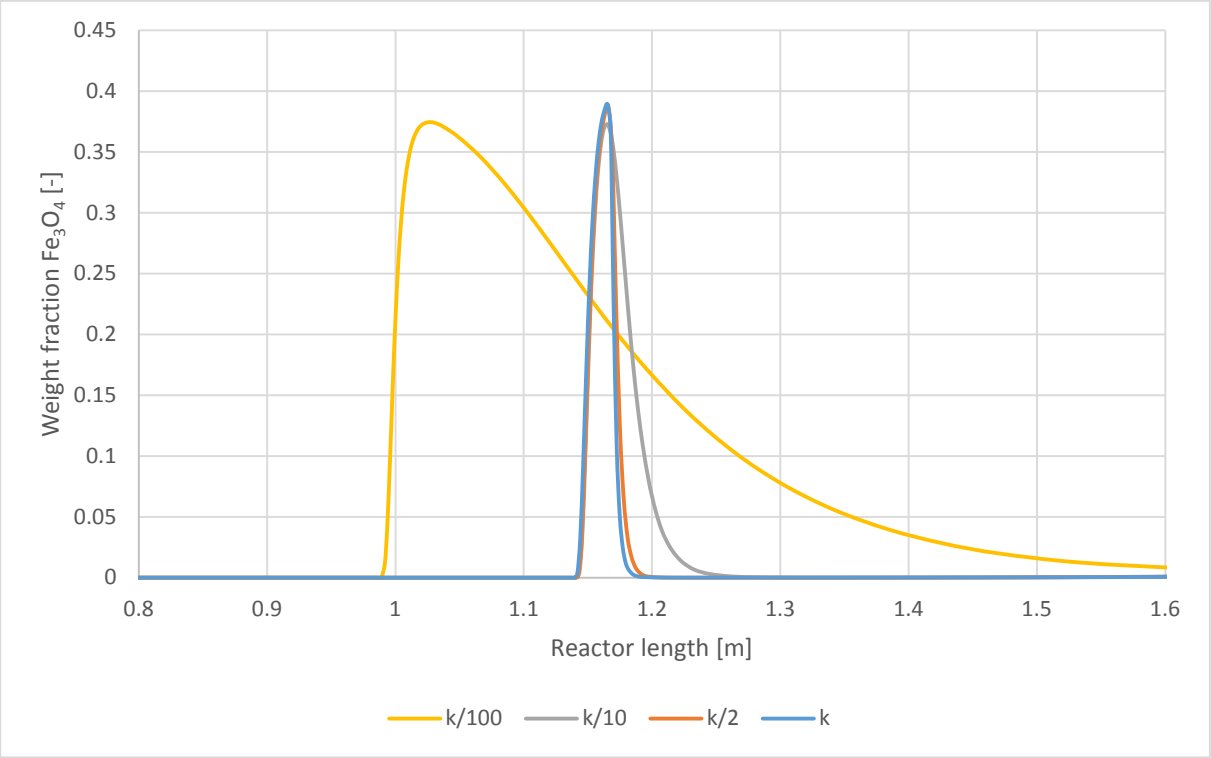

Figure 4.15 – Profiles of the weight fraction Fe3O4 as a function of the reactor length for the original case, and the cases that the reaction rate constant was divided by a factor 2, 10 and 100.

Figure 4.15 shows that Fe_3O_4 weight fraction profile is only changed at the front end of the reaction front for the case that the reaction rate constant for the steam oxidation is decreased by a factor 2 and 10. This means that the reaction rate for the steam oxidation is sufficient high, so that the reaction front for the oxidation of $FeAl_2O_4$ to Fe_3O_4 by steam is always faster than that of the oxidation of Fe_3O_4 to Fe_2O_3 by oxygen. Therefore, the oxidation of the oxygen carrier occurs via only pathway B, and a maximum amount of hydrogen is produced. From Figure 4.15 can also be seen that the height of the Fe_3O_4 front shows a small decrease when the reaction rate constant is decreased by a factor 10. This can be explained by a small overlap of the reaction fronts of the oxidation of $FeAl_2O_4$ to Fe_3O_4 by steam and the oxidation of Fe_3O_4 to Fe_2O_3 by steam. Therefore, a small amount of $FeAl_2O_4$ is directly oxidized to Fe_2O_3 by oxygen, which means that also the amount of produced hydrogen will show a small decrease. For the case that the reaction rate constant of the steam oxidation was decreased by a factor 100, the Fe_3O_4 weight fraction profile is shifted to the left. This is due to the fact that the steam oxidation kinetics are not sufficient fast, so that the reaction front for the oxidation of $FeAl_2O_4$ to Fe_3O_4 by steam has a high overlap with the reaction front for the oxidation of Fe_3O_4 to Fe_2O_3 by oxygen. Therefore, a larger amount of $FeAl_2O_4$ is directly oxidized to Fe_2O_3 by oxygen, and the produced amount of hydrogen shows a large decrease.

Table 4.4 also shows that the average temperature of the outflowing heat removal gas stream for the cases that the reaction rate constant for the steam oxidation is decreased by a factor 100 is 10˚C higher than that of the original case. This increase in temperature can be explained by the fact that part of the $FeAl_2O_4$ is directly oxidized to Fe_2O_3 by oxygen, which has a higher heat of reaction than that of the oxidation of $FeAl_2O_4$ to Fe_3O_4 by steam with the subsequent oxidation to Fe_2O_3 by oxygen.

For all four cases, the amount of hydrogen needed for pre-heating the air stream for the heat removal cycle is the same, and therefore the amount of hydrogen available for further heating of the heat removal outlet stream decreases with decreasing reaction rate constant. From simulations with the Aspen Plus model, the temperature of the outflowing heat removal stream after combustion with hydrogen was calculated. As can be seen from Table 4.4, the temperature of this gas stream entering the gas turbine decreases with decreasing reaction rate constant. For the case that the reaction rate constant was divided by a factor 100, this means that the increase in the temperature of the outflowing heat removal stream was overruled by the decrease in hydrogen available for heating this outflowing heat removal gas stream. Since the temperature of the gas stream entering the gas turbine decreases with decreasing reaction rate constant, the produced power by the gas turbine and therefore the turbine efficiency also decreases with decreasing reaction rate constant.

The effect of the steam oxidation kinetics on the reactor performance of the pre-combustion chemical looping concept is shown in Figure 4.16. From Figure 4.16, the decrease in turbine efficiency due to slower steam oxidation kinetics can be seen (green diamonds), which decreases by around 1.1 percent points when the reaction kinetics for the oxidation of $FeAl_2O_4$ to Fe_3O_4 by steam is a factor 100 smaller than suggested by the article of Coetsee et al. [27]. Since the steam oxidation kinetics has a significant effect on the power production by the gas turbine, the results from the ongoing research concerning the steam oxidation kinetics are needed for further analysis and optimization of the performance for the pre-combustion chemical looping concept for the production of power from coal-derived syngas.

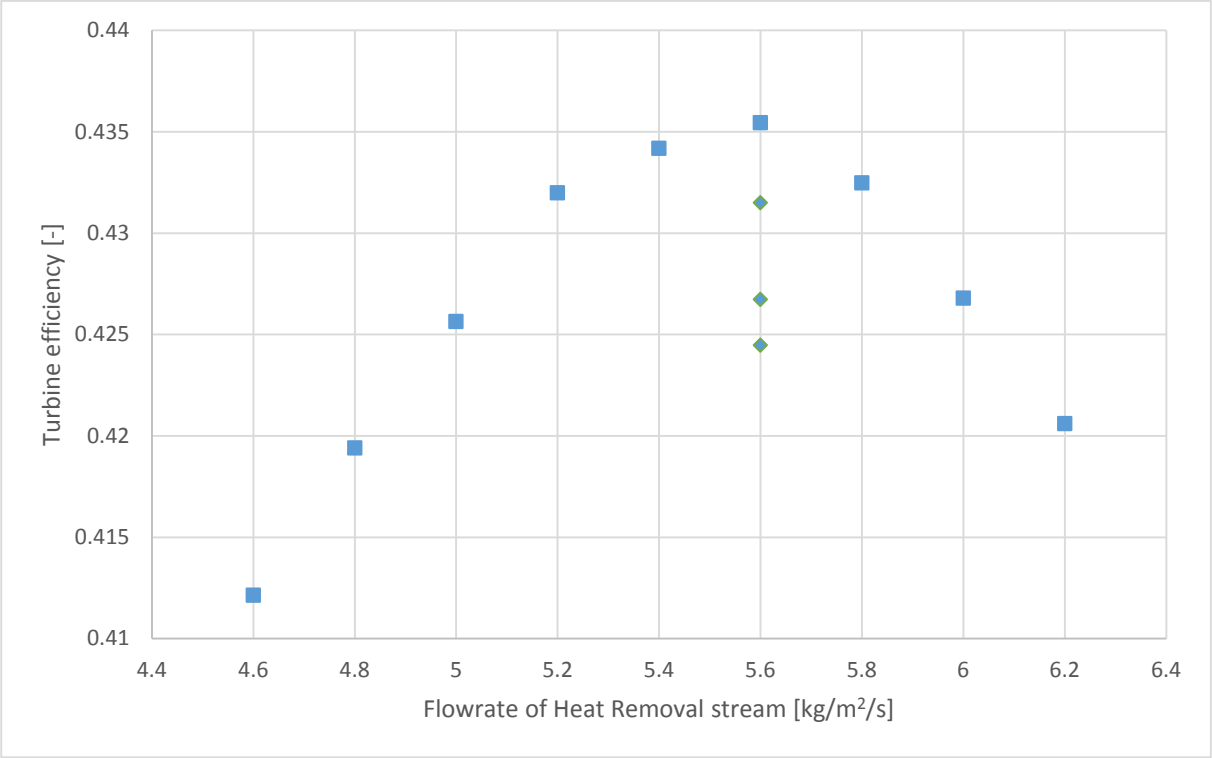

Figure 4.16 – Turbine efficiency as a function of the heat removal flowrate (blue squares: steam oxidation kinetics from Coetsee et al. [27], and green diamonds: from top down, steam oxidation kinetics from Coetsee et al. [27] divided by respectively a factor 2, 10 and 100

4.1.6 Ammonia production

The produced hydrogen during the oxidation cycle can also partially be used for the production of ammonia. When the part of the oxidant outlet stream that is not used for further heating of the outflowing heat removal stream, but for the production of ammonia, the outflowing stream from the heat removal cycle is directly fed to the gas turbine. Due to the lower temperature of the gas stream fed to the gas turbine, the produced power by the gas turbine, and therefore the turbine efficiency, will also be lower.

The ratio of hydrogen to nitrogen in the outflowing oxidant stream is around 0.94 for the optimized case with Al_2O_3 as inert material. For the production of ammonia, a mixture of hydrogen and nitrogen is needed with a hydrogen to nitrogen ratio of 3. This can be obtained by decreasing the air to steam ratio of the inflowing oxidant stream. When the ratio air to steam is decreased, the mole fraction of nitrogen is decreased, and the hydrogen to nitrogen ratio increases. Since the steam content is increased, the time needed for the oxidation of $FeAl_2O_4$ to Fe_3O_4 by steam decreases, and therefore the flowrate of the oxidant stream needs to be decreased. Due to the lower flowrate of the oxidant stream, and the lower oxygen content in the oxidant stream, not all Fe_3O_4 is oxidized to Fe_2O_3. Since the temperature rise in the reactor is mainly due to the oxidation of Fe_3O_4 to Fe_2O_3 by oxygen, an additional oxidation cycle is needed, in which air is fed to the reactor to complete the oxidation.

Since the steam oxidation of $FeAl_2O_4$ is an equilibrium reaction, the steam to hydrogen ratio, and therefore the hydrogen to nitrogen ratio during the oxidation cycle is dependent on the temperature. Therefore, additional research is needed for this heat management strategy in order to determine the air to steam ratio needed for producing an outflowing oxidant stream with a hydrogen to nitrogen ratio of 3. After determining the right air to steam ratio of the oxidant inlet stream, also additional research is needed for this heat management strategy in order to determine the performance of the pre-combustion chemical looping concept for the production of ammonia and integrated co-production of power for the case of coal-derived syngas as fuel.

4.2 Heat management strategy 2

Another heat management strategy is the removal of the stored heat after the reduction cycle. Since the oxygen carrier is then in reduced state, heat removal with air is not possible. Therefore, a pure nitrogen stream is needed for the heat removal cycle, which can be obtained from the air separation unit already present in the coal gasification plant, and by recirculation of the heat removal stream.

For this heat management strategy, it is not possible to pre-heat the heat removal stream by combustion of hydrogen, since no oxygen is available in the heat removal stream. Therefore, the heat removal inlet stream needs to be pre-heated by an external heater, which means that another additional energy input is needed. The operation sequence for this heat management strategy therefore is: (1) Oxidation by a mixture of steam and air, (2) Purge with a pure nitrogen stream, (3) Reduction by coal-derived syngas, and (4) Heat removal with a pure nitrogen stream.

For determining the performance of the PCCL concept for this heat management strategy, the operating cycles are simulated with the Delphi model for the case that the active weight fraction Fe_2O_3 is 0.4. Only this active weight fraction is simulated, since for this case the highest bed temperature after oxidation and reduction can be obtained. The inlet conditions during the simulations were the same as for heat management strategy 1, except for the composition of the inlet stream for the heat removal cycle (pure nitrogen).

The outlet gas temperature during the operating cycles as a function of time for both heat management strategies are shown in Figure 4.21. The second purge cycle with nitrogen during heat management strategy 1 is not included in this temperature profile. From Figure 4.21 can be seen that during heat management strategy 2 the temperature of the outflowing gas stream from the reduction cycle is almost as high as the temperature of the outflowing gas stream from the heat removal reactor. This means that part of the stored heat during the oxidation cycle is already removed from the reactor during the reduction cycle. This can also be seen from the bed temperature profiles at the start of the heat removal cycle, which is shown in Figure 4.22.

Also can be seen from Figure 4.21 that the outflowing heat removal stream shows a fast decrease in temperature at around 65 percent of the heat removal cycle time. This is due to the fact that the heat front is further along the reactor when the heat removal cycle is started compared to heat management strategy 1. In order to increase the turbine efficiency, the heat removal flowrate needs to be decreased. Even though it is possible to obtain an outflowing stream from the heat removal cycle with an average temperature comparable to that of heat management strategy 2, the gas stream will have a lower flowrate, which is disadvantageous for the power production.

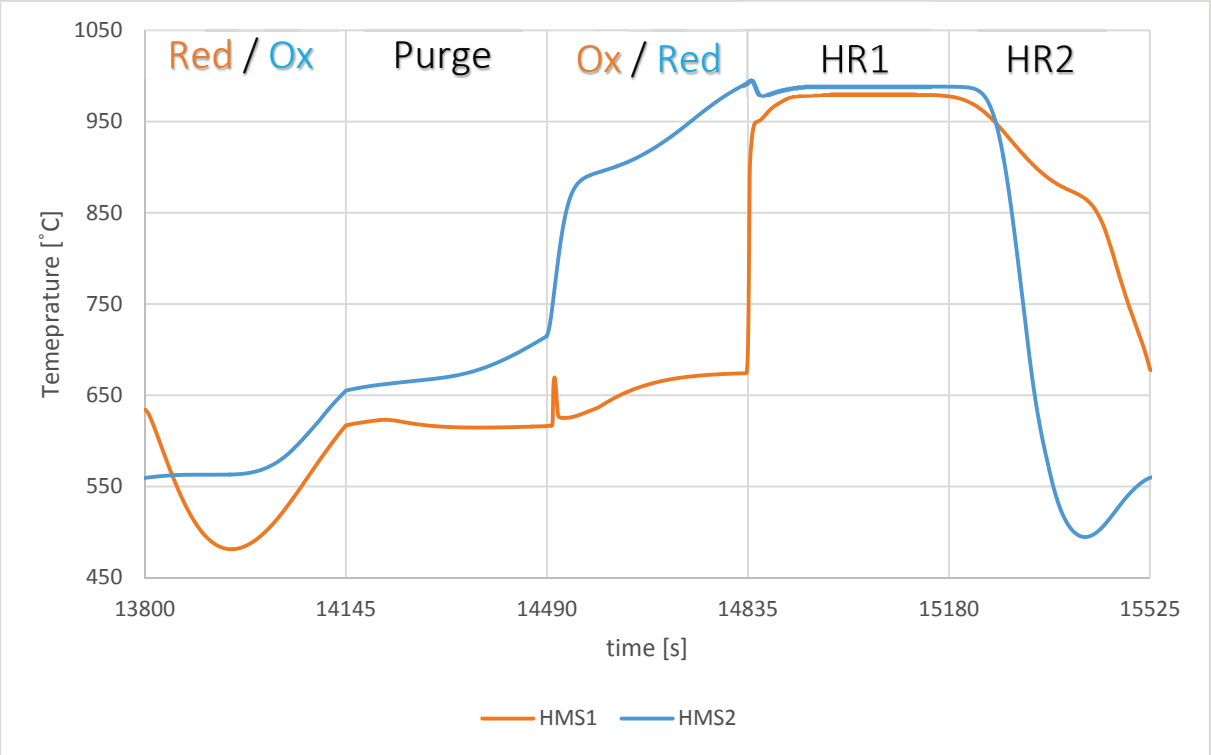

Figure 4.21 - Outlet gas temperature as a function of time for heat management strategies 1 and 2 for the case that the active weight fraction of Fe_2O_3 is 0.4

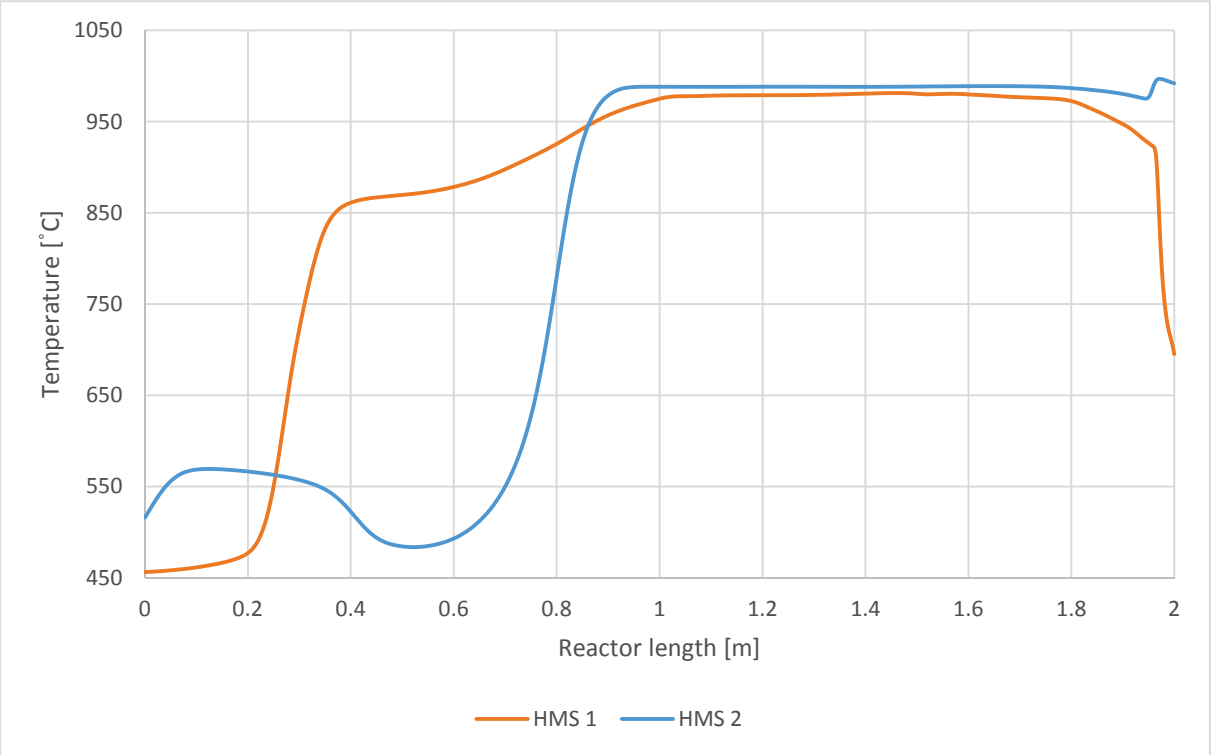

Figure 4.22 – Bed temperature as a function of the reactor length for heat management strategies 1 and 2 for the case that the active weight fraction of Fe_2O_3 is 0.4

The outflowing stream from the heat removal reactor cannot be further heated by combustion with hydrogen, since no oxygen is available in the gas stream. Since the temperature of the outflowing stream from the heat removal reactor is at relative low temperature, also the power production in the turbine and the turbine efficiency will be low. Therefore, this heat management strategy is not preferable for the production of power from coal-derived syngas.

For this heat management strategy, the produced hydrogen during the oxidation stage cannot be used for the heating the outflowing heat removal stream in order to produce power in a gas turbine with a high turbine efficiency. It is possible to use the produced hydrogen for the production of ammonia. Since still additional energy is needed for the separation unit and the pre-heating of the inflowing heat removal stream, and the gas stream entering the gas turbine has a lower and flowrate, the production of ammonia with the co-production of power from coal-derived syngas is also not preferable with this heat management strategy.

5 Results and discussion: Natural gas

For the case that natural gas is used as the fuel, only one heat management strategy is possible, since the produced heat during the oxidation cycle is already (partially) removed from the reactor during the reduction cycle due to the highly endothermic methane reforming reactions. For this case, also the effect of the active weight fraction of oxygen carrier on the performance of the PCCL concept will be discussed. The performance of the PCCL concept will be optimized for the production of a H_2/N_2-rich stream for the production of ammonia for the case that the preferable active weight fraction of oxygen carrier. Therefore, the steam to air ratio of the inflowing oxidant stream is varied, in order to obtain a hydrogen to nitrogen ratio of 3 in the outflowing oxidation stream. Finally, also the effect of the steam oxidation kinetics on the performance of the PCCL concept for the production of ammonia is analyzed.

5.1 Natural gas power plant integrated with the PCCL process

Natural gas can also be used as fuel for the production of power with the pre-combustion chemical looping concept. Since the reduction of Fe_2O_3 to $FeAl_2O_4$ by methane is highly endothermic, the stored heat during the oxidation cycle due to the highly exothermic oxidation of Fe_3O_4 to Fe_2O_3 by oxygen is already removed, which means that no additional heat removal cycle is needed. Therefore, the operation sequence will be: (1) Reduction by methane, (2) Purge with a pure nitrogen stream, (3) Oxidation by a steam/air mixture, and (4) Purge with a pure nitrogen stream. Since purge cycles are needed between the oxidation and reduction cycles, only one heat management strategy is possible.

Since no heat removal cycle is needed, the natural gas power plant integrated with the PCCL process will remain the same as already described in the article by Spallina et al. [?. For a description of the natural gas power plant integrated with the PCCL process, the reader is referred to the article Spallina et al. [36].

5.2 Determining flowrate for oxidant cycle

The ratio of oxidant to reductant flowrate is determined by the mole fractions of the reacting components according to equation 4.1, and the equilibrium constant for the steam oxidation.

The composition of the inlet streams were taken from Spallina et al. [36], even as the inlet temperatures and pressures, and are shown in Table 5.1 As can be seen from Table 5.1, there is in excess of steam and carbon dioxide in the gas stream fed to the reduction reactor for the methane reforming reactions, and therefore the only the mole fractions of methane, carbon monoxide and hydrogen have to be taken into account for determining the needed oxidant flowrate. Assumed is that during the reduction cycle there will be a full conversion of hydrogen and carbon monoxide to steam and carbon dioxide.

The equilibrium constant, which is temperature dependent, determines the ratio of produced hydrogen to unreacted steam, and therefore determines the flowrate needed for complete oxidation of the oxygen carrier during the oxidation cycle. From the Delphi model, the fraction of converted steam was calculated to be 0.477.

The needed flowrate for the oxidation cycle is determined by combining the results from the Delphi model with the Aspen Plus model. Therefore, the conversion of the water-splitting reaction was set to the fraction of converted steam as obtained from the Delphi model, and a design spec was introduced in which the oxidant flowrate was the changing variable in order to obtain the same outlet composition as obtained from the Delphi model. A ratio of oxidant to reduction flowrate of 1.94 was determined from the Aspen Plus model, which means that for a reductant flowrate of 1 kg/m^2/s an oxidant flowrate of 1.94 kg/m^2/s is needed for the case that natural gas is used as fuel. This oxidant inlet flowrate is much higher than for the case with coal-derived syngas as fuel since the mole fraction of methane is much lower than that of hydrogen/carbon monoxide in the inflowing reductant stream.

Table 5.1 – Inlet condition for the reduction, oxidation and purge cycle

		Reduction	**Oxidation**	**Purge**
Mole fraction [mol_i/mol_g]	**Ar**	-	0.004	-
	CH_4	0.229	-	-
	CO	0.003	-	-
	CO_2	0.196	-	-
	H_2	0.048	-	-
	H_2O	0.513	0.596	-
	N_2	0.010	0.315	1.0
	O_2	-	0.085	-
Temperature [˚C]		600.0	777.0	397.5
Pressure [bar]		25.49	20.5	20.0
Flowrate [kg/m^2/s]		1.00	1.94	0.10

In order to have a pseudo-continuous operation, the cycle time for each operating step needs to be the same, unless several reactors are operated in parallel for one operating step. The cycle time is dependent on the active weight fraction of the oxygen carrier, and the dimensions of the reactor. For the Delphi simulations, the reactor length was 2 meter and the reactor diameter was 0.5 meter, and therefore the needed cycle time for each operating step for the case that the active weight fraction of Fe_2O_3 is 0.2, 0,3 and 0.4 is respectively 65, 100 and 140 seconds.

For the case that natural gas is used as fuel, the operating steps with a cycle time of τ are shown in Figure 5.1 for each reactor.

	R1	R2	R3	R4
τ	**RED**	**P**	**OX**	**P**
τ	**P**	**OX**	**P**	**RED**
τ	**OX**	**P**	**RED**	**P**
τ	**P**	**RED**	**P**	**OX**

Figure 5.1 – Operating steps of each reactor for the case that natural gas is used as fuel

5.3 Effect of active weight fraction of Fe_2O_3 on performance of the PCCL concept

Now all the inlet conditions are known for the three cases with different active weight fractions of Fe_2O_3, the performance of the pre-combustion chemical looping concept can be determined for each case with the results from the Delphi model.

In order to determine if the temperature decrease due to the endothermic reduction reactions is indeed sufficient for removing the produced heat during the oxidation cycle, the bed temperature profiles after the reduction and oxidation cycle are needed. These bed temperature profiles are obtained from simulations with the Delphi model for each of the three different active weight fractions of Fe_2O_3. The bed temperature profiles after the reduction and the oxidation cycle are shown in Figure 5.2-5.4 for the case that the active weight fraction of Fe_2O_3 was respectively 0.2, 0.3 and 0.4.

From the bed temperature profiles of Figure 5.2-5.4 can be seen that a large amount of heat is removed from the reactor due to the methane reforming reactions during the reduction cycle, due to the absence of a heat plateau along the reactor. This indicates that a heat removal cycle is indeed not needed.

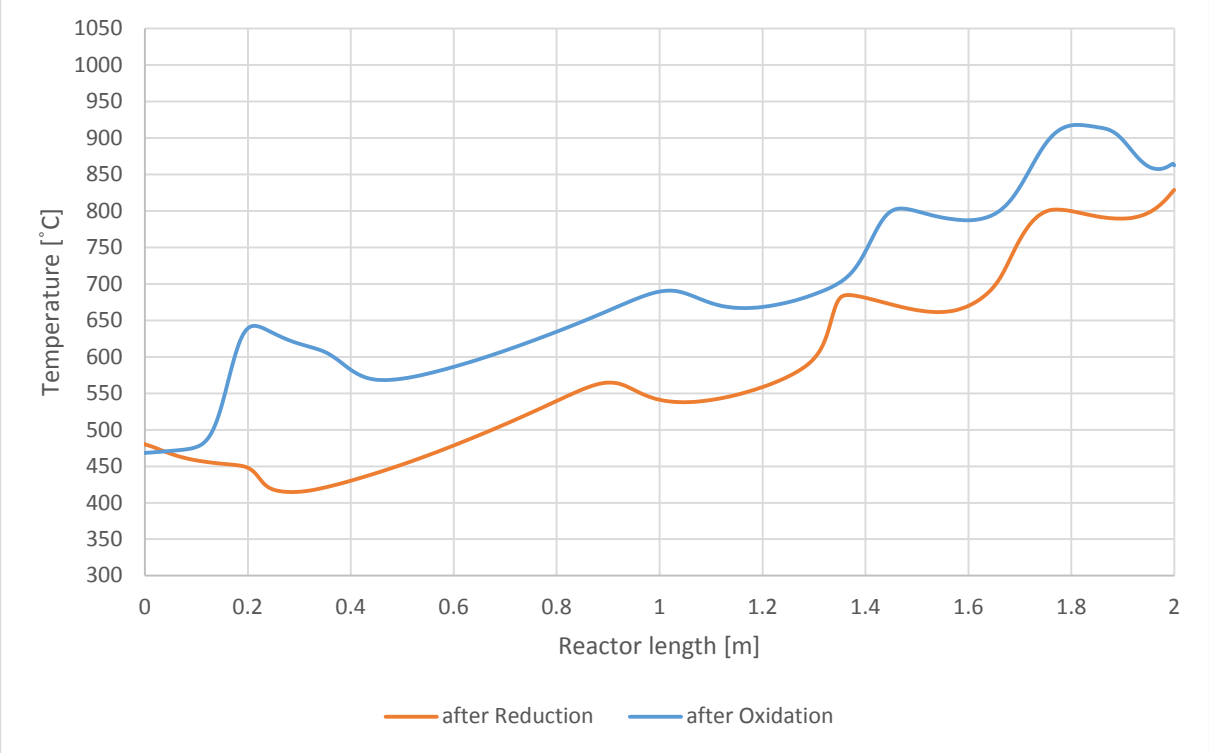

Figure 5.2 – Bed temperature profile after reduction and oxidation for the case that the active weight fraction Fe_2O_3 is 0.2

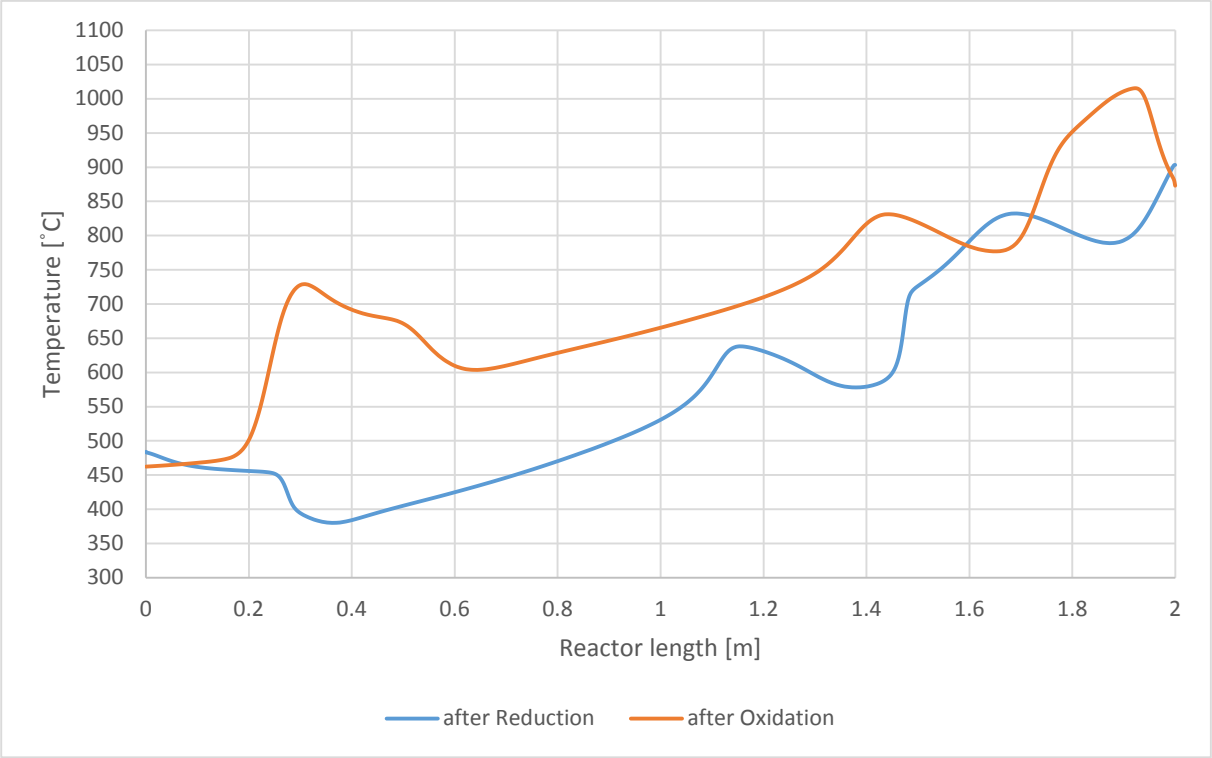

Figure 5.3 – Bed temperature profile after reduction and oxidation for the case that the active weight fraction Fe_2O_3 is 0.3

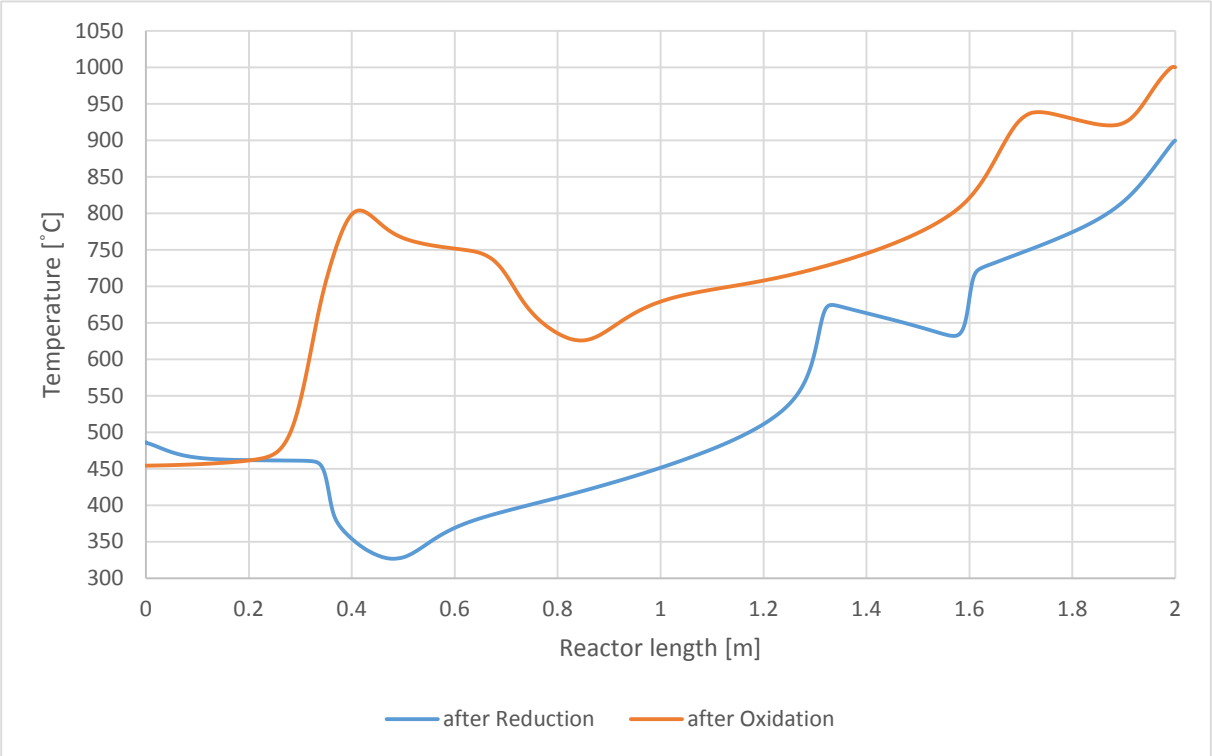

Figure 5.4 – Bed temperature profile after reduction and oxidation for the case that the active weight fraction Fe_2O_3 is 0.4

Also can be seen from Figure 5.2-5.4 that the maximal difference between the minimum and the maximum bed temperature is the lowest for the case that the active weight fraction of Fe_2O_3 is 0.2. This is advantageous for the life-time of the solid material, since it has to endure smaller temperature fluctuations during the sequentially switched reduction and oxidation cycles.

The outlet temperature profiles during each operating cycle are shown in Figure 5.5 for each of the simulated weight fractions of Fe_2O_3. From Figure 5.5 can be seen that the fluctuations in temperature of the outflowing N_2/H_2 stream from the oxidation reactor and the outflowing CO_2/H_2O stream from the reduction reactor is the lowest for the case that the active weight fraction of Fe_2O_3 is 0.2, which is advantageous for the pseudo-continuous power and ammonia production processes downstream. Therefore, the performance of the PCCL concept for the production of ammonia with natural gas as fuel will be optimized for the case that the active weight fraction of Fe_2O_3 is 0.2.

The average outlet composition of the outflowing reductant and oxidant stream for this case are shown in Table 5.2, and the outlet composition of the outflowing gas streams for each operating step as a function of time are shown in Figure 5.6. From both Table 5.2 and Figure 5.6 can be seen that during the reduction cycle there is almost no fuel slip, since the average mole fractions of hydrogen and carbon dioxide in the outflowing reductant is stream are almost zero, and the breakthrough of hydrogen and carbon monoxide is after the reduction cycle. Also can be seen from Figure 5.6 that the oxygen breakthrough is at the cycle switch between the oxidation and subsequent purge cycle, which means that the oxygen carrier is almost completely oxidized to Fe_2O_3. Nevertheless, the oxygen carrier is fully oxidized by the remaining oxygen from the oxidant stream that is blown out of the reactor during the purge stage. This can be seen from the increase in temperature of the outflowing gas stream during the purge with nitrogen after the oxidation cycle, and from the mole fraction of oxygen shown in Figure 5.6, which increases to the inlet mole fraction of oxygen halfway the subsequent purge cycle.

The carbon dioxide purity that can be obtained after water condensation of the reductant outlet stream can be calculated from the mole fractions of the outflowing gas components from the reduction cycle shown in Table 5.2, and has a value of 94.5 %.

Table 5.2 - Average outlet compositions during the reduction and oxidation cycle

		Reduction	**Oxidation**
Mole fraction [mol_i/mol_g]	**CH_4**	-	-
	CO	0.003	-
	CO_2	0.291	-
	H_2	0.006	0.362
	H_2O	0.692	0.254
	N_2	0.007	0.383
	O_2	-	-

From Table 5.2 also can be seen that the ratio of hydrogen to nitrogen in the outflowing gas stream of the oxidation cycle is 0.945. For the production of ammonia, the hydrogen to nitrogen ratio of the outflowing gas stream of the oxidation cycle needs to be 3. In order to obtain this hydrogen to nitrogen ratio, a sensitivity analysis of the oxygen content in the inflowing oxidant stream on the hydrogen to nitrogen ratio is performed. When the steam content of the oxidant stream is increased, the oxidation of $FeAl_2O_4$ to Fe_3O_4 by hydrogen is finished in a shorter time, which means that after that moment only steam and nitrogen is flowing out of the reactor. Therefore, the ratio of hydrogen to nitrogen decreases. In order to prevent this, the flowrate for this oxidant stream needs to be decreased.

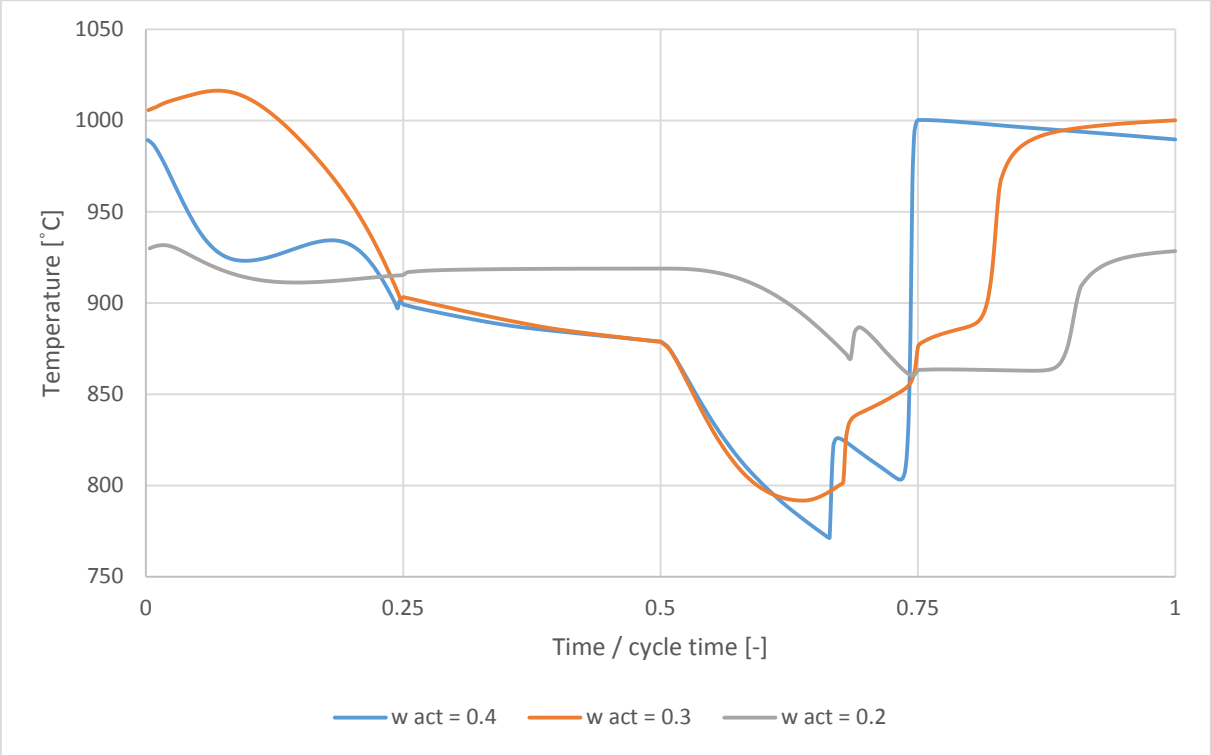

Figure 5.5 – Temperature of the outflowing gas stream during respectively the reduction, purge, oxidation and purge cycle for different active weight fraction of Fe_2O_3

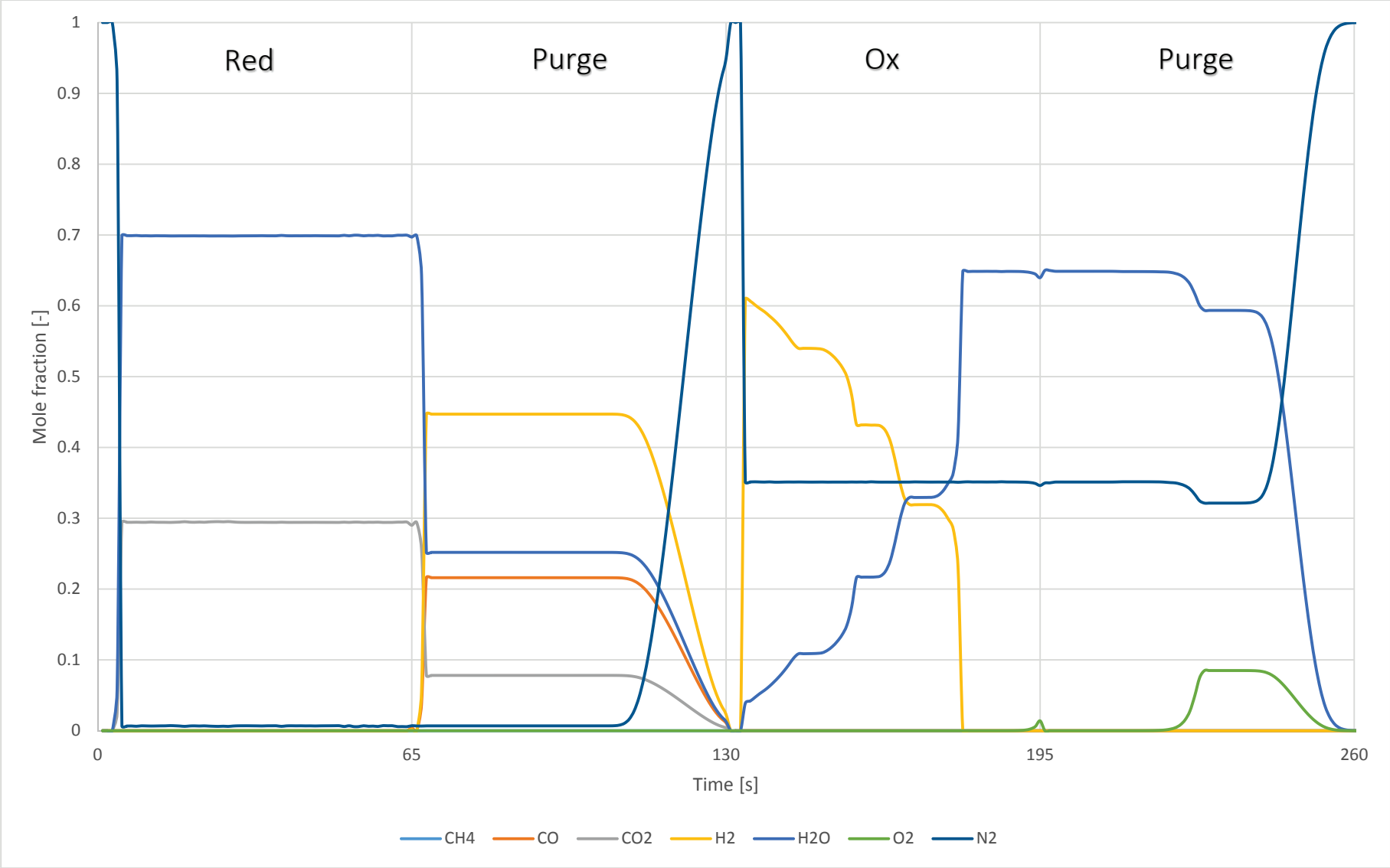

Figure 5.6 – Composition of the gas stream exiting sequentially the reduction, purge, oxidation and purge reactor as a function of the time

5.4 Effect of O_2 content in oxidant inlet stream on produced H_2/N_2 ratio

For the production of ammonia, a mixture of hydrogen and nitrogen with a ratio of 3 is needed. This can be obtained by decreasing the air to steam ratio of the inflowing oxidant stream. Due to the higher steam content of the inflowing oxidant stream, the time needed for full oxidation of $FeAl_2O_4$ to Fe_3O_4 by steam will be lower. Since the cycle times of each operating step needs to remain the same in order to have a pseudo-continuous operation, a smaller flowrate of the inflowing oxidant stream is needed. The needed oxidant flowrate decreases with decreasing oxygen content of the inflowing oxidant stream. Due to the lower oxygen content in the inflowing oxidant stream, not all Fe_3O_4 will be oxidized to Fe_2O_3 by oxygen during the oxidation cycle. In order to obtain a full conversion of the oxygen carrier, an additional oxidation cycle is needed in which air is fed to the reactor. The needed flowrate for the air oxidation cycle is equal to the original flowrate (1.94 kg/m^2/s) minus the flowrate needed during the first oxidation cycle, which therefore increases with decreasing oxygen content in the inflowing oxidant stream.

Since the hydrogen to nitrogen ratio of the outflowing oxidant stream is dependent on the bed temperature, it is hard to predict for which exact oxygen content the average hydrogen to nitrogen ratio of the outflowing oxidant stream will be 3. Therefore, different oxygen contents of the inflowing oxidant stream were simulated with the Delphi model. The different mole fraction of oxygen of the inflowing oxidant stream were 0.04, 0.045, 0.05, 0.055 and 0.06. The inlet compositions of the oxidant stream for both the first and second oxidation cycle, and the corresponding oxidant flowrates are shown in Table 4.8 for each simulated case.

The average hydrogen to nitrogen ratio of the outflowing gas stream from the first oxidation cycle is shown in Figure 5.7 for the five cases with different oxygen contents of the inlet oxidant stream. From Figure 5.7 can be seen that indeed the average hydrogen to nitrogen ratio of the outflowing oxidant stream increases with decreasing oxygen content of the inflowing oxidant stream. An estimate of the exact oxygen content of the oxidant inlet stream for obtaining an average hydrogen to nitrogen ratio of 3 of the oxidant outlet stream was made by fitting a parabolic line through the data points.

Table 4.8 – Inlet composition and flowrate for both oxidation cycles for different oxygen contents of the inlet flow for the first oxidation cycle

y_{O_2}		0.04		0.045		0.05		0.055		0.06	
Oxidation cycle		**1**	**2**	**1**	**2**	**1**	**2**	**1**	**2**	**1**	**2**
y_i [-]	**H_2O**	0.809	0.001	0.785	0.001	0.761	0.001	0.737	0.001	0.713	0.001
	N_2	0.151	0.772	0.170	0.772	0.189	0.772	0.208	0.772	0.227	0.772
	O_2	0.040	0.207	0.045	0.207	0.050	0.207	0.055	0.207	0.060	0.207
Flowrate [kg/m²/s]		1.125	0.817	1.175	0.767	1.230	0.712	1.284	0.658	1.344	0.598

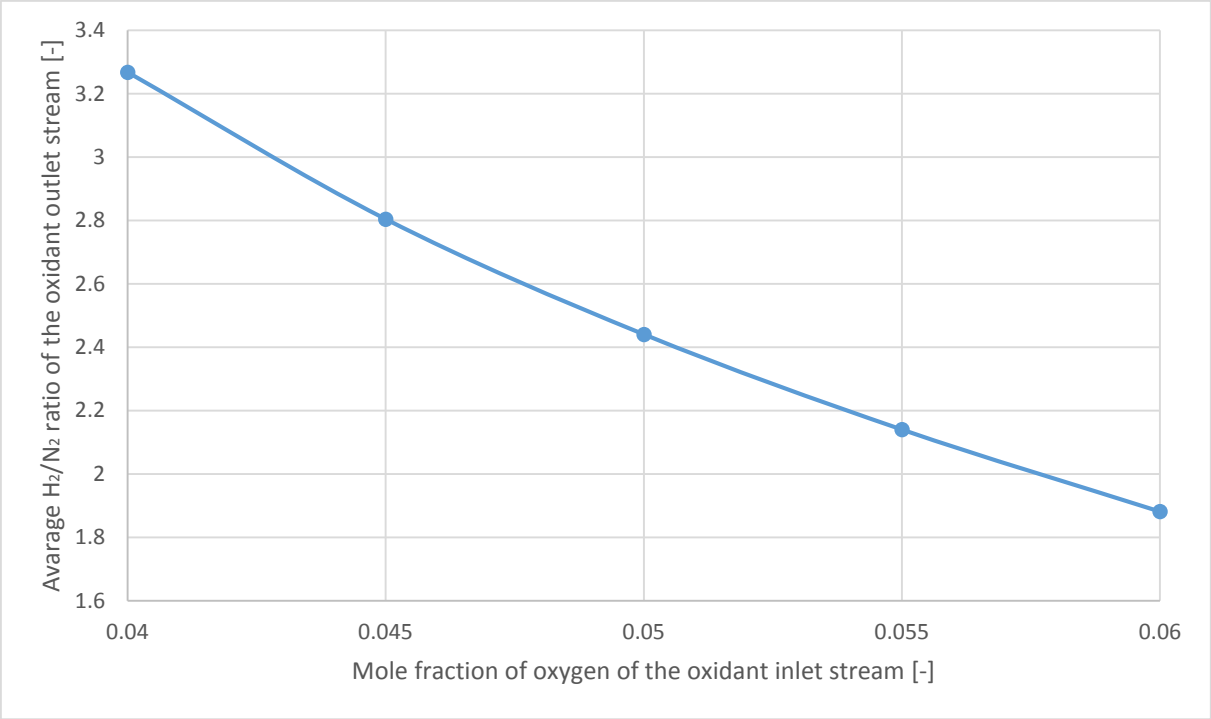

Figure 5.7 – Average hydrogen to nitrogen ratio of the outflowing oxidant stream as a function of the mole fraction of oxygen of the inflowing oxidant stream

The estimated oxygen content of the oxidant inlet stream is 0.0428. The inlet compositions and flowrates for this case are shown in Table 5.3 for both oxidation cycles. The temperature of the outflowing gas stream exiting sequentially the reduction, purge, first oxidation, second oxidation and second purge cycle is obtained from the Delphi model for the case that the oxygen content of the oxidant inlet stream is 0.0428, and is shown in Figure 5.8.The outlet composition of the gas stream exiting during each operating step as a function of the time is also obtained from the Delphi model for this case, and is shown in Figure 5.8.

From Figure 5.9 can be seen that the indeed the mole fraction of hydrogen during the first oxidation cycle is increased and the mole fraction of nitrogen is decreased in comparison with the previous case that the oxygen content of the oxidant inlet stream is 8.5%. Also can be seen from both Figure 5.8 and Figure 5.9 that the bed is fully oxidized to Fe_2O_3 by oxygen during the second oxidation cycle, since the mole fraction of oxygen increases to the inlet mole fraction after around 80% of the cycle time, and the temperature rise due to the oxidation of Fe_3O_4 to Fe_2O_3 by oxygen is coming out of the reactor at that same moment.

The plant performance can be increased by decreasing the air flowrate fed to the second oxidation reactor, since then less power is needed for the compression of this air stream to 20.5 bar. This further optimization of the PCCL performance beyond the scope of this research.

The average outlet compositions for the reduction cycle and both oxidation cycles are obtained from the Delphi model, and are shown in Table 5.4. From Table 5.4 can be seen that the outlet stream from the first oxidation cycle has a hydrogen to nitrogen ratio of 2.99, which is indeed close to 3. The carbon dioxide purity can be calculated from the mole fractions of the outflowing gas stream from the reduction cycle shown in Table 4.10, and has a value of 94.7%.

Table 5.3 – Inlet composition and flowrate for both oxidation cycles for the case that the oxygen content in the inflowing oxidant stream is 0.0428

		Oxidation 1	Oxidation 2
Mole fraction [mol_i/mol_g]	**H_2O**	0.7953	0.001
	N_2	0.1619	0.772
	O_2	0.0428	0.207
Flowrate [$kg/m^2/s$]		1.153	0.789

Table 5.4 - Average outlet compositions during the reduction cycle and oxidation cycles

		Reduction	Oxidation 1	Oxidation 2
Mole fraction [mol_i/mol_g]	**CH_4**	-	-	-
	CO	0.0035	-	-
	CO_2	0.2909	-	-
	H_2	0.0073	0.5052	-
	H_2O	0.6917	0.3256	0.0013
	N_2	0.0066	0.1692	0.9632
	O_2	-	-	0.0355

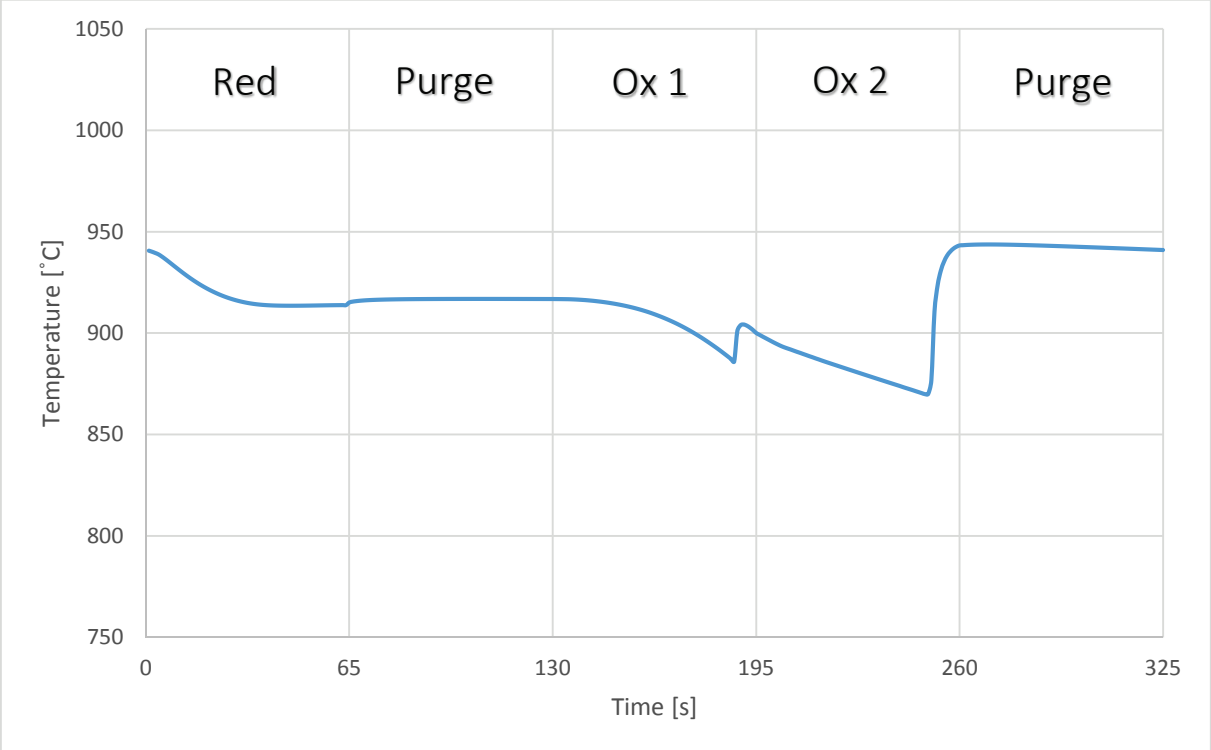

Figure 5.8 – Temperature of the outflowing gas stream from the operating steps

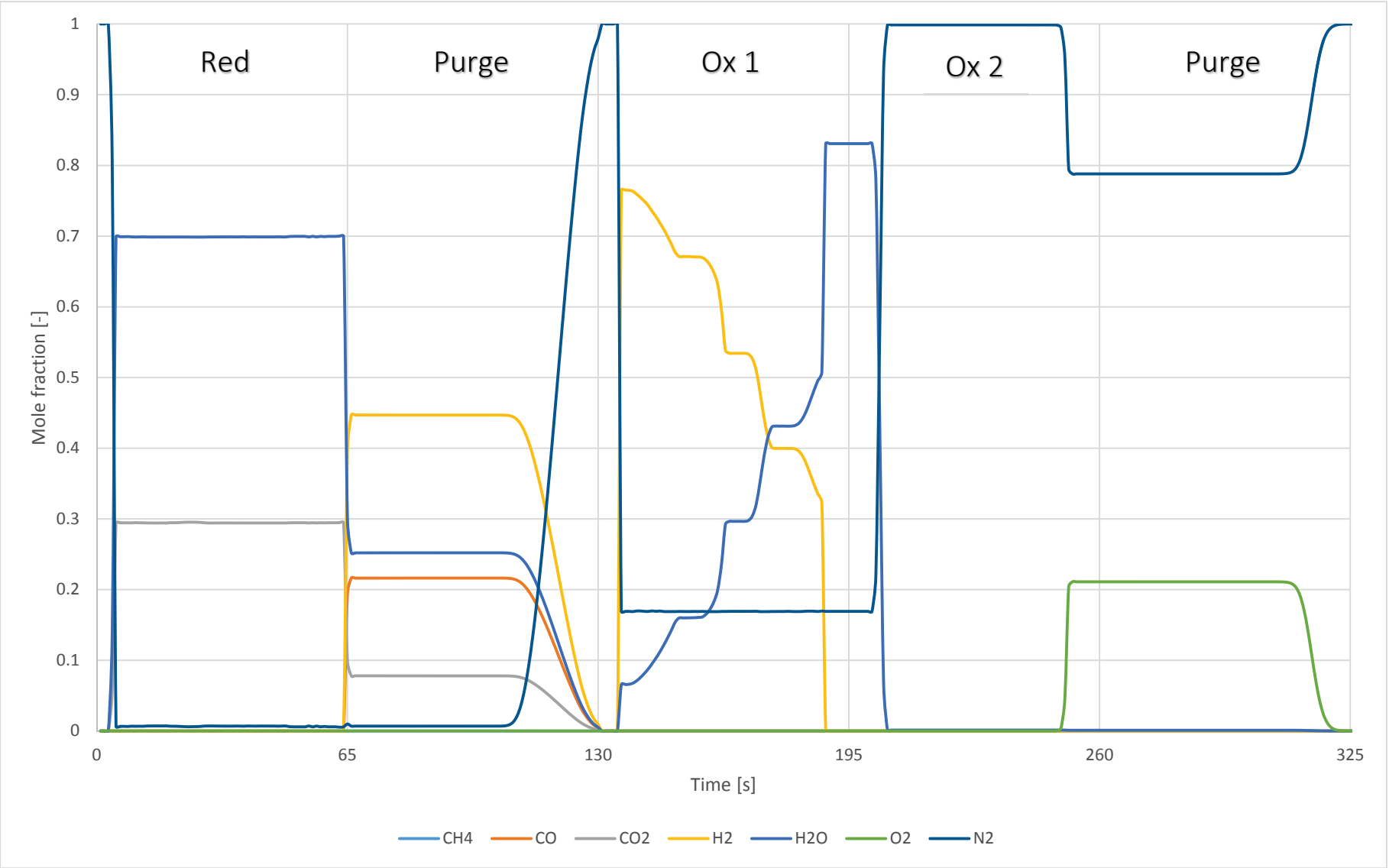

Figure 5.9 – Composition of the outflowing gas stream during each operating step

5.5 Effect of steam oxidation kinetics on the performance of the PCCL concept

As described in section 3.2, there are two possible pathways for the oxidation of the oxygen carrier, namely either the oxidation of $FeAl_2O_4$ to Fe_2O_3 by oxygen or the oxidation of $FeAl_2O_4$ to Fe_3O_4 by steam and the subsequent oxidation of Fe_3O_4 to Fe_2O_3 by oxygen. Since the oxidation of $FeAl_2O_4$ to Fe_3O_4 by steam is crucial for the hydrogen production during the oxidation cycle, the performance of the pre-combustion chemical looping concept for the production of ammonia and the co-production of power from natural gas is dependent on the steam oxidation kinetics.

Since the steam oxidation kinetics as suggested by Coetsee et al. [27] are not validated yet, the reaction rate constant for the oxidation of $FeAl_2O_4$ to Fe_3O_4 by steam as suggested by Coetsee et al. [27] were also decreased by a factor 2, 10 and 100 in order to determine the effect of the steam oxidation kinetics on the performance of the PCCL concept for the case of natural gas as fuel. The performance of the PCCL concept for ammonia production is mainly determined by the amount of produced hydrogen during the oxidation cycle, since the amount of nitrogen can be tuned with the steam to air ratio.

The case from section 5.4, in which the steam to air ratio of the inflowing gas stream to the first oxidation cycle was optimized for producing a hydrogen to nitrogen ratio of 3, was used as the base case for determining the effect of the steam oxidation kinetics on the performance of the PCCL concept for ammonia production. For the case that the reaction rate constant for the steam oxidation was decreased by a factor 2, 10 and 100, the same inlet conditions as for the base case were used. The obtained average outlet composition for both oxidation cycles with the corresponding hydrogen to nitrogen ratios are shown in Table 4.11 for the four cases with different values of the reaction rate constant for the steam oxidation.

Table 5.5 – Average outlet composition and hydrogen to nitrogen ratio of the outflowing oxidant streams for different values of the reaction rate constant for the steam oxidation

		k		**k/2**		**k/10**		**k/100**	
Oxidation cycle		**1**	**2**	**1**	**2**	**1**	**2**	**1**	**2**
Mole fraction [mol_i/mol_g]	**H_2**	0.5052	-	0.5018	-	0.4932	-	0.3960	0.0004
	H_2O	0.3256	0.0013	0.3290	0.0013	0.3377	0.0013	0.4348	0.0009
	N_2	0.1692	0.9632	0.1691	0.9631	0.1961	0.9719	0.1692	0.9987
	O_2	-	0.0355	-	0.0356	-	0.0268	-	-
Ratio H_2/N_2 [-]		2.986	-	2.967	-	2.916	-	2.341	0.0004

From Table 5.5 can be seen that the ratio hydrogen to nitrogen is decreasing with decreasing reaction rate constant. The hydrogen to nitrogen ratio can be increased by decreasing the oxygen content in the gas stream fed to the first oxidation cycle. Since the amount of $FeAl_2O_4$ oxidized by steam decreases with decreasing reaction rate constant, the flowrate fed to the first oxidation cycle needs to be decreased. As a consequence, a smaller product stream with a hydrogen to nitrogen ratio of 3 is produced.

The outlet composition of the gaseous components during the first oxidation cycle are shown in Figure 5.10. From both Table 5.5 and Figure 5.10 can be seen that the average mole fraction of hydrogen in the outflowing gas stream from the first oxidation cycle decreases with decreasing reaction rate constant for the steam oxidation. This is due to a higher amount of $FeAl_2O_4$ directly oxidized by oxygen instead of steam. Since only hydrogen is produced during the oxidation of $FeAl_2O_4$ to Fe_3O_4 by steam, the amount of produced hydrogen decreases when a higher amount of $FeAl_2O_4$ is oxidized by oxygen.

From Figure 5.10 can also be seen that the mole fraction of hydrogen is zero at the end of the first oxidation cycle for the original case and the case that the reaction rate constant is decreased by a factor 2 and 10. This means that for these cases there is a full conversion of $FeAl_2O_4$ to Fe_3O_4 by steam oxidation. For the case that the reaction rate constant for the steam oxidation is decreased by a factor 100, the mole fraction of hydrogen is not equal to zero at the end of the first oxidation cycle, which means that no full conversion of $FeAl_2O_4$ to Fe_3O_4 is obtained for this case, while the same amount of steam is fed to the first oxidation cycle. This can also be seen from the weight fraction of FeO as a function of the reactor length for the case that the reaction rate constant is decreased by a factor 100 as shown in Figure 5.11. This can be explained by the higher average bed temperature during the first oxidation cycle. The equilibrium constant for the oxidation of $FeAl_2O_4$ to Fe_3O_4 by steam increases with increasing temperature. Therefore, the steam to hydrogen ratio at equilibrium is higher, which means that the steam excess during the oxidation of $FeAl_2O_4$ to Fe_3O_4 increases, and therefore also the time needed for full oxidation of $FeAl_2O_4$ to Fe_3O_4 increases.

Figure 5.11 also shows that at around a reactor length of 0.5 m a small amount of the $FeAl_2O_4$ is not oxidized. This is due to low temperature in that part of the reactor which will lead to slower kinetics for the steam oxidation of $FeAl_2O_4$ to Fe_3O_4, and due to the fact that the oxygen from the inflowing gas stream did not yet reach this part of the reactor in which part of the $FeAl_2O_4$ is not totally oxidized. This can also be seen from Figure 5.12, which shows the Fe2O3 fraction along the reactor length at the end of the first oxidation cycle. When the weight fraction of Fe2O3 is zero, both FeAl2O4 and Fe3O4 are not oxidized by oxygen, which means that the oxygen from the inflowing oxidant stream did not yet reach this part of the reactor.

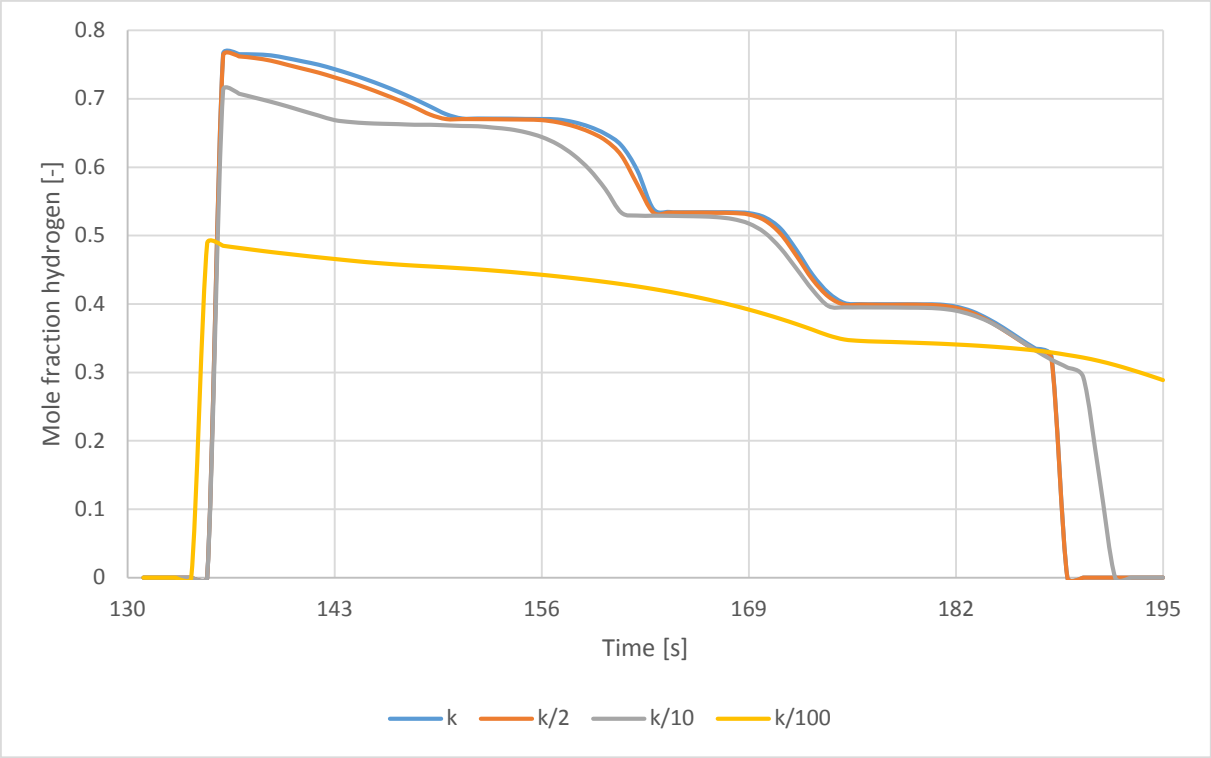

Figure 5.10 – Mole fractions of hydrogen in the outflowing gas stream from the first oxidation cycle for different values of the reaction rate constant for steam oxidation

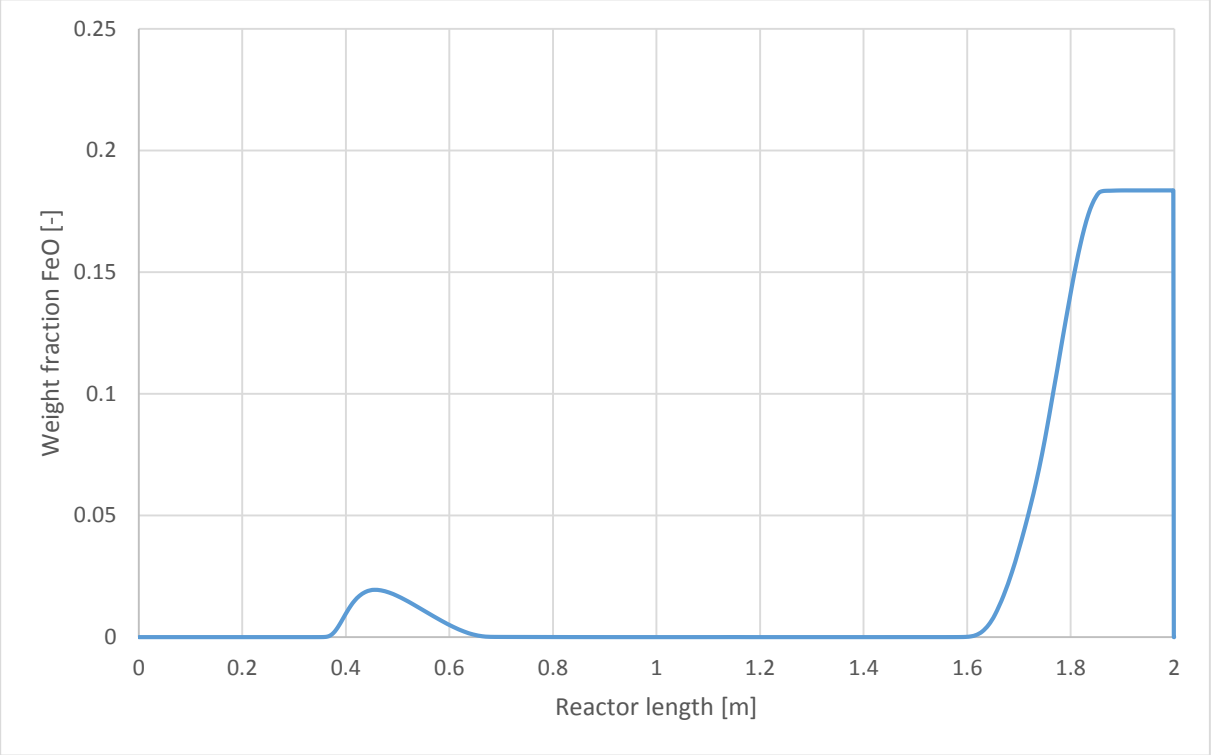

Figure 5.11 – Weight fraction FeO as a function of the reactor length after the first oxidation cycle for the case that the reaction rate constant for steam oxidation is decreased by factor 100

The increasing amount of $FeAl_2O_4$ oxidized by oxygen with decreasing value of the reaction rate constant for steam oxidation can also be seen from Figure 5.12, in which the weight fraction of Fe_2O_3 in the bed is plotted as a function of the reactor length. Figure 5.12 shows that the total amount of formed Fe_2O_3 decreases with decreasing value of the reaction rate constant for steam oxidation. Since the same amount of oxygen is fed to the first oxidation cycle for all cases, and a higher amount of oxygen is needed for the oxidation of $FeAl_2O_4$ to Fe_2O_3 than for the oxidation of Fe_3O_4 to Fe_2O_3, the amount of formed Fe_2O_3 during the first oxidation cycle decreases with increasing amount of $FeAl_2O_4$ oxidized by oxygen.

When a larger amount of $FeAl_2O_4$ is oxidized by air during the first oxidation cycle, also the temperature rise within the bed will be larger during this oxidation cycle, since the oxidation of $FeAl_2O_4$ to Fe_2O_3 by air is more exothermic than the oxidation of $FeAl_2O_4$ to Fe_3O_4 by oxygen and the subsequent oxidation to Fe_2O_3 by air. This will also lead to a higher average outlet temperature of the gas stream exiting the second oxidation cycle, which can be seen from Figure 5.13.

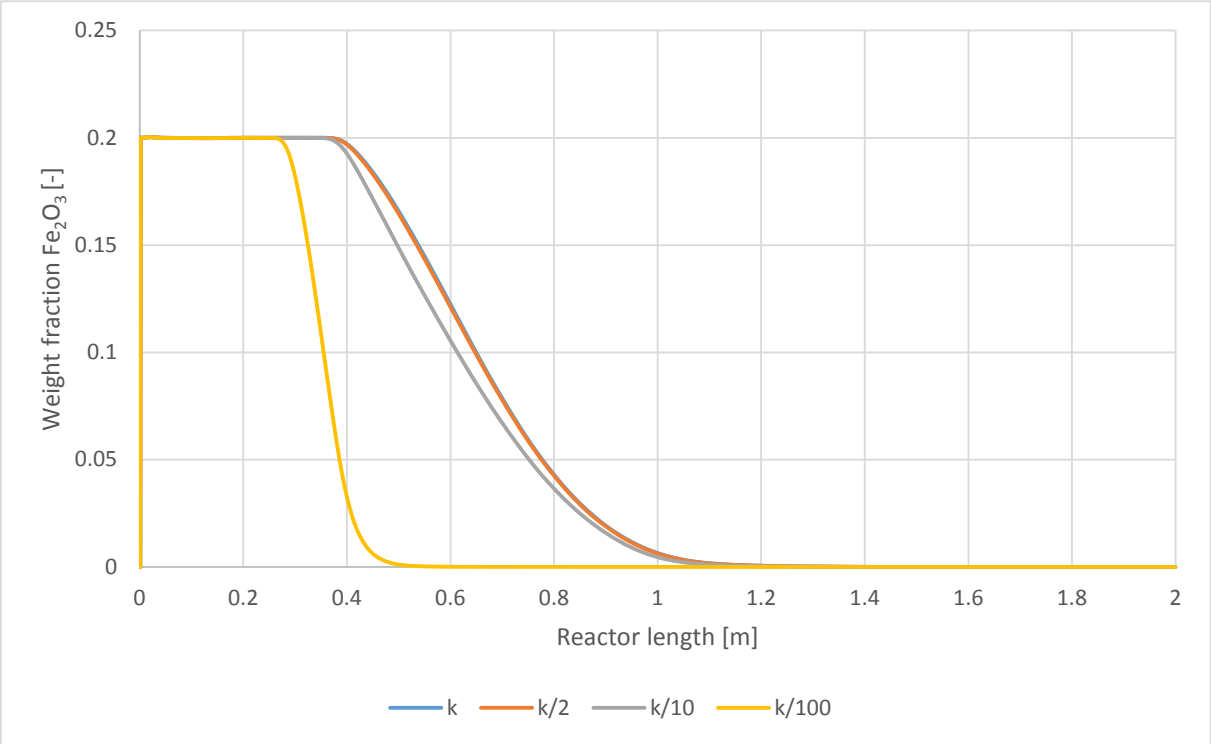

Figure 5.12 – Weight fraction Fe_2O_3 as a function of the reactor length after the first oxidation cycle for different values of the reaction rate constant for steam oxidation

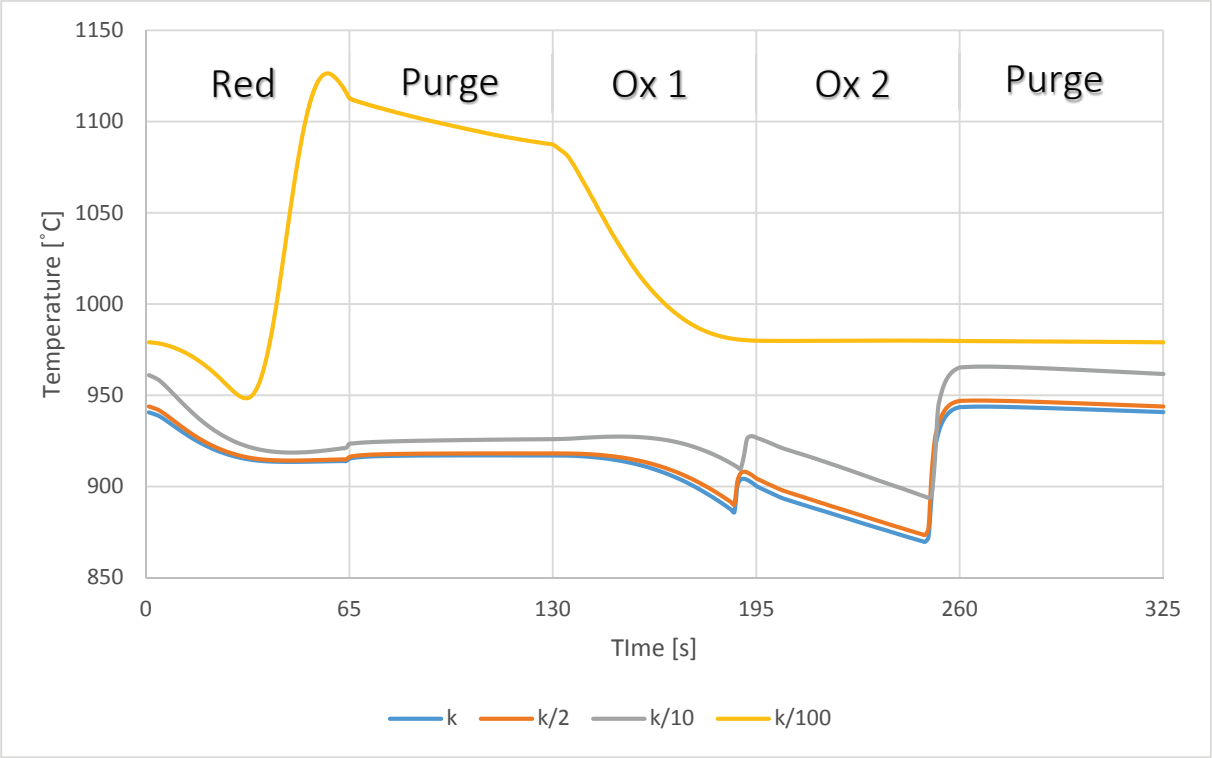

Figure 5.13 – Temperature of the outflowing gas stream during respectively the reduction, purge, first and second oxidation and purge cycle for different values of the reaction rate constant for steam oxidation

Since for the case that the reaction rate constant is decreased by a factor 100 the amount of formed Fe_3O_4 and Fe_2O_3 is much smaller than for the other three cases, more oxygen is needed for full conversion of the oxygen carrier to Fe_2O_3. Figure 5.14 shows the weight fraction of Fe_2O_3 as a function of the reactor length. From Figure 5.14 can be seen that the amount of oxygen fed during the second oxidation cycle is not sufficient for the full conversion of the oxygen carrier to Fe_2O_3, since part of the bed near the reactor outlet has a Fe_2O_3 weight fraction of zero. This can also be seen from the temperature profile of the outflowing gas stream for the case that the reaction rate constant for the steam oxidation is decreased by a factor 100. The heat produced by the exothermic oxidation of Fe_3O_4 to Fe_2O_3 by oxygen during the second oxidation cycle is removed from reactor at around half the cycle time of the subsequent reduction cycle, instead of at the end of the second oxidation cycle itself.

Since the production of a H_2/N_2 mixture with a ratio of 3 for the ammonia production is highly influenced by the steam oxidation kinetics, first a kinetic model for the steam oxidation of $FeAl_2O_4$ needs to be determined and validated. When these kinetics are obtained, the production of H_2/N_2 stream for the ammonia production can be further optimized by adjusting the oxygen content and the flowrate of the gas stream entering the first oxidation cycle.

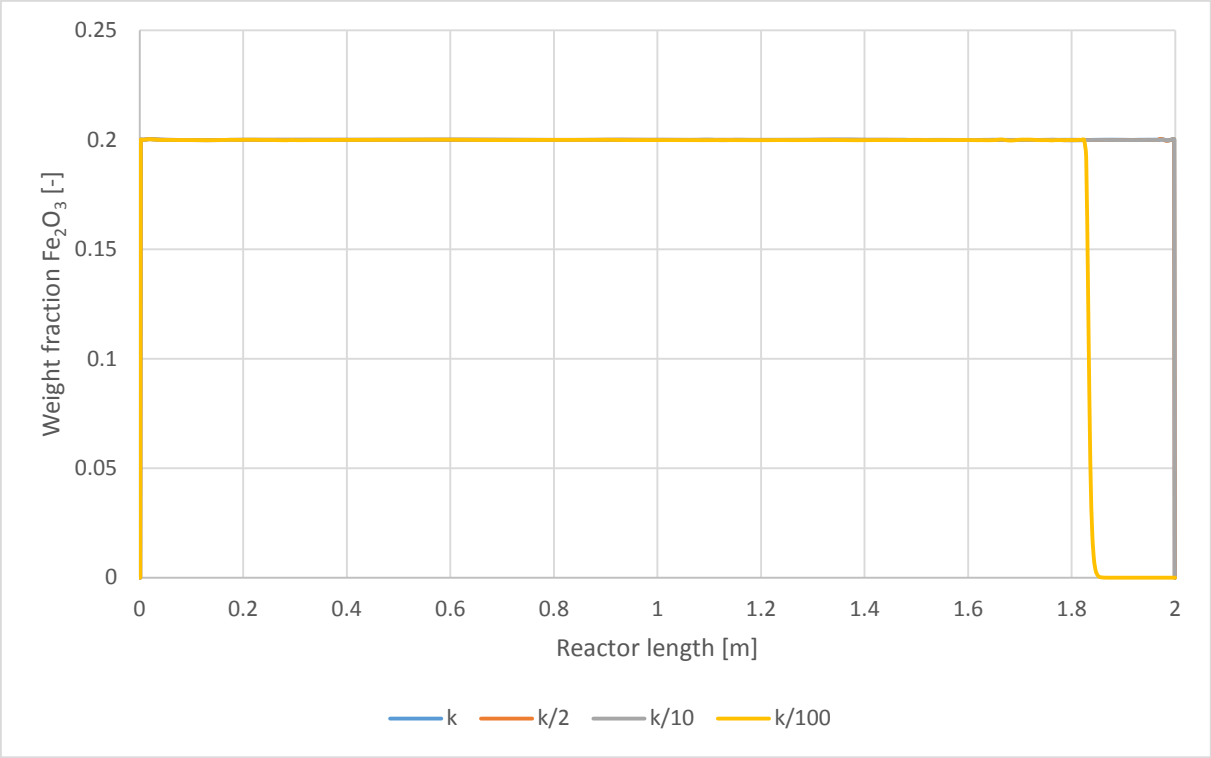

Figure 5.14 – Weight fraction Fe_2O_3 as a function of the reactor length after the second oxidation cycle for different values of the reaction rate constant for steam oxidation

6 Conclusion

The performance of the pre-combustion chemical looping carried out in dynamically operated packed bed reactors is determined for both the case that coal-derived syngas and natural gas are used as fuel for the reduction of the oxygen carrier.

For the case that coal-derived syngas is used as fuel for the reduction of the oxygen carrier, an active weight fraction Fe_2O_3 of 0.4 is preferred for the production of power in a gas turbine. This is due to the fact that a higher temperature rise is obtained when the active weight fraction of Fe_2O_3 is increased, and therefore, the temperature difference between the inflowing heat removal gas stream and the bed temperature before the heat removal cycle increases. Therefore, a smaller heat removal gas stream is needed for the heat removal cycle, and also a smaller amount of the produced hydrogen during the oxidation cycle is needed for pre-heating the air stream needed for the heat removal cycle. Since the temperature of the outflowing gas stream from the heat removal reactor is higher, and also more produced hydrogen can be combusted for further heating of the outflowing gas stream from the heat removal reactor, the temperature of the gas stream after this hydrogen combustion is higher when the active weight fraction of Fe_2O_3 is increased. The production of power in a gas turbine increases with increasing temperature of the inflowing gas stream, and therefore the highest power production is obtained when the active weight fraction of Fe_2O_3 is 0.4.

Heat removal after the oxidation cycle is preferred over heat removal after the reduction cycle, since in the latter case part of the stored heat during oxidation cycle is already removed from the reactor in the subsequent reduction cycle. For the case that the heat removal takes place after the oxidation cycle, a heat removal flowrate of 5.6 kg/m^2/s is preferred for the production of power in a gas turbine. This can be explained by the interaction between the power needed for compressing the ambient air stream and the power produced by expanding the high temperature and high pressure gas stream in the gas turbine. The power needed for compressing the air stream for the heat removal cycle increases with increasing heat removal flowrate. The power produced by the gas turbine increases with increasing heat removal flowrate and increasing temperature. When the heat removal flowrate increases, a higher amount of the produced hydrogen is needed for pre-heating the air stream for the heat removal cycle. Therefore, less hydrogen is available for further heating of the outflowing heat removal stream, which means that the temperature of the gas stream entering the gas turbine decreases with increasing heat removal flowrate. This temperature decrease hampers the power production in the gas turbine, and therefore a maximal power production can be obtained. Maximal power production takes place when the heat of the outflowing reductant stream is the lowest, since then a maximal amount of heat is sent to the gas turbine, which is the case for a heat removal flowrate

of 5.6 kg/m^2/s. The carbon dioxide purity that can be obtained with this case is 96.8%. A carbon dioxide purity of 100% cannot be reached due to the fact that a small amount of nitrogen is present in the fuel feed.

For this heat management strategy, active weight fraction Fe_2O_3 of 0.4, and a heat removal flowrate of 5.6 kg/m^2/s, the effect of the steam oxidation kinetics on the performance of the PCCL concept concerning the power production is determined. The power produced by the gas turbine decreases with decreasing reaction rate constant for the oxidation of $FeAl_2O_4$ to Fe_3O_4 by steam. This is due to the fact that the overlap between the reaction front for the oxidation of $FeAl_2O_4$ to Fe_3O_4 by steam and the reaction front for the subsequent oxidation of Fe_3O_4 to Fe_2O_3 by oxygen increases with decreasing reaction rate constant for the steam oxidation. Therefore, a higher amount of $FeAl_2O_4$ is directly oxidized to Fe_2O_3 by oxygen, which leads to a decrease in the hydrogen production. When the amount of produced hydrogen during the oxidation cycle is decreased, there is less hydrogen available for heating the outflowing gas stream from the heat removal cycle, and the temperature of the inflowing gas stream to gas turbine decreases. Therefore, the power production by the gas turbine decreases with decreasing reaction rate constant for the steam oxidation.

For the case that natural gas is used as fuel for the reduction of the oxygen carrier, the stored heat due to the highly exothermic oxidation reaction by oxygen during the oxidation cycle is already partially removed from the reactor due to the highly endothermic methane reforming reaction during the reduction cycle. Therefore, only one heat management strategy is possible, which is already optimized for the production of power in previous research. For the production of a H_2/N_2 gas stream during the oxidation cycle for the ammonia synthesis, an active weight fraction Fe_2O_3 of 0.2 is preferred. This is due to the fact that the changes in bed temperature between the reduction and oxidation cycle is decreases with decreasing active weigh fraction of Fe_2O_3, which is advantageous for the life-time of the solid material. Also the change in temperature of the outflowing gasses from both the reduction and oxidation cycle is the lowest for the case that the active weight fraction of Fe_2O_3 is 0.2, which is advantageous for the pseudo-continuous power and ammonia production processes downstream.

Since a hydrogen to nitrogen ratio of 3 in the outflowing oxidant gas stream is needed for the synthesis of ammonia, a sensitivity analysis of the oxygen content of the inflowing oxidant gas stream on the hydrogen to nitrogen ratio of the outflowing oxidant gas stream is performed. Therefore, the steam to air ratio of the inflowing oxidant gas stream was increased. Due to the lower oxygen content in the oxidant gas stream, the bed is not fully oxidized back to Fe_2O_3, and therefore an additional oxidation cycle is needed in which air is fed to the reactor. A hydrogen to nitrogen ratio of 3 was obtained when

the oxygen content of the inflowing oxidant gas stream is 0.0428. The carbon dioxide purity that can be obtained from this case is 94.7%.

For the case that natural gas is used as fuel for reduction cycle, an active weight fraction Fe_2O_3 of 0.2, and an oxygen mole fraction of 0.0428 of the inflowing oxidant gas stream, the effect of the steam oxidation kinetics on the performance of the PCCL concept concerning the amount of ammonia that can be produced from the outflowing oxidant gas stream. The amount of ammonia that can be produced from the outflowing oxidant gas stream decreases with decreasing reaction rate constant for the oxidation of $FeAl_2O_4$ to Fe_3O_4 by steam. This is also due to the fact that the overlap between the reaction front for the oxidation of $FeAl_2O_4$ to Fe_3O_4 by steam and the reaction front for the subsequent oxidation of Fe_3O_4 to Fe_2O_3 by oxygen increases with decreasing reaction rate constant for the steam oxidation. Therefore, a higher amount of $FeAl_2O_4$ is directly oxidized to Fe_2O_3 by oxygen, which leads to a decrease in the hydrogen production. Since the amount of hydrogen decreases with decreasing reaction rate constant for the steam oxidation, the hydrogen to nitrogen ratio also decreases, which means that the oxygen content of the inflowing oxidant stream needs to be further decreased in order to obtain a hydrogen to nitrogen ratio of 3. Therefore, the hydrogen/nitrogen content of the outflowing gas stream from the oxidation cycle decreases, which means that the amount of ammonia that can be produced decreases with decreasing reaction rate constant for the steam oxidation.

7 Recommendations

When the experimental results for the oxidation of $FeAl_2O_4$ to Fe_3O_4 by steam from the ongoing research at the Eindhoven University of Technology are available, and a kinetic expression for this steam oxidation is obtained, recommended is to adjust these kinetics in the reactor model.

For the case that coal-derived syngas is used as fuel for the reduction cycle, the implementation of the steam oxidation kinetics is needed because the performance of the PCCL concept concerning the power production is dependent on the steam oxidation kinetics. When the experimentally obtained kinetics for the steam oxidation are indeed much lower than that suggested by Coetsee et al. [27], there will be a significant decrease in hydrogen production during the oxidation cycle, and therefore also a significant decrease in power production by the gas turbine, as mentioned in the sensitivity analysis. Since it is not known at the moment if this will also have an effect on the optimal heat removal flowrate for maximal power production by the gas turbine, repeating the sensitivity analysis of the heat removal flowrate on the performance of the PCCL concept concerning the power production for the case that the new steam oxidation kinetics are implemented is recommended.

For the case that natural gas is used as fuel for the reduction cycle, the implementation of the steam oxidation kinetics is needed because the performance of the PCCL concept concerning the ammonia production is also dependent on the steam oxidation kinetics. Since the amount of produced hydrogen during the oxidation cycle is dependent on the steam oxidation kinetics, the determination of the optimal oxygen content of the inflowing oxidant stream for obtaining a hydrogen to nitrogen ratio of 3 in the outflowing oxidant gas stream is recommended. Therefore, the sensitivity analysis of the oxygen content in the inflowing oxidant stream needs to be repeated for the case that the new steam oxidation kinetics are implemented.

The needed oxygen content of the inflowing oxidant stream for the production of a outflowing oxidant stream with a hydrogen to nitrogen ratio of 3 for the case that coal-derived syngas is used as fuel during the reduction cycle was not determined in this research. In order to compare the reactor performance for the case that coal-derived syngas is used as fuel with the case that natural gas is used as fuel concerning the amount of produced hydrogen during the oxidation cycle, a sensitivity analysis of the oxygen content in the inflowing oxidant stream on the hydrogen to nitrogen ratio of the outflowing oxidant stream is recommended. For the production of a hydrogen/nitrogen stream for the ammonia synthesis it is preferable to have the heat removal cycle after the oxidation cycle instead of after the reduction cycle. This is due to the fact that in the latter case part of the heat that is produced during the oxidation cycle is already removed during the subsequent reduction cycle, which is disadvantageous for the downstream power production.

A complete plant analysis for both the case that coal-derived syngas and natural gas is used as fuel for the reduction cycle is also recommended, in order to determine the performance of the pre-combustion chemical looping concept for the production of power, or for the production of a H_2/N_2 gas stream for the ammonia synthesis with the co-production of power. For the case that coal-derived syngas is used as fuel, this plant analysis is useful since it is not known at the moment if the downstream power production from the heat of the outflowing gas streams from the gas turbine and the reduction reactor have an effect on for example the optimal heat removal flowrate as determined in this research.

Also a techno-economic analysis and optimization is recommended after full integration of the results obtained from the reactor modelling in this work. In order to determine the overall plant performance, for example the costs of ammonia synthesis, power production and the costs for carbon dioxide capture needs to be determined.

The reactor dimensions are for small-scale operation, since the reactor length and diameter are respectively 2 and 0.5 meters. In order to have a large-scale operation, these reactor dimensions should be increased, and therefore also the reductant, oxidant and heat removal flowrates and the cycle times for each operating step needs to be increased. Since it is not known at the moment what the optimal dimensions of the reactor and the optimal number of reactors are, it is recommended to research the engineering of the reactor.

Acknowledgements

Working on the same project for nine months, I thought it would takes forever when I started in September, but I couldn't be more wrong. They say that times flies when having fun, and that is exactly what I didn't expect that this master project would be. In the end, I am very happy with this master thesis and I am proud of what I achieved. There are a lot of people that had a contribution to this project in one way or another, and out of appreciation I would like to thank all of them.

First of all, I would to thank Martin van Sint Annaland for giving me the opportunity to do my master thesis within the SMR group. Although I was sometimes very confused after the meetings, since you always had a lot of suggestions for taking the project to a higher level, all of the comments were very useful for me and positively affected the final result. I also would like to thank Fausto Gallucci for your critical point of view and pointing out the parts of the presentation that can give a rise to questions. I also would like to thank John van der Schaaf for being my external committee member. A special thanks to my supervisor Vincenzo Spallina, for helping me with the project providing me with comments from sometimes a different point of view, and by improving my skills to clearly and structurally discuss and present results.

I also would like to thank all the (PhD-) students from the SMR group for providing a nice atmosphere during the many coffee breaks. Special thanks to Annelies, Beatrice, Fabio, Floris, Francesca, Gianmaria, James, Jan-Willem, Jeroen, Martin, Max, Rhea, Rik, Rosa, Sander, Stella and Tom for all the nice conversations, without all of you this nine months wouldn't have been the same!

There is one name that I would like to mention twice, since she always has been there for me during the last 7 (!) years of university. Rhea, I am really thankful that I met you, and that we spent lots of time together during the lectures, the study sessions at home, and during all the binge watching sessions.

Also special thanks goes to my parents for always being there for me. Fun story, last week they told me that they are doubting whether they adopted me or not, since they have no clue how a son of them can be so smart (not my words!). I also would like to thank my brother Richard and my best friend Jill for keeping me down to earths and always supporting me, even while they have no clue of what I have been doing for the last couple of years.

Finally I also would like to thank and Laura, Marilous and my two second mothers José and Janine, for all the time we spent together in front of the building, and discussing all the newest gossip.

Nomenclature

List of Symbols

A	$[m^2]$	Area
b	$[-]$	Stoichiometric factor
C	$[mol/m^3]$	Concentration
C_p	$[J/mol/K]$	Heat capacity
d_p	$[m]$	Particle diameter
D_{ax}	$[m^2/s]$	Axial dispersion coefficient
D_R	$[m]$	Reactor diameter
E_a	$[J/mol]$	Activation energy
F	$[kg/m^2/s]$	Flowrate
H_R	$[J/mol]$	Reaction enthalpy
K_{ad}	$[*]$	Adsorption constant
K	$[*]$	Equilibrium constant
k_0	$[*]$	Pre-exponential factor
k_R	$[*]$	Reaction rate constant
L_R	$[m]$	Reactor length
m	$[kg]$	Mass
M	$[kg/mol]$	Molar weight
M_v	$[kg/m^3]$	Mass per pellet volume
n	$[-]$	Reaction order
n_i	$[mol]$	Number of moles of component i
Nu	$[-]$	Nusselt number
p	$[Pa]$	Pressure
P	$[W]$	Power
Pe	$[-]$	Péclet number
Pr	$[-]$	Prandtl number
r	$[mol/m^3/s]$	Reaction rate
R	$[J/mol/K]$	Gas constant
Re	$[-]$	Reynolds number
r_g	$[m]$	Grain radius
Sc	$[-]$	Schmidt number
t	$[s]$	Time
T	$[K]$	Temperature

v	$[m/s]$	Velocity
V	$[m^3]$	Volume
w	$[kg/kg]$	Weight fraction
w_1	$[m/s]$	Reaction front velocity
w_2	$[m/s]$	Heat front velocity
x	$[m]$	Distance
y	$[mol/mol]$	Mole fraction

Greek letters

Δ	$[-]$	Difference
ε	$[m^3/m^3]$	Porosity
η	$[-]$	Efficiency
λ	$[W/m/K]$	Heat dispersion coefficient
ρ	$[kg/m^3]$	Density
ζ	$[-]$	Stoichiometric factor

Subscripts/superscripts

0	At time is 0
act	Active
ax	Axial
cat	Catalyst
DR	Dry Reforming
eff	Effective
eq	Equilibrium
g	Gas
i	Component i
m	Molar
s	Solid
SR	Steam Reforming
WGS	Water Gas Shift

Abbreviations

CCS	Carbon Capture and Storage
CLC	Chemical Looping Combustion
LHV	Lower Heating Value

$[*]$ means that this symbol has different units for different components or reactions.

Bibliography

[1] IPCC, 2013. Climate change 2013: The physical science basis. Stockholm.

[2] IEA. World Energy Outlook 2006. OECD/IEA, Paris, France, 2006.

[3] IPCC, 2014. Climate change 2014: Mitigation of Climate Change.

[4] Finkenrath, M., 2011. Costs and Performance of Carbon Dioxide Capture for Power Generation.

[5] IPCC, 2005. Carbon Dioxide Capture and Storage. Cambridge University Press, UK.

[6] DOE/NETL, Carbon dioxide capture and storage RD&D roadmap, 2010.

[7] S. Consonni, G. Lozza, G. Pelliccia, S. Rossini, F. Saviano, Chemical-Looping Combustion for Combined Cycles With CO[sub 2] Capture, J. Eng. Gas Turbines Power. 128 (2006) 525.

[8] O. Brandvoll, O. Bolland, Inherent CO[sub 2] Capture Using Chemical Looping Combustion in a Natural Gas Fired Power Cycle, J. Eng. Gas Turbines Power. 126 (2004) 316.

[9] R. Naqvi, O. Bolland, Multi-stage chemical looping combustion (CLC) for combined cycles with CO2 capture, Int. J. Greenh. Gas Control. 1 (2007) 19–30.

[10] B. Erlach, M. Schmidt, G. Tsatsaronis, Comparison of carbon capture IGCC with pre-combustion decarbonisation and with chemical-looping combustion, Energy. 36 (2011) 3804–3815.

[11] S. Rezvani, Y. Huang, D. McIlveen-Wright, N. Hewitt, J.D. Mondol, Comparative assessment of coal fired IGCC systems with CO2 capture using physical absorption, membrane reactors and chemical looping, Fuel. 88 (2009) 2463–2472.

[12] F. Gallucci, H.P. Hamers, M. van Zanten, M. van Sint Annaland, Experimental demonstration of chemical looping combustion of syngas in packed bed reactors with ilmenite, Chem. Eng. J. 274 (2015) 156-168.

[13] L. Han, Z. Zhou, G.M. Bollas, Heterogeneous modeling of chemical-looping combustion. Part 1: Reactor model, Chem. Eng. Sci. 104 (2013) 233–249.

[14] H.P. Hamers, F. Gallucci, P.D. Cobden, E. Kimball, M. van Sint Annaland, A novel reactor configuration for packed bed chemical-looping combustion of syngas, Int. J. Greenh. Gas Control. 16 (2013) 1-12.

[15] Spallina, V., Gallucci, F., Romano, M.C., Chiesa, P., Lozza, G., van Sint Annaland, M., 2013. Investigation of heat management for CLC of syngas in packed bed reactors. Chemical Engineering Journal 225, 174-191.

[16] K. Piotrowski, K. Mondal, H. Lorethova, L. Stonawski, T. Szymanski, T. Wiltowski, Effect of gas composition on the kinetics of iron oxide reduction in a hydrogen production process, Int. J. Hydrogen Energy. 30 (2005) 1543–1554.

[17] A. Singh, F. Al-Raqom, J. Klausner, J. Petrasch, Production of hydrogen via an Iron/Iron oxide looping cycle: Thermodynamic modeling and experimental validation, Int. J. Hydrogen Energy. 37 (2012) 7442–7450.

[18] P. Gupta, L. Velazquez-Vargas, L. Fan, Syngas redox (SGR) process to produce hydrogen from coal derived syngas, Energy & Fuels. (2007) 2900–2908.

[19] J. Plou, P. Duran, J. Herguido, J. a. Peña, Steam-iron process kinetic model using integral data regression, Int. J. Hydrogen Energy. 37 (2012) 6995–7004.

[20] G. Lozza, P. Chiesa, M.C. Romano, P. Savoldelli, Three Reactors Chemical Looping Combustion For High Efficiency Electricity Generation With CO2 Capture From Natural Gas, Proc. ASME Turbo Expo 2006, GT2006-90345. (2006) 1–11.

[21] P. Chiesa, G. Lozza, a Malandrino, M. Romano, V. Piccolo, Three-reactors chemical looping process for hydrogen production, Int. J. Hydrogen Energy. 33 (2008) 2233–2245.

[22] F. Li, L. Zeng, L.-S. Fan, Biomass direct chemical looping process: Process simulation, Fuel. 89 (2010) 3773–3784.

[23] M. Sorgenfrei, G. Tsatsaronis, Design and evaluation of an IGCC power plant using iron-based syngas chemical-looping (SCL) combustion, Appl. Energy. 113 (2013) 1958–1964.

[24] C. Cormos, Evaluation of iron based chemical looping for hydrogen and electricity co-production by gasification process with carbon capture and storage, Int. J. Hydrogen Energy. 35 (2010) 2278–2289.

[25] C.D. Bohn, C.R. Müller, J.P. Cleeton, A.N. Hayhurst, J.F. Davidson, S. a. Scott, et al., Production of very pure hydrogen with simultaneous capture of carbon dioxide using the redox reactions of iron oxides in packed beds, Ind. Eng. Chem. Res. 47 (2008) 7623-7630.

[26] E. Lorente, J.A. Peña, J. Herguido, Cycle behavior of iron ores in the steam-iron process, Int. J. Hydrogen Energy. 163 (2011) 7043-7050.

[27] T. Coetsee, P.C. Pistorius, E.E. de Villiers, Rate-determining steps for reduction in magnetite-coal pellets, 2002. Minerals Engineering 15, 919-929.

[28] M.S. Valipour, M.Y. Motamed Hashemi, Y. Saboohi, Mathematical modeling of the reaction in an iron ore pellet using a mixture of hydrogen, water vapor, carbon monoxide and carbon dioxide: an isothermal study, 2006. Advanced Powder Technology 17, 227-295.

[29] V. Patrick, G.R. Gavalas, P.K. Sharma. Ind. Eng. Chem. Res. 32 (1993) 519-532.

[30] A. Abad, F. García-Labiano, L.F. de Diego, P Gaýan, J. Adánez, Reduction kinetics of Cu- Ni-, and Fe-based oxygen carriers using syngas (CO+H2) for chemical looping combustion. Energy & Fuels 21 (2007) 1843-1853.

[31] M.E.E. Abashar, Coupling of steam and dry reforming of methane in catalytic fluidized bed membrane reactors. International Journal of Hydrogen Energy 29 (2004) 799-808.

[32] V. Spallina, P. Chiesa, E. Martelli, F. Gallucci, M.C. Romano, G. Lozza, M. van Sint Annaland, Reactor design and operation strategies for a large-scale packed bed CLC power plant with coal syngas. International Journal of Greenhouse Gas Control 36 (2015) 34-50.

[33] Monsen, B. E.; Olsen, S. E.; Kolbeinsen, L. Kinetics of magnetite oxidation. Scand. J. Metall. 1994, 23, 74−80.

[34] S. Noorman, F. Gallucci, M. van Sint Annaland, J.A.M. Kuipers, Grid adaptation with WENO schemes for non-uniform grids to solve convection-dominated partial differential equations. Chemical Engineering Science 60 (2005), 2609-2619.

[35] V. Spallina, F.C. Arienti, M.C. Romano, F. Gallucci, M. van Sint Annaland, Thermodynamic analysis of a pre-combustion chemical looping process for power production integrated with a coal gasification combined cycle (2014).

[36] V. Spallina, F. Gallucci, M. Romano, M. van Sint Annaland, Pre-combustion packed bed chemical looping (PCCL) technology for efficient H_2-rich gas processes.

Appendix

Appendix A - Solid porosity

During reduction, oxygen is transferred from the oxygen carrier to the fuel, and during oxidation, oxygen is transferred from air and steam back to the oxygen carrier. Therefore, the solid porosity changes during every reduction-oxidation cycle. The solid porosity changes at the reactor front, which means that the solid porosity changes along the reactor length. In order to calculate the solid porosity at each point in the reactor, equations A1-A9 are implemented in the reactor model.

The solid porosity for the case that the oxygen carrier is in the most oxidized state (Fe_2O_3) is assumed to be 0.55. In order to calculate the solid porosities of the reduced states, the amount of moles of Fe_2O_3 in the reactor is needed, which is calculated with the following equation:

$$n_{Fe_2O_3} = \frac{m_{Fe_2O_3}}{M_{Fe_2O_3}} = \frac{w_{Fe_2O_3} m_s}{M_{Fe_2O_3}} = \frac{w_{Fe_2O_3} \rho_s V_s}{M_{Fe_2O_3}} = \left. \frac{w_{Fe_2O_3} \frac{\pi}{4} {D_R}^2 L_R \varepsilon_{bed} \varepsilon_{s,Fe_2O_3}}{M_{Fe_2O_3} \left(w_{Fe_2O_3} / \rho_{Fe_2O_3} + w_{Al_2O_3} / \rho_{Al_2O_3} \right)} \right|_{t=0} \quad [A1]$$

The change in solid porosity can be calculated from the change in solid volume. During reduction and oxidation, the volume inert (Al_2O_3) remains the same. Therefore, the solid volumes for each reduced state are calculated with the following equations:

$$V_{Fe_3O_4} = \frac{2 n_{Fe_2O_3} M_{Fe_3O_4}}{3 \rho_{Fe_3O_4}} \quad [A2]$$

$$V_{FeO} = \frac{2 n_{Fe_2O_3} M_{FeO}}{\rho_{FeO}} \quad [A3]$$

$$V_{Fe} = \frac{2 n_{Fe_2O_3} M_{Fe}}{\rho_{Fe}} \quad [A4]$$

$$V_{Al_2O_3} = w_{Al_2O_3} m_s = w_{Al_2O_3} \rho_s V_s = \left. \frac{w_{Al_2O_3} \frac{\pi}{4} {D_R}^2 L_R \varepsilon_{bed} \varepsilon_{s,Fe_2O_3}}{w_{Fe_2O_3} / \rho_{Fe_2O_3} + w_{Al_2O_3} / \rho_{Al_2O_3}} \right|_{t=0} \quad [A5]$$

The total solid volume for each reduced state can be calculated by the sum of the inert volume and either the volume of either Fe_3O_4, FeO or Fe. The total solid volume for each reduced state also can be calculated by multiplying the reactor volume with the total porosity ($\varepsilon_{bed} \varepsilon_{s,i}$). Therefore, the solid porosity for each reduced state can be calculated for each reduced state with equation 8.6-8.8.

$$\varepsilon_{s,Fe_3O_4} = \frac{4 V_{total}}{\pi {D_R}^2 L_R \varepsilon_{bed}} = \frac{4}{\pi {D_R}^2 L_R \varepsilon_{bed}} \left(V_{Fe_3O_4} + V_{Al_2O_3} \right) \quad [A6]$$

$$\varepsilon_{s,FeO} = \frac{4 V_{total}}{\pi {D_R}^2 L_R \varepsilon_{bed}} = \frac{4}{\pi {D_R}^2 L_R \varepsilon_{bed}} \left(V_{FeO} + V_{Al_2O_3} \right) \quad [A7]$$

$$\varepsilon_{s,Fe} = \frac{4 V_{total}}{\pi {D_R}^2 L_R \varepsilon_{bed}} = \frac{4}{\pi {D_R}^2 L_R \varepsilon_{bed}} \left(V_{Fe} + V_{Al_2O_3} \right) \quad [A8]$$

Finally, the average solid porosity can be calculated every time step at each point in the reactor by the weighted average of the solid porosities of each reduced state with the following equation.

$$\varepsilon_s = \frac{\varepsilon_{s,Fe} w_{Fe}}{(1-w_{Al_2O_3})} + \frac{\varepsilon_{s,FeO} w_{FeO}}{(1-w_{Al_2O_3})} + \frac{\varepsilon_{s,Fe_3O_4} w_{Fe_3O_4}}{(1-w_{Al_2O_3})} + \frac{\varepsilon_{s,Fe_2O_3} w_{Fe_2O_3}}{(1-w_{Al_2O_3})}\Bigg|_{t=t} \quad \text{[A9]}$$

Appendix B - Physical properties

B1 Heat of reaction

The heat of reaction of all gas-solid and gas-gas reactions are needed to simulate the temperature changes within the reactor due to chemical reaction. The heat of reaction is temperature dependent, and can be described by the following polynomial equation:

$$\Delta H_R \left[\frac{J}{mol}\right] = AT^3 + BT^2 + CT + D \quad \text{[B1]}$$

For this research, the enthalpy for each reaction is calculated from the data provided by the book of Barin (Thermochemical Data of Pure Substances) [35]. For some of the reactions, the heat of reaction cannot be described by only one polynomial expressions. Therefore, the heat of reaction needed to be divided into multiple temperature intervals for some of the reactions.

The heat of reaction for all reactions, including the fitted expressions according to equation B1, are graphically shown in Figure B1-B8. An overview of the fitted values for coefficients A to D of equation B1 can be found in Table B1.

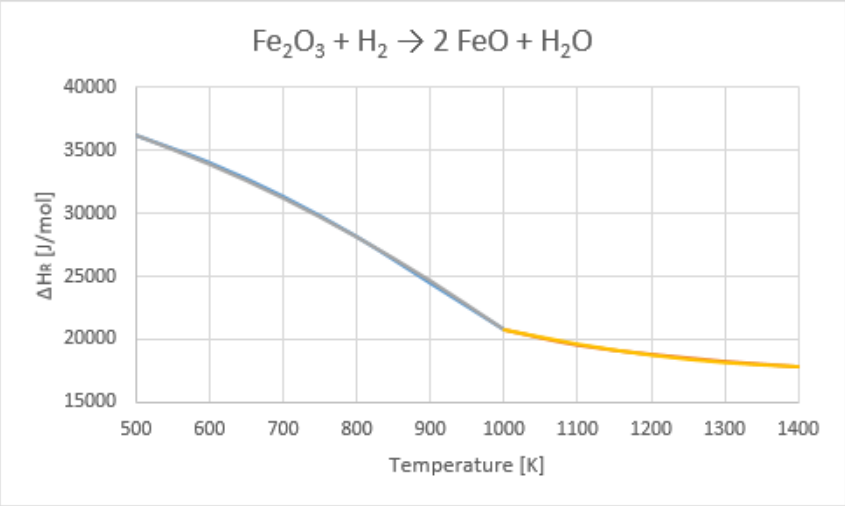

Figure B1 – Heat of reaction for the reduction of Fe_2O_3 to FeO by hydrogen

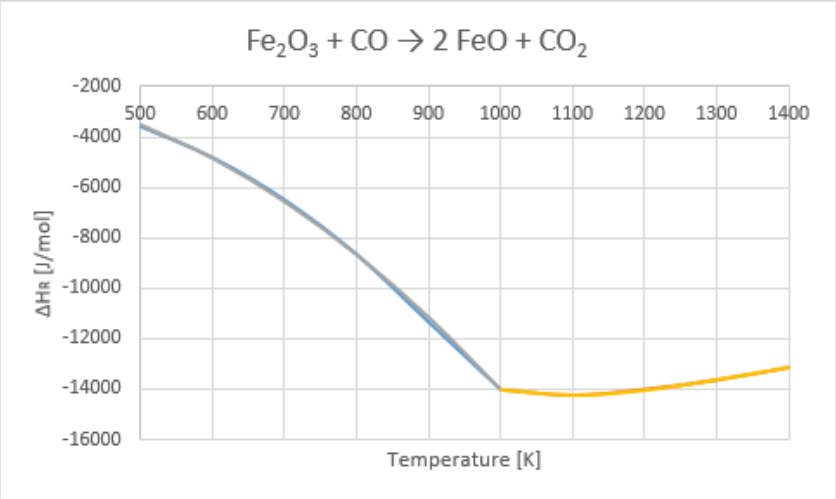

Figure B2 – Heat of reaction for the reduction of Fe_2O_3 to FeO by carbon monoxide

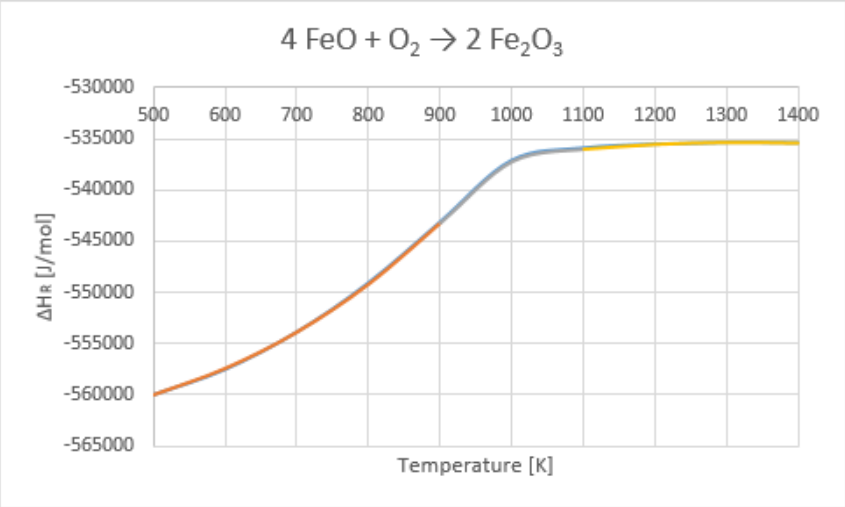

Figure B3 – Heat of reaction for the oxidation of FeO to Fe_2O_3 by oxygen

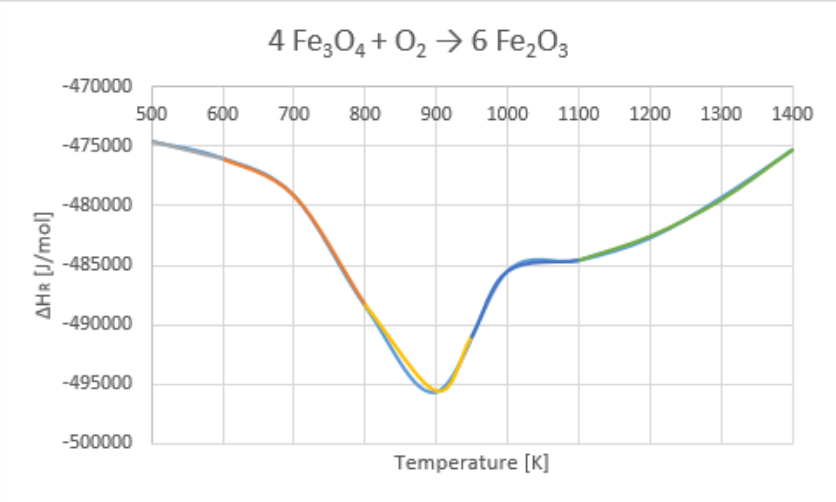

Figure B4 – Heat of reaction for the oxidation of Fe_3O_4 to Fe_2O_3 by oxygen

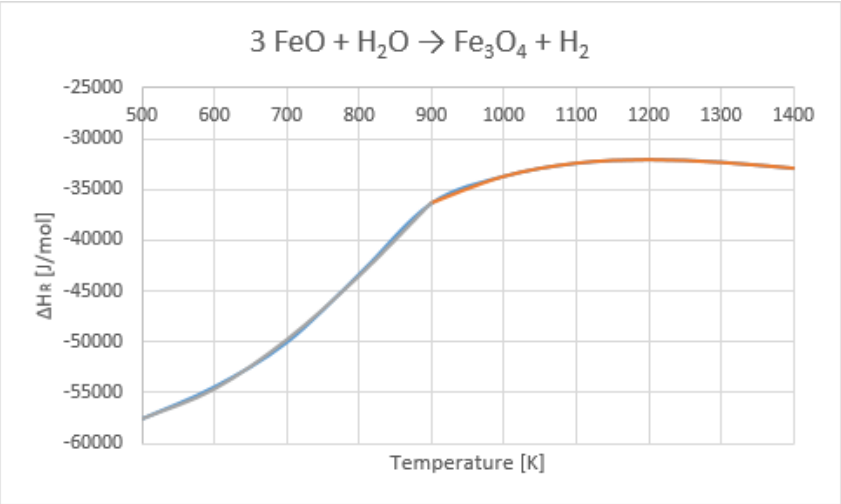

Figure B5 – Heat of reaction for the oxidation of FeO to Fe_3O_4 by steam

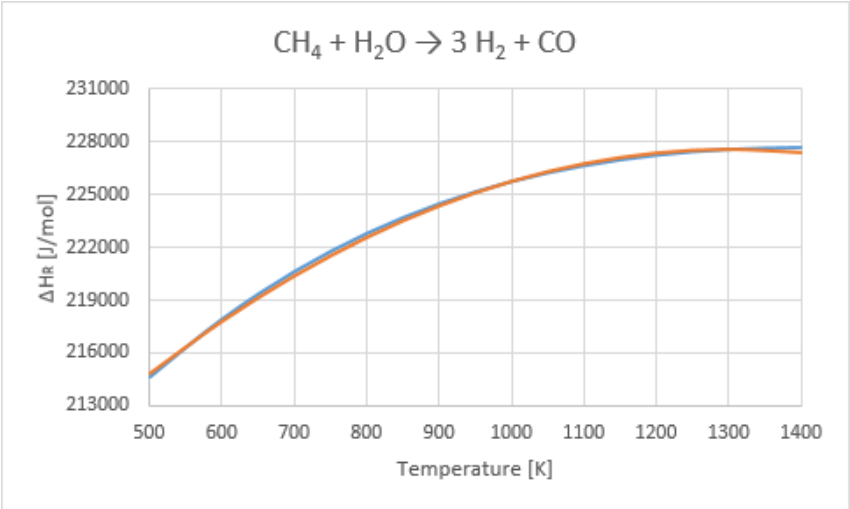

Figure B6 – Heat of reaction for methane steam reforming

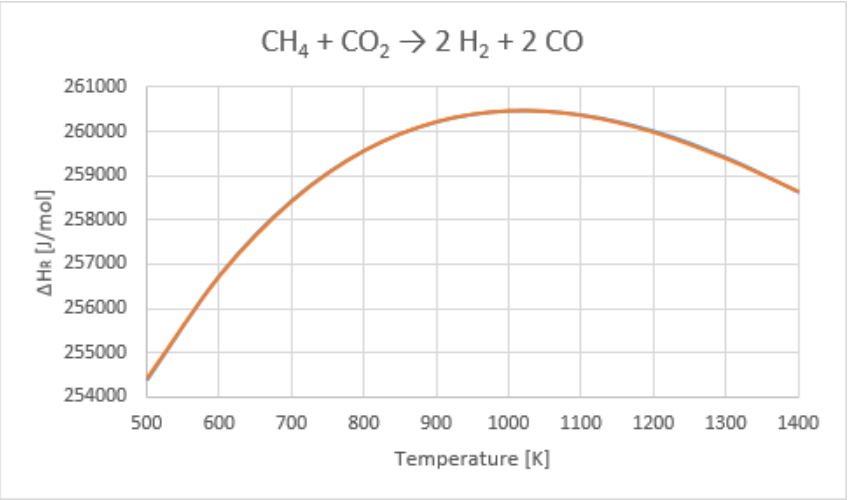

Figure B7 – Heat of reaction for methane dry reforming

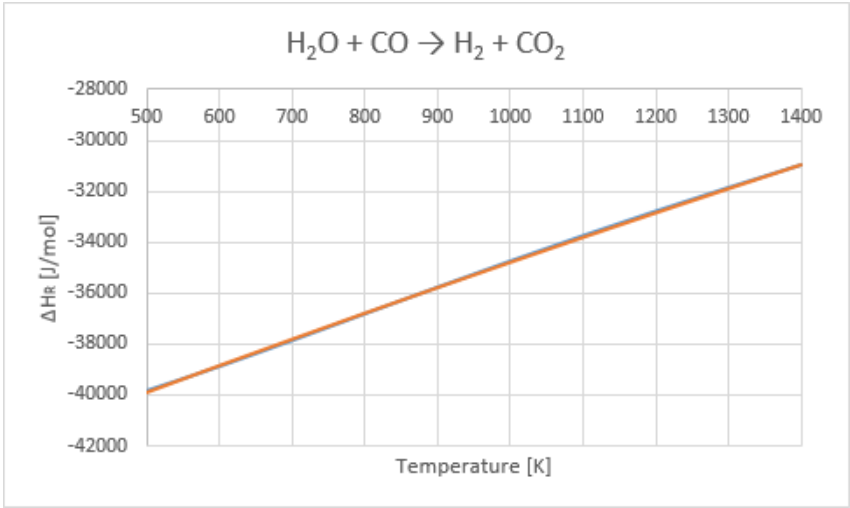

Figure B8 – Heat of reaction for the water gas shift

Table B1 – overview heat of reaction coefficients for gas-solid reactions

Gas-Solid Reactions	A	B	C	D	T interval	R^2
$Fe_2O_3 + H_2 \rightarrow 2\ FeO + H_2O$ [1]	-	-1.980E-02	-1381E+00	4.191E+04	500-1000	0.9997
	-	1.332E-02	-3.914E+01	4.665E+04	1000-1400	0.9978
$Fe_2O_3 + CO \rightarrow 2\ FeO + CO_2$ [1]	-	-1.907E-02	7.681E+00	-2.620E+03	500-1000	0.9995
	2.736E-05	1.097E-01	-1.419E+02	4.552E+04	1000-1400	0.9982
$FeO + O_2 \rightarrow Fe_2O_3$	2.623E-05	1.868E-03	-3.065E-02	-5.638E+05	500-900	0.9999
	8.893E-06	-2.680E-01	5.454E+02	-8.235E+05	900-1100	>0.9999
	-9.081E-07	-7.746E-03	2.533E+01	-5.533E+05	1100-1400	0.9989
$Fe_3O_4 + O_2 \rightarrow Fe_2O_3$	-	-	-1.410E+01	-4.676E+05	500-600	1
	-1.442E-04	-3.440E-03	1.565E+02	-5.375E+05	600-800	>0.9999
	4.183E-04	-4.001E-03	-9.735E+02	7.877E+04	800-950	>0.9999
	-2.199E-04	7.045E-04	7.355E+02	-1.002E+06	950-1100	>0.9999
	1.441E-05	7.042E-04	-3.856E+01	-4.622E+05	1100-1400	0.9978
$FeO + H_2O \rightarrow Fe_3O_4 + H_2$	-8.076E-05	2.407E-01	-1.621E+02	-2.657E+02	500-900	0.9995
	5.653E-05	-2.351E-01	3.199E+02	-1.750E+05	900-1400	0.9999

Table B2 – overview heat of reaction coefficients for gas-gas reactions

Gas-Gas Reactions	A	B	C	D	T interval	R^2
$CH_4 + H_2O \rightarrow 3\ H_2 + CO$	1.483E-09	-1.975E-02	5.151E+01	1.940E+05	500-1400	0.9986
$CH_4 + CO_2 \rightarrow 2\ H_2 + 2\ CO$	1.123E-05	-5.106E-02	6.902E+01	2.313E+05	500-1400	0.9999
$H_2O + CO \rightarrow H_2 + CO_2$	-	-7.095E-04	1.126E+01	-4.533E+04	500-1400	0.9998

[1] For the reductions of Fe_2O_3 to $FeAl_2O_4$, assumed is that the $FeAl_2O_4$ is a combination of FeO and Al_2O_3, and the Al_2O_3 does not have an influence on the heat of reaction

B2 Solid heat capacity

Besides the heat of reaction, also the solid heat capacities are needed to simulate the temperature changes within the reactor due to chemical reaction. The solid heat capacity is also temperature dependent, and can be described by the following polynomial equation:

$$C_{p,s}\left[\frac{J}{mol\,K}\right] = AT^3 + BT^2 + CT + D \qquad [B2]$$

For this research, data for the solid heat capacity of each compound at different temperatures is used from the book of Barin (Thermochemical Data of Pure Substances) [35]. For some of the compounds, the solid heat capacity cannot be described by only one polynomial expressions. Therefore, the solid heat capacity needed to be divided into multiple temperature intervals for some of the compounds.

The solid heat capacities for all compounds, including the fitted expressions according to equation B2, are graphically shown in Figure B9-B14. An overview of the fitted values for coefficients A to D of equation B2 can be found in Table B2.

Table B2 - overview solid heat capacity coefficients for all compounds

Compound	A	B	C	D	T interval	R^2
Fe	-	4.832E-05	-3.460E-02	3.510E+01	500-900	0.9972
	-	4.105E-03	-7.686E+00	3.635E+03	900-1042	>0.9999
	-	4.109E-03	-9.444E+00	5.463E+03	1042-1184	>0.9999
	-	4.331E-07	7.234E-03	2.471E+01	1184-1400	>0.9999
FeO	-	-4.328E-06	1.824E-02	4.545E+01	500-1400	0.9996
Fe_3O_4	2.323E-06	-3.972E-03	2.415E+00	-3.124E+02	500-850	>0.9999
	-1.924E-07	8.245E-04	-1.172E+00	7.484E+02	850-1400	>0.9999
Fe_2O_3	-	-1.527E-05	1.079E-01	8.177E+01	500-960	>0.9999
	-	2.978E-03	-6.353E+00	3.525E+03	960-1100	>0.9999
	-	3.448E-06	-1.811E-03	1.387E+02	1100-1400	0.9990
$CaAl_2O_4$	2.979E-08	-1.050E-04	1.488E-01	9.935E+01	500-1400	0.9997
Al_2O_3	3.610^{E}-08	-1.284^{E}-04	1.666^{E}-01	5.069^{E}+01	500-1400	0.9992

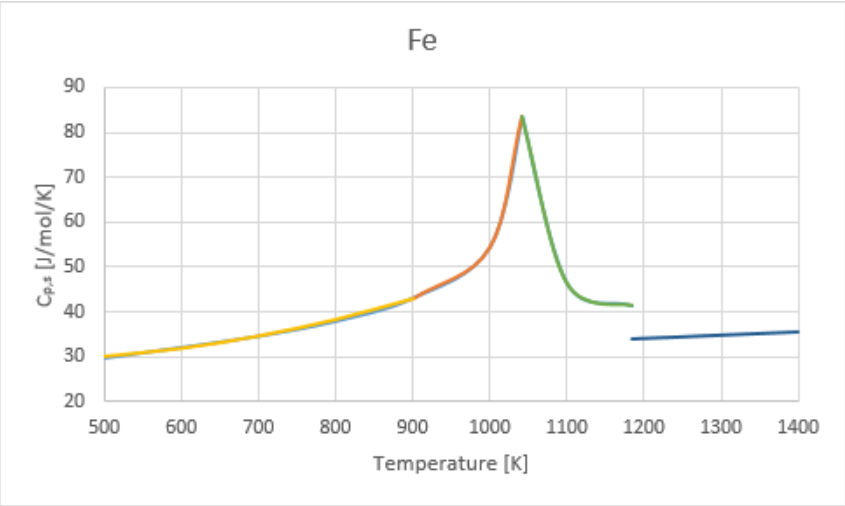

Figure B9 – Solid heat capacity of Fe

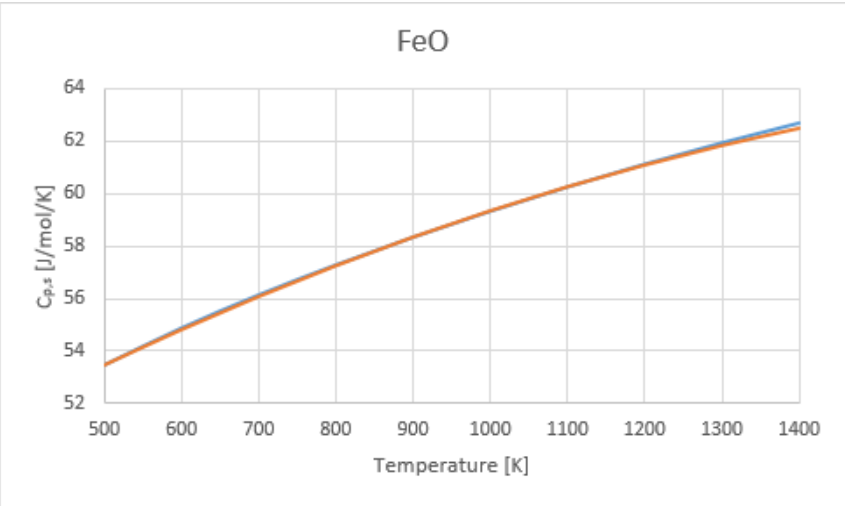

Figure B10 – Solid heat capacity of FeO

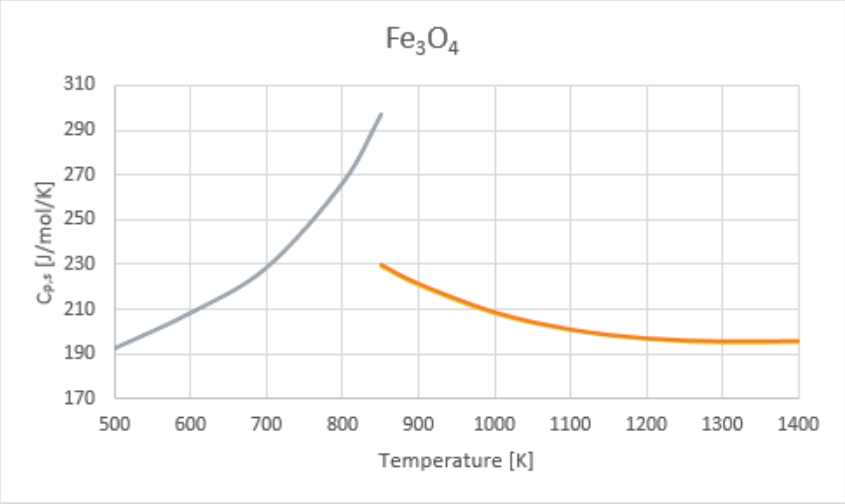

Figure B11 – Solid heat capacity of Fe_3O_4

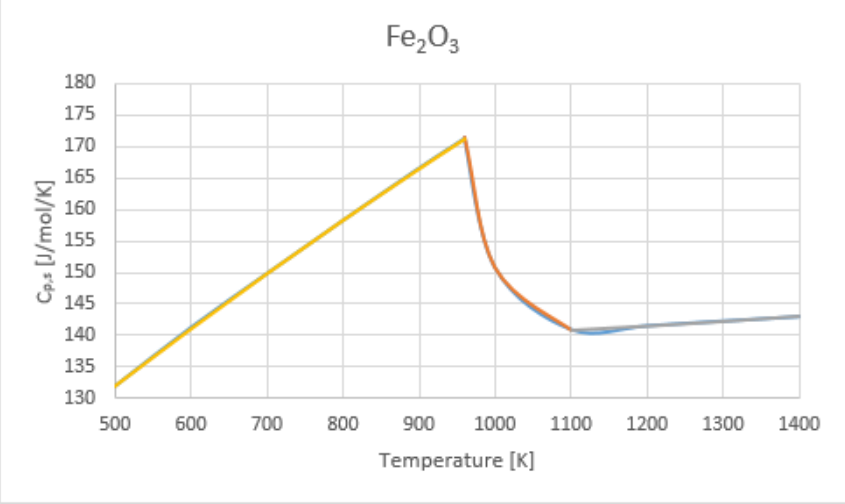

Figure B12 – Solid heat capacity of Fe_2O_3

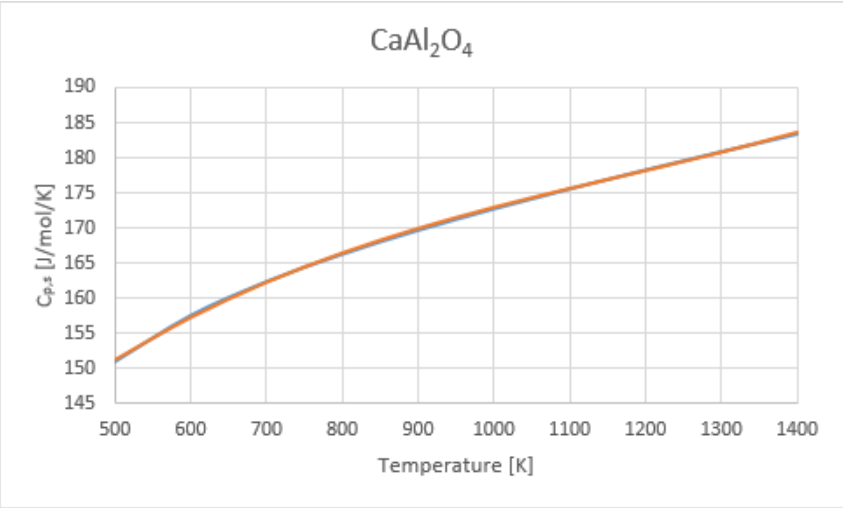

Figure B13 – Solid heat capacity of $CaAl_2O_4$

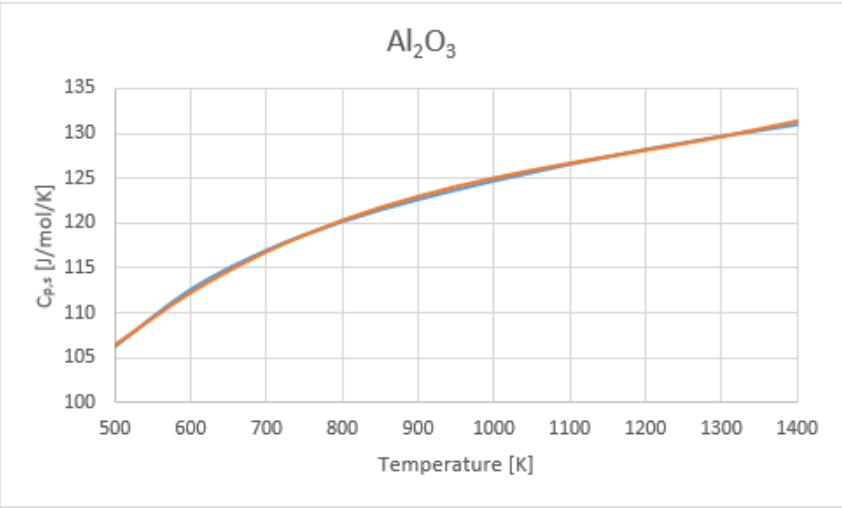

Figure B14 – Solid heat capacity of Al_2O_3